THE JOURNAL
OF
CHEMICAL PHYSICS

VOLUME 16, NUMBER 3 March, 1948

The Effect of Trapping Centers on Dielectric Breakdown in Alkali Halides*, **

CHARLES F. MEYER AND ROBERT C. HERMAN
Applied Physics Laboratory, The Johns Hopkins University, Silver Spring, Maryland
(Received September 8, 1947)

The Seeger-Teller theory of dielectric breakdown for the alkali halides has been extended to account for the effect of trapping at low temperatures. The cross section of ionized *F*-centers has been estimated classically, as well as from recent experiments of Domanic on the photoelectric yield of *F'*-centers, to be about 3×10^{-13} cm² near liquid air temperatures. The increase in the breakdown field for NaCl is given as a function of the concentration of vacant halogen ion sites. An observable increase, of about 10 percent, in breakdown voltage is predicted at a concentration of 2×10^{18} centers per cm³.

I. INTRODUCTION

THE chief theoretical ideas in the field of dielectric breakdown of the alkali halides have been formulated by Fröhlich, Seeger and Teller, and Seitz and von Hippel. These theories are concerned primarily with a description of the breakdown phenomenon in perfect crystals, i.e., crystals which do not contain any localized discrete energy states. Various types of crystal imperfections such as vacant lattice sites, interstitial atoms, strains, internal cracks, etc., give rise to localized states which act as electron traps. It is well known that trapping centers for electrons explain many of the phenomena associated with the coloration and photo-conductivity of the alkali halides, semi-conduction and the luminescence of certain types of phosphors. The behavior of the alkali halide crystals, investigated principally by Pohl and collaborators, has been explained by the introduction of the so-called color centers (Farbzentren) or localized regions where electrons are trapped in discrete energy states. A model proposed by de Boer[1] for these color centers is that empty *F*-centers are vacant halogen ion sites in the lattice, while the *F*-centers themselves are such sites which contain one electron. To explain the phenomena observed in the alkali halides it is necessary to introduce in addition the *F'*-center, which is a vacant halogen site containing two electrons. In this paper the vacant halogen ion sites are referred to as "ionized" *F*-centers. Thus, an ionized *F*-center may capture an electron to become an *F*-center which in turn may be converted into an *F'*-center by the capture of an additional electron. Recently, Seitz[2] has discussed the properties of multiple lattice vacancies in alkali halide crystals. Although such aggregates consisting of several adjacent vacancies can also trap electrons, their concentration is small compared to that of the simpler, single vacant sites.

While most of the calculations of the breakdown field in alkali halide crystals have been

* A portion of the work described in this paper has been supported by the Bureau of Ordnance, U. S. Navy, under Contract NOrd-7386.
** A preliminary account of this paper was presented at the Conference on Electrical Insulation, National Research Council at the Massachusetts Institute of Technology, Cambridge, Massachusetts, September 24–27, 1947.

[1] J. H. de Boer, Rec. des Trav. Chim. Pays Bas **56**, 301 (1937).
[2] F. Seitz, Rev. Mod. Phys. **18**, 384 (1946).

confined to crystals in which there are no trapping centers,[3–5] there have been discussions by Seeger and Teller,[6] von Hippel and Lee,[7] Meyer,[8] Seeger,[9] and most recently by Fröhlich,[10] concerning the influence of electron trapping on the breakdown phenomenon. In particular, there have been considerations to determine whether or not avalanche formation is possible for various concentrations of empty trapping centers.[8,9] These calculations are based on the idea that at sufficiently low temperatures electrons will be removed permanently from an avalanche by the trapping mechanism, thus causing an increase in the voltage required for breakdown. On the other hand, if the electrons are not trapped for long enough times, such as at sufficiently high temperatures, the breakdown voltage is not affected significantly. It should be noted that Fröhlich's recent investigation[10] shows that trapped electrons are of importance in determining the decrease in breakdown voltage at higher temperatures.

The purpose of this paper is to study the effect of trapping centers in alkali halide crystals on the formation of an avalanche of electrons in an applied electric field. This study, based on the Seeger-Teller breakdown theory, permits a determination of the order of magnitude of the empty trap concentration required to give a measurable increase in breakdown voltage at low temperatures.

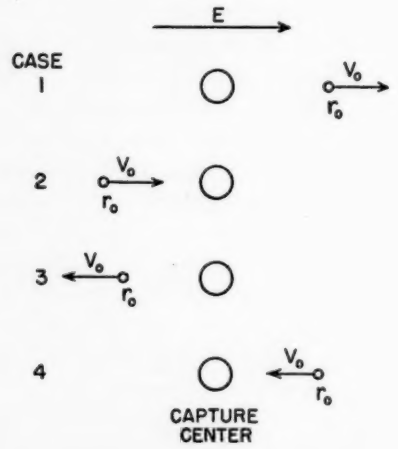

FIG. 1. Initial positions of electron with respect to a Coulomb center employed in calculating the classical capture cross section.

II. CAPTURE CROSS SECTION OF IONIZED *F*-CENTERS

In many phenomena involving the motion of electrons through a lattice, an important factor in determining the rate of change of concentration of electrons is the capture cross section of the trapping centers. At the present time there is not available an adequate quantum-mechanical calculation of the capture cross section, for conduction electrons, of ionized *F*-centers in alkali halides. Among the difficulties is the lack of adequate information concerning the potential function in the neighborhood of an ionized *F*-center and the wave function of low velocity conduction electrons. However, estimates of the cross section in the presence of an applied electric field have been made on the basis of a greatly simplified classical picture.[8] It was assumed that the ionized *F*-center has a Coulomb potential with cut-off similar to that used by Tibbs,[11] and that the conduction electrons may lose energy to the lattice by the mechanism suggested by von Hippel[12] and developed by Seeger and Teller.[3] The problem was treated in the one-dimensional case (i.e., for the case of electrons traveling straight-line paths directed through the center of the Coulomb field) since the three-dimensional problem leads to serious computational difficulties. It was believed that this approximation would give the correct order of magnitude for the dependence of the cross section on the velocity of the conduction electron. In the one-dimensional case, attention is focused on an electron at a distance r_0 from a capture center. The problem is to determine the minimum velocity which this electron must have in order to escape to infinity. The electron is considered to be moving under the influence of the Coulomb field of the center, the applied electric field and the frictional field

[3] R. J. Seeger and E. Teller, Phys. Rev. **54**, 515 (1938).
[4] H. Fröhlich, Proc. Roy. Soc. (A)**160**, 230 (1937).
[5] F. Seitz, *Modern Theory of Solids* (McGraw-Hill Publishing Company, Inc., New York, 1940).
[6] R. J. Seeger and E. Teller, Phys. Rev. **56**, 353 (1939).
[7] A. von Hippel and G. M. Lee, Phys. Rev. **59**, 824 (1941).
[8] C. F. Meyer, Thesis, George Washington University (1942).
[9] R. J. Seeger, J. Wash. Acad. Sci. **36**, 285 (1946).
[10] H. Fröhlich, Proc. Roy. Soc. (A)**188**, 521 (1947).
[11] S. R. Tibbs, Trans. Faraday Soc. **35**, 1471 (1939).
[12] A. von Hippel, J. App. Phys. **8**, 815 (1937).

postulated by Seeger and Teller.[3] It is possible to consider four distinct cases, as shown in Fig. 1, depending on the direction of the electron velocity vector with respect to the applied electric field and the field of the center. The differential equation for any case is given by

$$d^2r/dt^2 = \pm(e^2/mKr^2) - A(dr/dt)^{-2} \times \ln[b^2(dr/dt)^2] + (eE/m), \quad (1)$$

where

$$A = 4\pi^2 e^2 \nu_T^2 \left(\frac{1}{K'} - \frac{1}{K}\right)\left(\frac{K}{K'}\right), \quad (1a)$$

and

$$b^2 = (m/2h\nu_T)(K'/K)^{\frac{1}{2}}.$$

In these equations, K is the normal dielectric constant, K' the dielectric constant when the ions are kept fixed (which can be evaluated by extrapolating the square of the index of refraction to infinite wave-lengths), E is the applied electric field, and ν_T the transverse lattice vibration frequency. Equation (1) can be solved conveniently by means of the Runge-Kutta method.[13] This equation has been solved for r_0 as a function of v (the conduction electron velocity) for all cases shown in Fig. 1. Since there are only minor differences between the results, we have chosen to list in Table I the values of the cross section for Case 2. The cross section σ_v is defined as $\sigma_v = \pi r_0^2$, where r_0 is the distance an electron of velocity v must be away from the center if it is just to escape. In these calculations the applied field was set equal to the classical breakdown field of 2.9×10^5 volt/cm in NaCl as calculated by Seeger and Teller.[3] Cross sections have been calculated for other values of the applied field with the result that no strong effect of the electric field is observed. Calculations have also been carried out for the two-dimensional case where there is a finite impact parameter. The cross section is then only slightly larger than in the one-dimensional case.

In addition to the above classical calculation it is possible to estimate capture cross sections from experiment. For example, Mott and Gurney[14] have estimated the capture cross section of F-centers from measurements of the range of electrons in KCl, obtaining a result of the order of 10^{-14} to 10^{-15} cm^2. Since that time the experiments of Domanic[15] on the photoelectric yield of F'-centers in KCl permit a similar determination of the cross section of ionized F-centers. These experiments give the variation of $\eta\beta\tau$ as a function of temperature, where η is the quantum yield of photoelectrons for irradiation in the F' band, β the electron mobility, and τ is the time an electron in the conduction band spends in the free state. Following a suggestion by Seitz[16] these data may be interpreted as follows. When the crystal is irradiated at low temperature with light lying in the F'-band, the F'-centers go over into F-centers by losing electrons which are then captured by ionized F-centers to form further F-centers. This is borne out by the fact that for each photon absorbed by an F'-center, two F-centers are formed at low temperatures.[17] According to Domanic, $\eta\beta\tau$ for KCl at 90°K is about 10^{-9} cm^2/volt. The quantity τ is given by

TABLE I. Classical capture cross section of ionized F-centers in NaCl.

Conduction electron velocity $v\times10^{-7}$ cm/sec.	Capture cross section $\sigma_v\times10^{14}$ cm^2	Conduction electron velocity $v\times10^{-7}$ cm/sec.	Capture cross section $\sigma_v\times10^{14}$ cm
4.88	0.357	1.41	20.4
4.56	0.461	1.37	21.6
4.31	0.570	1.34	22.6
4.10	0.685	1.30	23.8
3.93	0.804	1.26	24.8
3.78	0.930	1.22	25.9
3.64	1.06	1.18	27.0
3.43	1.33	1.14	28.1
3.25	1.61	1.09	29.0
3.10	1.90	1.04	30.2
2.97	2.21	0.986	31.2
2.81	2.68	0.937	32.0
2.67	3.17	0.808	33.0
2.56	3.66	0.840	33.8
2.46	4.23	0.792	34.6
2.37	4.67	0.745	35.5
2.24	5.81	0.698	36.1
2.14	6.52	0.652	37.0
2.05	7.55	0.606	37.6
1.96	8.55	0.561	38.3
1.89	9.51	0.516	38.7
1.83	10.5	0.478	39.4
1.77	11.6	0.433	39.8
1.71	12.7	0.388	40.3
1.66	13.7	0.393	40.7
1.62	14.8	0.399	40.9
1.57	15.9	0.255	41.2
1.53	17.3	0.211	41.4
1.49	18.1	0.167	41.6
1.45	19.3	0.123	41.9

[13] J. B. Scarborough, *Numerical Mathematical Analysis* (The Johns Hopkins Press, Balitmore, 1930).
[14] N. F. Mott and R. W. Gurney, *Electronic Processes in Ionic Crystals* (Oxford University Press, London 1940).
[15] F. Domanic, Ann. d. Physik **43**, 187 (1943).
[16] Private communication.
[17] H. Pick, Ann. d. Physik **31**, 365 (1938).

$\tau=(N_0 v\sigma_v)^{-1}$, where N_0 is the density of vacant sites, v is the velocity of conduction electrons, and σ_v is the capture cross section of ionized F-centers for electrons of velocity v. If it is assumed that most of the F-centers were converted to F'-centers before the experiment, then the density of vacant sites is about 3×10^{16} cm^{-3}. At a temperature of 90°K, η may be taken as unity[17] and, according to the theory of Fröhlich and Mott,[18] $\beta/v\cong10^{-5}$ cm/volt with $v\cong7\times10^{6}$ cm/sec. Thus:

$$\sigma_v=(\eta/N_0)(\beta/v)(\eta\beta\tau)_{\text{exp}}^{-1},$$

which gives

$$\sigma_v\cong3\times10^{-13}\text{ cm}^2.$$

Since the physical characteristics of KCl and NaCl are not very different, this value of σ_v for KCl might be compared with the value of about 4×10^{-13} cm^2 for NaCl given in Table I for the same conduction electron velocity. The close agreement between the values of σ_v obtained by these crude approximations is certainly not significant. Further refinements must be made by means of quantum-mechanical methods and will be justified when more adequate information is available on the potential function of the centers.

III. CALCULATION OF THE ELECTRIC BREAKDOWN FIELD FOR AN ALKALI HALIDE CRYSTAL CONTAINING TRAPPING CENTERS

The purpose of this section is to develop a theory for estimating the increase in the electric breakdown voltage at low temperatures as a function of the vacant trap concentration. It is well known that breakdown can occur when the relatively few conduction electrons normally present in a crystal are accelerated by the applied electric field and gain sufficient energy to remove electrons from the halogen negative ions. An avalanche may be created in this manner. Suppose that there are N_0 trapping centers per cm^3 of the crystal. Let n be the number of conduction electrons per cm^3 at the time t, and N_i the value of n when the electric field, E, is first applied. It is assumed throughout that all the conduction electrons have the same velocity as a function of time. According to the simplified picture given here, n will start with the value N_i and decrease with time unless an avalanche begins. As the conduction electrons accelerate in the applied field, they acquire an energy sufficient to form secondary electrons which are stripped from the halogen negative ions. During this period of acceleration, some of the conduction electrons are trapped, thus reducing the number of electrons available for avalanche formation. The breakdown criterion in the case of these two competing processes may be stated as follows: There can be no breakdown if $n\leqq N_i/2$ at the time when the conduction electrons have an energy sufficient to form secondary electrons. On the other hand, if $n>N_i/2$ under the energy condition stated, an avalanche is possible since the rate of formation of secondaries is greater than the rate of loss of electrons to the trapping centers. The above condition presupposes that the secondary electrons are produced with an efficiency equal to unity. It is also assumed that once an electron is trapped it is removed permanently from the avalanche. This will be true for low temperatures where kT is sufficiently smaller than the energy depth of the trap.

If the trap concentration, N_0, is very much greater than the initial concentration of conduction electrons, the variation with time of the conduction electron concentration is given by

$$dn/dt=-N_0\sigma_v vn, \tag{2}$$

where v is the conduction electron velocity and $\sigma_v=\pi r_0^2$ is the capture cross section of a trapping center for a conduction electron of velocity v. The velocity of the conduction electrons as a function of time has the form

$$m(dv/dt)=eE-(A/v^2)\ln(b^2v^2), \tag{3}$$

where A and b^2 are defined in Eq. (1a). According to the Seeger-Teller theory $(1/b)$ is the characteristic velocity below which there is no frictional drag on the conduction electron. The second term on the right-hand side of Eq. (3) represents the frictional force on the electron.[3] The term (e^2/Kr^2), which represents the Coulomb field of the trapping center, has been omitted from Eq. (3) because the time average of the field of the center is small. Equations (2) and (3) may be combined in the form

$$\frac{dn}{dv}=-\frac{mN_0\sigma_v vn}{eE-(A/v^2)\ln(b^2v^2)}. \tag{4}$$

[18] H. Fröhlich and N. F. Mott, Proc. Roy. Soc. (A)171, 496 (1939).

For convenience, define the following quantities

$$\xi = n/N_i,$$
$$D = (A/ev^2)\ln(b^2v^2), \tag{5}$$

and

$$\alpha = E/E_B,$$

where E_B, the breakdown field for zero trap concentration,[3] is given by

$$E_B = \frac{0.74\pi^2 mev_T}{h}\left(\frac{1}{K'}-\frac{1}{K}\right)\left(\frac{K}{K'}\right)^{\frac{1}{2}}. \tag{5a}$$

The problem is now to determine the minimum value of α required to produce breakdown for a given value of N_0. Substitution of the quantities ξ, D, and α from Eq. (5) into Eq. (4), yields

$$\left(\frac{e}{mN_0}\right)\frac{d\xi}{\xi} = -\frac{\sigma_v v dv}{\alpha E_B - D}. \tag{6}$$

It should be remarked that D is the electric field inside the crystal which gives rise to the frictional effects in the Seeger-Teller theory. The applied breakdown field, E_B, is that which just exceeds the maximum value of D. Thus,

$$D = (1/e)(dw/ds) \quad \text{and} \quad E_B = (1/e)(dw/ds)_{\max},$$

where dw/ds is the energy lost per cm to the lattice. Equation (6) may be integrated subject to the condition that $\xi = \frac{1}{2}$ when the electron velocity reaches the value v_c, required to remove the electron from the halogen ion. This procedure leads to a relationship between N_0 and α_c, where α_c is the minimum value of α which will cause breakdown when there is a trap concentration N_0. The integration of Eq. (6) yields

$$\frac{eE_B \ln 2}{mN_0} = \int_{v_0}^{v_c} \frac{\sigma_v v dv}{\alpha_c - (D/E_B)}. \tag{7}$$

The lower limit of integration, v_0, in the integral remaining in Eq. (7) represents the average thermal velocity of the conduction electrons. For convenience, Eq. (7) may be written in the form

$$N_0 = \gamma E_B / I_0, \tag{8}$$

where

$$\gamma = (e/m)\ln 2, \tag{8a}$$

and

$$I_0 = \int_{v_0}^{v_c} \frac{\sigma_v v dv}{\alpha_c - (2.718/b^2v^2)\ln(b^2v^2)}. \tag{8b}$$

The integral I_0 should be evaluated numerically from $v = v_0$ to $v = v_c$. The upper limit, v_c, is the critical velocity required to ionize the halogen ion in the alkali halide crystal. For NaCl, $v_c = 18.4 \times 10^7$ cm/sec. since the energy[19] required is 9.6 ev. In Section II, σ_v, the capture cross section of ionized F-centers, was evaluated for velocities up to 4.9×10^7 cm/sec. Beyond this value of velocity σ_v is relatively small. Consequently, the integrand of I_0 is small in the interval of 4.9×10^7 cm/sec. $\leqq v \leqq v_c$ and it suffices to evaluate the integral up to $v = 4.9\times10^7$ cm/sec. The choice of the lower limit, v_0, which represents the average thermal velocity is not critical to the evaluation of I_0. The contribution to I_0 from the interval $0 \leqq v \leqq v_0$ is of the order of one percent of the contribution from $v_0 \leqq v \leqq 4.9\times10^7$ cm/sec. The integral was finally evaluated in the range

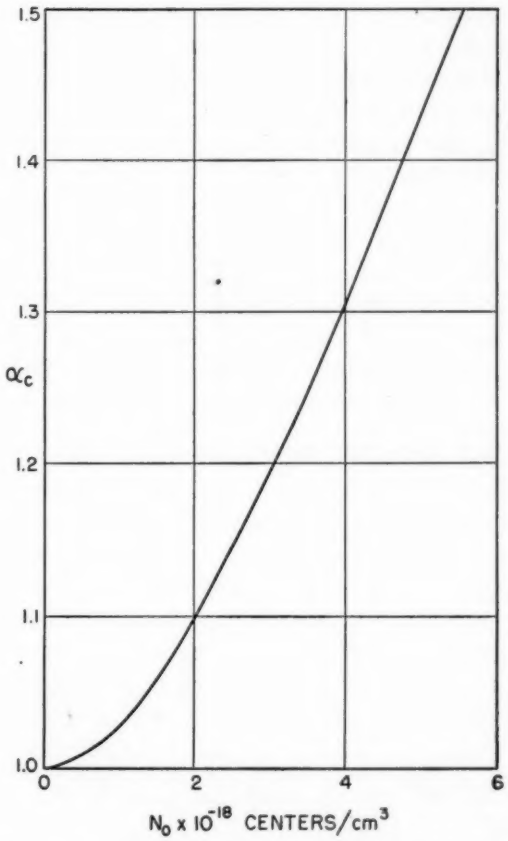

FIG. 2. The variation of breakdown field with concentration of vacant sites N_0. ($\alpha_c = E_c/E_B$, where E_B is the breakdown field for $N_0 = 0$ and E_c is the breakdown field for a finite value of N_0.)

[19] Reference 5, p. 97.

$0 \leqq v \leqq 4.9 \times 10^7$ cm/sec. which includes the interval $0 \leqq v \leqq v_0$ in order to partially compensate for the omission of the interval between $v = 4.9 \times 10^7$ cm/sec. and $v = v_c$.

Equation (8) has been employed to determine the value of N_0 required to yield a given value of α_e. The procedure followed was to evaluate the integral I_0, by numerical integration for various values of α_e and then to determine the corresponding values of N_0 from Eq. (8). This calculation has been carried out for the case of NaCl since values of the cross section for capture as a function of velocity were available for that crystal only. The values of the parameters for NaCl are as follows: $K = 5.9$, $K' = 2.19$, and $\nu_T = 4.91 \times 10^{12}$ sec.$^{-1}$. The values employed for the universal constants are those given by Birge.[20] The results obtained are shown in Fig. 2 where $\alpha_e = E_e/E_B$ is plotted against $N_0 \times 10^{-18}$ centers per cm^3. The quantity E_e is the electric breakdown field for the given value of N_0. To this approximation the curve indicates that the trapping centers increase the breakdown voltage noticeably at concentrations greater than about 2×10^{18} centers per cm^3.

This result clearly depends upon the fact that we have been considering ionized F-centers as the electron traps. If we were to estimate the effect of F-centers as traps on the breakdown voltage, higher trap concentrations would be required to produce measurable effects. This is so, because the cross section for capture of an electron seems to be about 10–100 times smaller for an F-center than for an ionized F-center. The only recorded measurements of breakdown in crystals containing F-centers are those of Kalobuchow[21] and Worobjew.[22] The latter found that NaCl colored by x-ray exposure showed a lower breakdown strength in the light than in the dark. This lowering was a function of the light intensity and not the frequency in the visible region. No measurements were made with varying concentrations of F-centers. The result observed may be due to space-charge effects which might make it difficult to determine the effects of empty trap concentration unless the experiments are performed in the dark. Although the above calculations could be extended to other alkali halides, it seems to us that such calculations would be worth while only if better values of the cross section of an ionized F-center became available.

[20] R. T. Birge, Rev. Mod. Phys. **13**, 233 (1941).

ACKNOWLEDGMENTS

We wish to thank Dr. Frederick Seitz, of the Carnegie Institute of Technology, for profitable suggestions and criticisms of this paper. We also wish to thank Dr. R. J. Seeger, Naval Ordnance Laboratory, and Dr. E. Teller, University of Chicago, for discussions on this subject. Our appreciation is extended to Dr. F. T. McClure for many suggestions concerning the presentation of the material in this paper.

[21] N. Kalobuchow, Zeits f. Physik **92**, 143 (1934).
[22] A. Worobjew, Zeits f. Physik **93**, 269 (1935).

THE JOURNAL OF CHEMICAL PHYSICS VOLUME 16, NUMBER 3 MARCH, 1948

Studies of Surface Films by Reflection of Polarized Light. I. A More Rigorous Algebraic Method for Computing Results*

F. A. Lucy
Stanford University, Stanford University, California

(Received July 30, 1947)

Plane-polarized light is in general elliptically polarized by reflection. Since the molecules in a very thin surface layer are those chiefly concerned in the process of reflection, the ellipticity is very sensitive to the interface conditions such as the presence of thin films. Since light changes phase 360° in a single wave-length, determination of phase changes to within a few minutes of arc should allow film thickness measurements to the nearest angstrom unit. The method has been used for many years to treat problems of wide variety. The instruments and techniques employed have, on the whole, been adequate, but the interpretation of results has often been more or less unsatisfactory. The algebraic relationship between instrument readings and film constants is not exactly known. Reasonably precise graphical solution is tedious. Algebraic solutions have been preferred by most workers.

This paper reports an algebraic method containing fewer approximations than used hitherto and compares results with values found by two prior methods. Drude's original equations give results in rather poor agreement with those of the more precise equations developed in this paper. Results obtained with the equations of Tronstad, on the other hand, agree fairly well in a favorable case.

PLANE-POLARIZED light, reflected from an interface at angles of incidence and azimuth not equal to $n\pi/2$ (n integral), becomes more or less elliptically polarized. The ellipticity results because the components in and perpendicular to the plane of incidence are, in general, differently retarded by reflection, and accordingly recombine out of phase. Also, in general, the reflected components are differently attenuated by the reflection. As a result, when the phase difference is removed by a compensator, the azimuth of the reconstituted plane-polarized light ordinarily cannot be obtained by a simple change of sign of the azimuth of the incident light.

When the interface is covered by a relatively transparent film, the observed beam is provided in part by reflection at the interface between the first medium and the film, in part by reflection at the interface between the film and the basis material. Consequently, the changes of phase and azimuth for reflection from filmed basis material generally are not the same as the changes observed in the case of reflection from bare basis material. When film and basis are both transparent, the difference in attenuation produced by the film is seldom enough to give a usable experimental value of azimuth change. The result is that, in principle, two data such as refractive index (leading to chemical identification in favorable cases) and thickness may be determined for a film on a metallically reflecting base, but only one such datum for a thin film on a base of high transparency.

The difference produced by the film between the path length of the components is roughly of the order of the film thickness. Since light changes phase 360° in a single wave-length, measurement of phase change precisely and accurately to a few minutes of arc should allow determination of the film thickness to the nearest angstrom unit.

The mathematical relation of shifts in phase and azimuth to the refractive index and thickness of the film producing them is complicated. Graphical solutions have been obtained, valid over a wide range of film thicknesses,[1–3] as well as analytical (algebraic) solutions[4–7] which yield precise values only for extremely thin films.

Most workers have studied films of relatively small absorption index, or highly absorbing film

* The work here reported was performed under contract between the U. S. Navy and Stanford University, designated as N6ori 154, Task Order II, under the direction of Professor James W. McBain, Department of Chemistry, and was based in part upon work performed by the author in the laboratory of the Pennsylvania Salt Manufacturing Company.

[1] A. Vašiček, J. Opt. Soc. Am. **37**, 145 (1947).
[2] A. B. Winterbottom, Trans. Faraday Soc. **42**, 487 (1946).
[3] A. Rothen, Rev. Sci. Inst. **16**, 26 (1945).
[4] P. Drude, Wied. Ann. **36**, 865 (1889).
[5] H. Hauschild, Ann. d. Physik [4] **63**, 816 (1920).
[6] L. Tronstad, Kgl. norske Vid. Sels. Skr. Nr. 1 (1931) (abridged in Zeits. f. physik. Chemie **158A**, 369 (1932); see reference 22 for correct equations).
[7] G. Szivessy, *Handbuch der Physik* XX, pp. 240–253 for other references.

material in extremely thin layers, so that in either case film absorption could be neglected. The case of thicker films of absorbing material has also been considered.[2, 8, 9]

It should be noted that changes in reflected polarized light can be produced by agencies other than film formation. Thus, altered polishing or burnishing conditions can produce large changes in the optical constants of metals.[10, 11] Some objections[12] to the methods usually employed deserve consideration, though stated at present in speculative and non-quantitative form. It is safest, when possible, to work with a liquid basis, thereby avoiding any possible difficulties from surface strains, polarized scattering from surface defects, difference between projected and actual film thickness, etc. Further objections to the method and its interpretation have been raised, but apparently are ill-founded.[13, 14]

Apparatus used by various investigators differs somewhat in detail. Typically, a surface film analyzer comprises a source of light, a filter or prism monochromator, a collimating lens, a polarizing prism, the sample under test (a flat reflecting surface), a compensator provided with an ellipticity half-shade, an analyzing prism provided with a polarimetric half-shade, and a viewing magnifier which gives an enlarged view of either half-shade or of the sample surface, at the same time condensing the light beam into the observer's pupil. The elements are usually mounted on two optical benches which are pivoted about an axis lying in the plane of the sample. Divided circles and verniers give the values of angle of incidence and of the azimuths of polarizer, compensator, and analyzer. Alternately, it is possible to place the compensator just following the polarizer, adjusting the ellipticity to a value such that reflection from the sample makes the beam again plane polarized. Other variants are described in the references given, especially by Herschkowitsch.[14]

The method has been applied to numerous problems, such as studies of natural and artificial tarnish films on glasses,[15] sorption of gases on metals,[14] oxidation and other corrosion of metals and mineral surfaces,[8, 16, 17] the nature of the transition layer between gas and liquid,[18, 19] passivating films,[6] monomolecular layers of fatty acid on water,[19] etc. Indeed, a complete bibliography of the subject would contain several hundred literature references, many at least as important as those quoted here. Bibliographies in the references given will serve as guides to the others.

As to the interpretation of the results, Adam[20] observes, with some justice, "The nature of the light reflected depends on the structure of the films, but the interpretation is so difficult in terms of molecules that most writers merely give an 'optical thickness' for the film, which has an unknown relation even to the actual thickness. Strachan[21] has attempted to treat the film as a two-dimensional assembly of oriented molecules each of which scatters light, but his expressions for the optical constants are of such mathematical complexity that the connection between the optical properties and the molecules is not easy to understand."

Nearly every worker in this field has used apparatus fully capable of the precision desired for his problem. The somewhat unsatisfactory nature of the results obtained by many investigators therefore results from difficulties of explanation rather than of technique. Most of the workers have used the equations of Drude, or similar expressions. These were derived with the use of several simplifying assumptions, justifiable for the purposes of Drude himself, but leading to errors in the results of various other experiments, errors which seriously reduce the value of the conclusions. Thus, if one is merely trying to see

[8] C. E. Leberknight and B. Lustman, J. Opt. Soc. Am. **29**, 59 (1939).
[9] B. Lustman and R. F. Mehl, Am. Inst. Mining and Met. Eng. Trans. **143**, Inst. Met. Div. 246 (1941).
[10] J. Conroy, Proc. Roy. Soc. **31**, 486 (1881).
[11] P. Drude, Wied Ann. **36**, 865 (1889), see also numerous earlier articles by Drude in the same journal.
[12] H. Schulz and R. Hanemann, Zeits. f. Physik. **16**, 200 (1923); **22**, 222 (1924).
[13] R. W. Wood, *Physical Optics* (The Macmillan Company, New York, 1939), third edition, p. 415.
[14] E. Herschkowitsch, Ann. d. Physik [5] **10**, 993 (1931).
[15] A. Vašiček, Phys. Rev. **57**, 925 (1940).
[16] P. Drude, Wied Ann. **39**, 481 (1890).
[17] H. Freundlich, G. Patscheke, and H. Zocher, Zeits. f. physik. Chemie **128A**, 321 (1927); **130A**, 289 (1927).
[18] J. W. McBain, R. C. Bacon, and H. D. Bruce, J. Chem. Phys. **7**, 818 (1939).
[19] C. Bouhet, Ann. de physique [10] **15**, 5, 102 (1931).
[20] N. K. Adam, *Physics and Chemistry of Surfaces* (Clarendon Press, Oxford), third edition, p. 36.
[21] C. Strachan, Proc. Camb. Phil. Soc. **29**, 116 (1933); see also C. G. Darwin, Trans. Camb. Phil. Soc. **23**, 137 (1924).

whether the surface of a mineral is attacked more rapidly by damp air than by dry air, discrepancies of several fold may be tolerable, but if one desires the equations relating thickness of film to time of exposure, much greater precision is necessary.

The derivation has been given in more or less detail many times previously.[4–6, 22] The approximations used are such that the calculated results approach the correct values as the reciprocal of the film thickness approaches infinity. However, the approach is not asymptotic, and in unfavorable cases not even monotonic. Together with the unavoidable inapplicability to thick films, this situation has led to the adoption of graphical methods[1–3] which, for general work, are decidedly more tedious than algebraic methods, though sometimes less tedious if the problems to be studied fall in a narrow range.

There is a middle course. It is possible to develop an explicit algebraic method for calculating film constants in which the only approximation is the dropping of higher terms in L/λ, where L is film thickness and λ wave-length of the light used. Then, as L/λ approaches zero, the calculated values approach the true values asymptotically. Of course, in any method *experimental* errors become relatively more serious as the film becomes thinner. Consequently, there will be a range of refractive index and thickness values for which a particular computing method gives best results. For most of the problems handled by the polarized light method, it is desirable to have this range extended to films as thin as possible.

In one approach frequently used, the basis material, film, and outer medium are considered to be bounded by parallel planes (Fig. 1a). An incident ray is partly reflected, partly refracted. The refracted ray, in turn, is similarly divided at the film-basis interface. Multiple reflections within the film are assumed. The amplitude and phase relations for components in and perpendicular to the plane of incidence are derived in terms of film thickness and optical constants of medium, film, and basis. Tables or graphs are then constructed, giving expected amplitude and phase relations of the summed reflected beam in terms of the properties of the incident light for ranges of angle

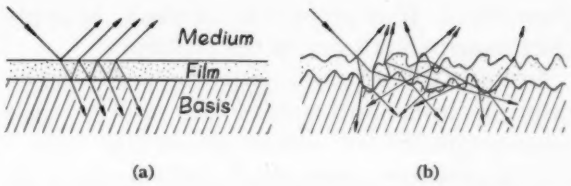

FIG. 1. Schematic representation of the multiple reflection to be expected (on the basis of geometrical optics) within an ideal plane-parallel film (1a) and within a film closer to the form actually existing on polished metal (1b).

of incidence, wave-length, and film constants. Knowing the constants for medium and basis, and observing the actual properties of the reflected beam, one may, by successive approximations and interpolation, in most cases arrive at values of film thickness and refractive index. The precision depends, *inter alia*, upon the precision of the graphs and tables. To prepare these so as to cover any very wide range of conditions is a decidedly tedious matter, especially if fairly precise results are desired for polished metal bases. Slight differences in polishing conditions cause every specimen to differ from every other. For films of thickness more than about 100A such interpolation methods are the only ones available, but problems involving films of less thickness (and these are very numerous) are preferably handled algebraically.

A straightforward application of the multiple-reflection method meets with difficulties when the interfaces are not true planes. Electron micrographs of silica replicas of optically flat polished metal mirrors, for example, reveal innumerable pits and scratches, with rounded areas of flowed metal between. If angles of reflection and refraction were to be calculated by geometrical optics, the situation would be that shown in Fig. 1b, where the path length within the film is highly uncertain, and where a ray may even leave the film and re-enter it. It is a matter of experience that when the interfacial irregularities are small with respect to the wave-length of incident light, the diffusion suggested by Fig. 1b does not actually occur.

It is therefore conceptually preferable to treat the film material and the basis material as distributions of polarizable matter, sending out light waves under the influence of the incident beam. Interference then produces the observed

[22] L. Tronstad, Trans. Faraday Soc. **31**, 1151 (1935), correcting an error in the equations of reference 6.

phenomena. It is preferable, in short, to apply electromagnetic theory to the problem.

In this treatment, because of the superposition principle, irregularities small with respect to the wave-length do not matter unless they form a porous structure: pores small with respect to the wave-length lower the effective refractive index.

The electromagnetic derivation has already been carried part way with the desired precision.[6,23–25] The procedure is to start from Maxwell's equations, derive the appropriate boundary conditions, express the amplitudes of incident, refracted, and reflected beams in simultaneous equations, expand, collect, eliminate the data for the refracted beam, and express the constants of the reflected light for the case of basis plus film in terms of the constants for bare basis material plus a correction factor, where the latter involves the film constants, and finally to obtain an explicit solution for the film constants in terms of instrument readings.

Work of earlier investigators has brought the process to the stage in which the correction factor has been derived before introduction of approximations other than the neglect of higher terms in L/λ. The notation of Born[25] for the correction factor σ is

$$\sigma=\frac{4\pi L}{\lambda_0}\cdot\frac{(\epsilon_1)^{\frac{1}{2}}\epsilon_2\eta}{\epsilon_2-\epsilon_1}\cdot\frac{\cos\phi\sin^2\phi}{\epsilon_2\cos^2\phi-\epsilon_1\sin^2\phi}, \tag{1}$$

where

$$\eta=\bar{\epsilon}+\epsilon_1\epsilon_2/\tilde{\epsilon}-\epsilon_1-\epsilon_2. \tag{2}$$

L is film thickness, λ_0 is the vacuum wave-length of the light used, ϕ is the angle of incidence, ϵ_1 is the dielectric constant of the surrounding medium, ϵ_2 is that of the basis material, and $\bar{\epsilon}$ and $\tilde{\epsilon}$ are effective averages of the film dielectric constant for electric fields in perpendicular directions. The last two quantities will, in the following, be taken as the same and equal to ϵ, since the derivation of the present paper is intended to apply to practically isotropic film materials only. Drude and Tronstad proceed to neglect $\epsilon_1\sin^2\phi$, but this term will be retained in the present derivation.

Division of numerator and denominator by $\cos^2\phi$ changes (1) to

$$\sigma=\frac{4\pi L}{\lambda_0}\cdot\frac{(\epsilon_1)^{\frac{1}{2}}\epsilon_2\eta}{\epsilon_2-\epsilon_1}\cdot\frac{\sin\phi\tan\phi}{\epsilon_2-\epsilon_1\tan^2\phi}. \tag{3}$$

Introducing (2) in (1) and collecting, we have

$$\sigma=C\frac{(\epsilon_1)^{\frac{1}{2}}\epsilon_2(\epsilon_2-\epsilon_1)(\epsilon-\epsilon_2)}{\epsilon(\epsilon_2-\epsilon_1)(\epsilon_2-\epsilon_1\tan^2\phi)},$$

with (4)

$$C=\frac{4\pi L}{\lambda_0}\sin\phi\tan\phi.$$

Further compactness results from setting

$$D=\frac{(\epsilon_1)^{\frac{1}{2}}(\epsilon-\epsilon_1)}{\epsilon}. \tag{5}$$

Then,

$$\sigma=\frac{CD\epsilon_2(\epsilon-\epsilon_2)}{(\epsilon_2-\epsilon_1)(\epsilon_2-\epsilon_1\tan^2\phi)}. \tag{6}$$

When the basis material is strongly absorbing, as in the case of reflection from a metal, it is best to take ϵ_2 as complex. In place of the Maxwell relation $\epsilon_2^{\frac{1}{2}}=n$, it is then customary to set

$$\epsilon_2^{\frac{1}{2}}=n_2-ik \quad \text{or} \quad \epsilon_2^{\frac{1}{2}}=n_2(1-i\kappa), \tag{7}$$

where n is the real part of the refractive index, expressing the ratio of phase speeds, as usual, and k is the absorption coefficient. Squaring both sides of (7) gives

$$\epsilon_2=n^2-k^2-2ink. \tag{8}$$

For compactness, introduce

$$\alpha=n^2-k^2=n^2(1-\kappa^2), \quad \beta=2nk=2n^2\kappa. \tag{9}$$

That is, write $\epsilon_2=\alpha+i\beta$. Then

$$\sigma=\frac{CD(\alpha-i\beta)(\epsilon-\alpha+i\beta)}{(\alpha-i\beta-\epsilon_1)(\alpha-i\beta-\epsilon_1\tan^2\phi)}. \tag{10}$$

It is possible to carry ϵ_1 explicitly in the further work, and necessary to do so if experiments are to be made on samples immersed in a transparent liquid, but since the numerical examples below refer to air as the first medium, ϵ_1 will be set equal to unity in the following. Further abbrevia-

[23] P. Drude, *Lehrbuch der Optik* (Leipzig, 1900), p. 266.
[24] P. Drude, *Theory of Optics* (translated by Mann and Millikan), pp. 287–291.
[25] M. Born, *Optik* (Verlag, Julius Springer, Berlin, 1933), p. 36, reprinted by Edwards Brothers, Ann Arbor, Michigan, 1943.

tions are convenient:

$$\alpha-1=p, \quad \alpha-\tan^2\phi=q. \tag{11}$$

The factor for rationalizing the denominator is

$$(p+i\beta)(q+i\beta)=pq+ip\beta+iq\beta-\beta^2.$$

This may be written $r+is$, where

$$\left.\begin{aligned} r&=pq-\beta^2,\\ s&=\beta(p+q).\end{aligned}\right\} \tag{12}$$

The rationalized denominator is then simply r^2+s^2, while the numerator consists of a real part:

$$\epsilon(\alpha r+\beta s)+(\beta^2-\alpha^2)r-2\alpha\beta s,$$

and an imaginary part:

$$i[\epsilon(\alpha s-\beta r)+(\beta^2-\alpha^2)s+2\alpha\beta r],$$

each multiplied by CD. Again for compactness, set

$$CD/(r^2+s^2)=LA, \tag{13}$$

where L is, as noted, the film thickness.

The effect of reflection from the filmed sample is described by the expression $\tan\psi e^{i\Delta}$. Here $\tan\psi$ is the relative attenuation in amplitude suffered by components perpendicular and parallel to the plane of incidence, and Δ is the phase difference of the components in the elliptical beam. For a fuller discussion, see below, and see also references 2, 5–7, 13 (p. 542), etc. The state of the light beam reflected by the sample in the absence of the film in question is, similarly, described by $\tan\psi' e^{i\Delta'}$. The quotient of these two quantities is[25]

$$\tan\psi e^{i\Delta}/\tan\psi' e^{i\Delta'}=1+i\sigma+\cdots. \tag{14}$$

The left side of (14) may alternatively be written

$$\frac{\tan\psi}{\tan\psi'}e^{i(\Delta-\Delta')}. \tag{15}$$

In the Drude-Tronstad formulation,[6,22] this is replaced by an approximation. The exponential is expanded and terms after the first in $\Delta-\Delta'$ are dropped. The quotient of tangents is replaced by $(2\psi-2\psi')/\sin 2\psi'$, so that the equation derived from the real parts may be expressed in terms of ψ and ψ' alone, and that derived from the imaginary parts in terms of Δ and Δ' alone.

In the present development, however, the exponential is exactly expressed by de Moivre's theorem. Then

$$\frac{\tan\psi}{\tan\psi'}[\cos(\Delta-\Delta')+i\sin(\Delta-\Delta')]=1+i\sigma+\cdots. \tag{16}$$

Separation of real and imaginary parts gives

$$\left.\begin{aligned} 1/LA&=[\epsilon(\alpha s-\beta r)+(\beta^2-\alpha^2)s+2\alpha\beta r]\Big/\left[1-\frac{\tan\psi}{\tan\psi'}\cos(\Delta-\Delta')\right],\\ \text{and}\qquad 1/LA&=[\epsilon(\alpha r+\beta s)+(\beta^2-\alpha^2)r-2\alpha\beta s]\Big/\left[\frac{\tan\psi}{\tan\psi'}\sin(\Delta-\Delta')\right].\end{aligned}\right\} \tag{17}$$

The Eqs. (17) are of the form

$$\left.\begin{aligned} 1/LA&=a_1\epsilon+b_1,\\ \text{and}\qquad 1/LA&=a_2\epsilon+b_2.\end{aligned}\right\} \tag{18}$$

Therefore, with the definitions of a and b obvious from (17),

$$\epsilon=(b_2-b_1)/(a_1-a_2), \tag{19}$$

and L may be found by eliminating ϵ or by substitution in either of Eqs. (18):

$$L=1/\mathrm{A}(a_1\epsilon+b_1)=1/\mathrm{A}(a_2\epsilon+b_2)=(a_1-a_2)/\mathrm{A}(a_1b_2-a_2b_1). \tag{20}$$

The square root of the film dielectric constant is the film refractive index:

$$n=\epsilon^{\frac{1}{2}}. \tag{21}$$

From the definitions of C and D above, it follows that

$$A=\frac{4\pi\sin\phi\tan\phi}{\lambda(r^2+s^2)}\cdot\frac{\epsilon-1}{\epsilon}. \tag{22}$$

Because of the factor $(\epsilon-1)/\epsilon$ in A, plots of $1/L$ against ϵ according to (17) are hyperbolae intersecting trivially at $1/L=0$, $\epsilon=1$, and at some other point which is the desired solution. When the curves intersect at a very small angle, a slight error in the slopes of the curves near the intersection point will seriously affect ϵ even

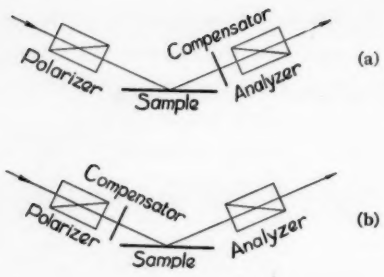

FIG. 2. Alternate arrangements of essential elements of surface-film analyzer.

though the error makes little difference in L. Crudities of approximation will have the same effect. It is desirable to choose experimental conditions, when time for varying them is available, in such a way that the curves intersect at as large an angle as possible.

If the quotient in (15) had been formed the other side up, namely, as

$$\frac{\tan\psi'}{\tan\psi}\exp i(\Delta'-\Delta), \tag{23}$$

which is equally legitimate, the right side of (16) would become $1-i\sigma+\cdots$, changing the denominators in (17) so that

$$\left.\begin{aligned} 1/LA&=\left[\epsilon(\alpha s-\beta r)+(\beta^2-\alpha^2)s+2\alpha\beta r\right]\Big/\\ &\qquad\left[\frac{\tan\psi'}{\tan\psi}\cos(\Delta'-\Delta)-1\right],\\ 1/LA&=-\left[\epsilon(\alpha r+\beta s)+(\beta^2-\alpha^2)r-2\alpha\beta s\right]\Big/\\ &\qquad\left[\frac{\tan\psi'}{\tan\psi}\sin(\Delta'-\Delta)\right]. \end{aligned}\right\} \tag{24}$$

The terms discarded in this case differ from those discarded in (16): it is not quite true to say that $1-\sigma=1/(1+\sigma)$. With a given set of experimental data, values of ϵ and L determined by (17) will accordingly differ slightly from those found with (24). Because higher terms in L/λ were discarded at several other points in the derivation, it is not possible to say *a priori* whether (17) or (24) will give best results in a given case. Calibration experiments on known films may show, for instance, that (17) applies better than (24) with film materials of low refractive index, making (24) preferable for film material of high index.

To use these equations, the experimenter may treat his data in the manner of Tronstad.[6] Assume an instrument (Fig. 2) containing a polarizer, analyzer, and de Sénarmont compensator (the last being a mica plate of constant retardation, rotatable in azimuth). Obtain compensation for the unfilmed surface. Define the azimuths as follows: let the polarizer be in null position when the electric vector of the transmitted light is in the plane of the sample (thus perpendicular to the plane of incidence), let the analyzer be in null position when extinguishing the light from the polarizer so set, and let the compensator be in null position when the fast direction of the mica is in the plane of incidence. Designate these azimuths, respectively, as P, A, and Q. This A is, of course, not to be confused with the A of Eq. (22).

If the reflected components are equally attenuated, compensation of the phase difference will give a plane vibration with azimuth θ defined below. Call the retardation of the compensator δ. Then,[17] expressing the difference between polarizer and compensator azimuths as PQ,

$$\cos2\theta=\cos2PQ\cos2Q+\sin2PQ\sin2Q\cos\delta. \tag{25}$$

This defines θ. Further,

$$\sin\Delta'=\sin2PQ\sin\delta/\sin2\theta, \tag{26}$$

where Δ' is the phase difference of the components in the elliptically polarized beam, referring to axes parallel and perpendicular to the plane of incidence. As in (17) and (24), this phase difference, referring as it does to the unfilmed sample, is called Δ', while Δ is the analogous quantity for the filmed sample. Also calculate

$$\tan\psi'=\tan\theta/\tan A. \tag{27}$$

Then, approximately,

$$\left.\begin{aligned} \kappa&=\sin\Delta'\tan2\psi',\\ n&=\sin\phi\tan\phi\cos2\psi'/(1+\cos\Delta'\sin2\psi'). \end{aligned}\right\} \tag{28}$$

These are the customary definitions. In the derivation of (28), $\sin^2\phi$ was neglected at one point relative to the modulus of ϵ_2. This approximation is nominally of the same order as Drude's neglect of $\epsilon_1\sin^2\phi$ relative to $\epsilon_2\cos^2\phi$ in his derivation of the film equations, but insertion of

TABLE I. Comparison of polarizer azimuth P, compensator azimuth Q, and analyzer azimuth A, for thin films of ferric oxide on steel after different times of treatment. (Wave-length 5461A, bath Na_2SO_4-NaOH, pH 13.4, 85°C, work anodic, current density 12 amp./dm^2, rinse water vacuum distilled and collected under nitrogen, used boiling, sample dried hot in nitrogen at reduced pressure, measured in nitrogen.)

Period of treatment (seconds)	P	Q	A
0	45°	19° 07′	−47° 20′
10	45°	18° 48′	−47° 30′
(Repolished)			
0	45°	19° 36′	−47° 52′
20	45°	18° 58′	−48° 11′

experimental data shows that it is in most cases much less serious in magnitude. It affects the film equations slightly but unsymmetrically, and the investigator may prefer to use the much more complicated exact formulae.[26] Readings on the filmed sample similarly yield $\tan\psi$ and Δ for substitution in the film equations. With n and κ, the investigator then computes (9), (11), and (12). Since ϕ, the angle of incidence, is read from the instrument dial, all the quantities necessary for calculating ϵ and L are at hand. Substitution into (17) or (24), followed by evaluation of (20) and (22), solves the problem. Methods giving a less closely approximate result require nearly as much time. At the expense of lowered precision, the saving is seldom worth while.

Tronstad's solution may be recast into comparable form. Let

$$\frac{4\pi}{\lambda}\cdot\frac{\cos\phi\sin^2\phi}{(\cos^2\phi-\alpha)^2+\alpha'^2}\cdot\frac{\epsilon-1}{\epsilon}=\mathrm{B}, \tag{29}$$

where

$$\alpha=\frac{1-\kappa^2}{n^2(1+\kappa^2)^2}, \tag{30}$$

and

$$\alpha'=\frac{2\kappa}{n^2(1+\kappa^2)^2}. \tag{31}$$

Here α and α' are quantities introduced by Drude and are not related to the α defined in (11). Tronstad's equations[22] corresponding to (17) then

[26] *Handbuch der Physik*, Vol. 20, pp. 240–245; O. Wiener, Abh. d. Math.-Phys. Kl. d. Sächs. Ges. d. Wiss. **30**, 495 (1908).

TABLE II. Evaluation by four different equations of refractive index, n, and thickness of film, L, for the films of Table I.

Period of treatment	Equations (17) n	(17) L	(24) n	(24) L	(32) n	(32) L	Drude[11] n	Drude[11] L
10 sec.	3.34	2.82A	3.34	2.81A	3.17	3.06A	3.07	5.26A
20 sec.	3.36	5.56	3.28	5.82	3.18	5.99	3.08	10.15

become

$$\begin{aligned}1/LB&=-\frac{\sin2\psi'}{2(\psi-\psi')}\alpha'(\epsilon\cos^2\phi-1)=a_1\epsilon+b_1,\\ 1/LB&=\frac{1}{\Delta-\Delta'}[\epsilon(\alpha\cos^2\phi-\alpha^2-\alpha'^2)\\ &\qquad+\alpha-\cos^2\phi]=a_2\epsilon+b_2,\end{aligned} \tag{32}$$

whence

$$\begin{aligned}\epsilon&=(b_2-b_1)/(a_1-a_2),\\ L&=1/\mathrm{B}(a_1\epsilon+b_1)=1/\mathrm{B}(a_2\epsilon+b_2).\end{aligned} \tag{33}$$

The form of the solution is the same as that of the present paper, but the coefficients differ from those of (18).

Graphical determination of Δ and ψ is possible. While slower and less precise than the analytical method, it gives a clearer description of the phenomenon and is a help in selecting plus and minus signs. A single example (following Tronstad[6]) is given in Fig. 3.

The instrument is assumed to be of the type shown in Fig. 2b, with polarizer, mica compensator, sample, and analyzer in sequence. In the Stanford instrument, the sample is horizontal, while incident and reflected light beams lie in a vertical plane. To an observer of the oncoming

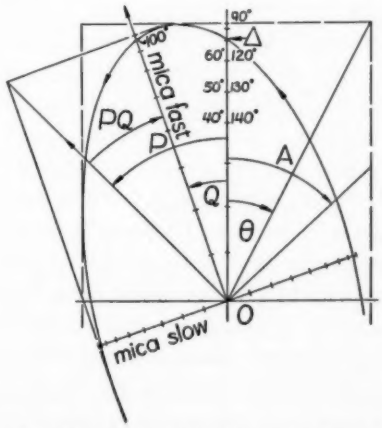

FIG. 3. Graphical determination of phase shift and relative amplitude weakening when plane-polarized light is reflected from steel.

light, azimuth angles are positive counterclockwise, by the usual convention, but are taken as zero in the vertical plane of incidence. The diagram is drawn by laying out horizontal and vertical axes, then drawing P as chosen and Q as found in an experiment. The slow direction of the mica is also drawn. From an arbitrary point on OP, perpendiculars are dropped to the compensator axes. The segments thus delimited are divided from 0° to 90° by a sine scale. OP represents light leaving the polarizer. This is decomposed by the compensator, which in this case has a retardation of 100°, and is thus approximately a quarter-wave plate. After passing the compensator, the components recombine with this phase difference, giving the ellipse shown. Relative to any other axes, this same ellipse represents components with a different phase difference. In particular, relative to the plane of incidence, the retardation is Δ, which may be read from a sine scale of degrees on the vertical axis. This phase difference is removed by reflection from the sample, and the horizontal and vertical components would recombine to give plane-polarized light in azimuth θ, if it were not for the fact that the vertical component is more attenuated than the horizontal one. The vibration plane of the reflected light actually, therefore, has the azimuth A, from which ψ is found by (27).

In conclusion, some numerical examples will be given to illustrate the magnitude of the discrepancies between results obtained with the various equations, using data of Table I.

The differences between (24) and (32) are not so great as they may appear. In favorable cases, close agreement is found between results calculated by the two systems from a given set of experimental data. One favorable case is that of a thin ferric oxide film on steel: the refractive index is high, the difference between ψ and ψ' is relatively large, while $\cos(\Delta-\Delta')$ is very close to unity. In consequence, Tronstad's omissions and approximations have little effect on the answer. The equations of Drude[11] omit three more terms, namely, those making up the coefficient a_2 in (32). It is true that these are individually small. On the other hand, all have the same sign (α is negative for steel) and are multiplied by ϵ, which here has a large numerical value. As a result, $a_2\epsilon$ in the present case is not much smaller than b_2. The value of L, the film thickness, largely determined by the Δ equation, is brought out much too high by the Drude equation. Table II gives the comparison. It will be noted that the refractive indices are close to that of bulk ferric oxide. The latter, measured on the same instrument, is $n=3.19$ for the wave-length used.

Since the differences in azimuth angles are known to only two figures, with the second somewhat uncertain, the third figure in the results is not significant, but is retained to facilitate comparisons. It is seen that (17) and (24) give identical results with the thinner film, but that neglect of higher terms makes a perceptible difference in the case of the thicker film.

The data in the tables refer to a mirror of low carbon steel, polished metallographically, then alternately etched with a mixture of acetic and hydrochloric acids, rinsed, and polished on paper with Barnesite 85 in kerosene. This alternation of etching and polishing removes inclusions and intergranular material and partially spreads the ferrite across the pits and crevices so formed. If etching is not performed, specks of impurity pull out and scratch the ferrite. As the final step, the mirror was polished for two minutes with Barnesite in dilute aqueous trisodium phosphate, rinsed, and dried in vacuum. On the basis of previous work[17] this mirror probably bore a layer of oxide about one molecule thick. Exposed to dry air, a mirror so treated required about four hours to develop a further monomolecular layer of oxide.

A much greater rate of oxidation resulted from anodic treatment at 12 amp./dm² in an alkaline bath. As the tables show, oxide was formed electrolytically at the rate of approximately six molecular layers per minute. After anodizing, the mirror was rinsed quickly in two changes of boiling water and dried in nitrogen at reduced pressure. The water used had been distilled (without boiling) in the absence of air and collected under nitrogen. Practically all of the oxide, therefore, was that electrolytically produced.

For thicker films, when $\cos(\Delta-\Delta')$ differs more from unity, and, in general, when the conditions are less favorable for the validity of the Drude-Tronstad approximations, wider discrepancies than those shown in Table II are to be expected.

THE JOURNAL OF CHEMICAL PHYSICS VOLUME 16, NUMBER 3 MARCH, 1948

An X-Ray Study of the Stepwise Melting of Anhydrous Sodium Palmitate*

H. NORDSIECK, F. B. ROSEVEAR, AND R. H. FERGUSON
Chemical Division, Procter and Gamble Company, Ivorydale, Ohio
(Received October 3, 1947)

X-ray powder patterns on anhydrous sodium palmitate show that the five phases already known to occur between crystal and isotropic melt can be grouped into two basic structures. Both structures are liquid crystalline, i.e., crystalline in the direction of the long spacing and liquid-like laterally. Between the lower temperature "waxy" structure, which includes the previously known subwaxy, waxy, and superwaxy phases, and the higher temperature "neat" structure, which includes subneat and neat, there is a pronounced break in the curve of long spacing *vs.* temperature; in addition, the three waxy phases exhibit two diffuse short spacing rings, whereas the neat phases exhibit only one. These pattern differences lead to the interpretation that the waxy phases contain structural restraints on molecular position and motion not present in the neat phases.

I. INTRODUCTION

THE present paper describes an x-ray study of the progressive melting behavior of anhydrous sodium palmitate. Previously, six phase transitions have been reported to occur in anhydrous sodium palmitate between the crystalline state and isotropic melt. The present study was carried out more to investigate the structure of these high temperature phases than to check previous transition temperatures. The data to be presented show that, as the soap is heated, it transforms from the fully crystalline state to the isotropic liquid state, or "nigre," by way of two intermediate basic structures, one of which embraces the three waxy phases (subwaxy, waxy, and superwaxy) and the other the two neat phases (neat and subneat).

For background, Table I lists chronologically the transition temperatures obtained by various recent investigators and the experimental methods used. Vold, Rosevear, and Ferguson,[1] who discuss the work prior to 1939, report the determination of four transition temperatures found by the dilatometer and polarizing microscope. These results are corroborated, with slight differences in transition temperatures, by Vold and Vold[2] who, in addition, resolved the waxy phase into two phases, subwaxy and waxy. These same investigators[3] later discovered with the dilatometer and the hot wire microscope technique of Bernal[4] the waxy-superwaxy transition at 172°C, bringing the total of waxy phases to three. Chesley[5] examined the melting behavior of anhydrous sodium palmitate by taking x-ray patterns from room temperature up to 300°C and listed all of the previously described transitions, except the waxy-superwaxy one at 172°C. Finally, R. D. Vold[6] applied a differential calorimeter technique to the problem and found all of the transitions except the waxy-superwaxy one at 172°C. Thus, the phase sequence on heating is crystal, subwaxy, waxy, superwaxy, subneat, neat, and, finally, isotropic liquid or nigre above 295°C.

II. X-RAY EVIDENCE ON THE HIGH TEMPERATURE PHASES

In Fig. 1 are reproduced illustrative x-ray powder patterns of each of the phases formed as anhydrous sodium palmitate is heated to the temperatures indicated in the figure. Exact reproduction of the patterns in such a figure is difficult, so that most of the details are dealt with graphically in Fig. 2. Nevertheless, certain features should be noted: (a) The long spacing rings are grouped near the center of the pattern and the short spacing rings farther out. (b) There are

* Presented at the meeting of the American Society for X-ray and Electron Diffraction, December 5, 1946, Pittsburgh, Pennsylvania.

[1] R. D. Vold, F. B. Rosevear, and R. H. Ferguson, Oil and Soap **16**, 48 (1939).

[2] M. J. Vold and R. D. Vold, J. Am. Chem. Soc. **61**, 808 (1939).

[3] R. D. Vold, Soap and Sanitary Chemicals (June, 1940); M. J. Vold, J. Am. Chem. Soc. **63**, 160 (1941).

[4] J. D. Bernal and D. Crowfoot, Trans. Faraday Soc. **29**, 1032 (1933).

[5] F. G. Chesley, M. S. Thesis, M.I.T. (1940); J. Chem. Phys. **8**, 643 (1940).

[6] R. D. Vold, J. Am. Chem. Soc. **63**, 2915 (1941).

TABLE I. Phase transitions on heating anhydrous sodium palmitate.

Reference	Vold, Rosevear, and Ferguson (1939)[a]	Vold and Vold (1939)[b]	R. D. Vold (1940) M. J. Vold (1941)[c]	Chesley (1940)[d]	R. D. Vold (1941)[e]
Method	Dilatometer and microscope	Dilatometer and microscope	Dilatometer and microscope hot wire	X-ray	Calorimeter
Phase	Transition temperatures, °C				
Crystal	125	117	117	117	114
Subwaxy	—	135	135	138	135
Waxy	—	—	172	—	—
Superwaxy	195	208	208	205	209
Subneat	255	253	253	257	237
Neat	297	292	295	290	292
Nigre					

[a] See reference 1.
[b] See reference 2.
[c] See reference 3.
[d] See reference 5.
[e] See reference 6.

several sharp short spacing rings up to 110°C; at the higher temperatures, any short spacings are diffuse. (c) The patterns of the three waxy phases (subwaxy, waxy, and superwaxy) are similar. (d) The patterns of the two neat phases (neat and subneat) are similar. (e) The long spacing rings of all the phases except nigre are sharp.

Figure 2 shows diagrammatically the dependence of x-ray pattern on temperature as anhydrous sodium palmitate is heated. The transition temperatures (Table I) are indicated by the vertical lines. These data, coupled with certain features displayed in Fig. 1, lead to the following description of the various phases.

The Crystalline Region

In the present work the starting material was omega phase, which is the crystalline phase obtained on cooling the anhydrous soap from the subwaxy or higher regions to room temperature. Below 117°C the soap remains essentially crystalline, as shown by the several sharp diffractions in Fig. 1. The relatively slight change in the long spacing and the strongest short spacing between 25°C and 110°C indicates that omega phase persists, any differences in these and other spacings being possibly the result of Thiessen's[7] genotypical effect, or of Chesley's[5] change at 67°, or of simple thermal expansion. Since, on the basis of the evidence in Figs. 1 and 2, there can be no doubt as to the existence of a discontinuity near 120°, and since the details of behavior in the crystalline region are not the concern of this paper, the pairs of points at 25° and 110° are deemed sufficient.

[7] P. A. Thiessen and Eva Ehrlich, Zeits. f. physik. Chemie **A165**, 453, 464 (1933).

The Waxy Phases

On the basis of the x-ray evidence, the subwaxy, waxy, and superwaxy phases appear to fall into one inclusive structural group. Specifically, all three phases exhibit sharp long spacing rings and two diffuse short spacing halos. In addition, the long spacings of all three phases lie on the same curve for spacing *versus* temperature; the short spacings, though diffuse, likewise appear to fall on continuous curves. The above curve for long spacing *versus* temperature and the presence of two diffuse short spacings serve to distinguish the waxy structure from the crystalline phase, which exhibits several sharp, short spacing rings and long spacing curve which is discontinuous with that of the waxy structure, and from the neat structure, which exhibits only a single, diffuse, short spacing ring and a separate curve for long spacing *versus* temperature. An additional distinction between the waxy and crystalline structures is furnished by the intensity sequence of the long spacing rings (Fig. 1); these rings in the case of the waxy phases show a progressive decrease in intensity with order, while the crystal phase exhibits long spacing rings with odd orders strong.

By way of interpretation, the waxy structure can be described as liquid crystalline, i.e., crystalline in the long spacing direction because the long spacings are sharp, and liquid or amorphous laterally because the short spacings, at 2.9 and 4.8A, are diffuse. The halo at 4.8A probably represents the average lateral separation of the hydrocarbon chains in a loose hexagonal packing, and the halo at 2.9A indicates an additional structural restriction such as an average common orientation of the dipolar end groups of the soap molecules. This restriction of molecular motion may account for the stiffness of the waxy phases.

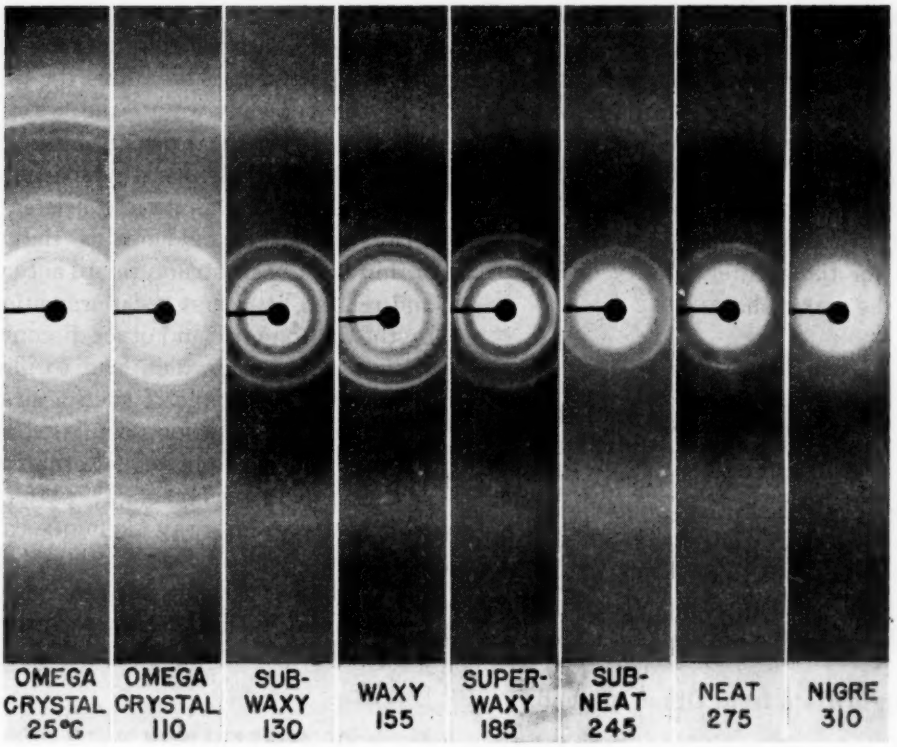

FIG. 1. X-ray patterns of the high temperature phases of anhydrous sodium palmitate.

The Neat Phases

As in the waxy phases, the subneat and neat phases appear to belong to an inclusive basic structure, to judge by the x-ray evidence. Both phases share a common curve for long spacing *versus* temperature.** Furthermore, both show only a single, diffuse, short spacing ring, the 2.9A ring of the waxy phases having disappeared in the transition to subneat.

The distinction of the neat structure from the adjacent waxy structure is discussed in the preceding section. The distinction between the neat and the nigre phases is less clear cut on the basis of x-ray pattern alone, although there seems to be a definite discontinuity in long spacing. The chief pattern difference lies in the character of the long spacing diffractions (Fig. 1); the neat phases exhibit three or four relatively sharp orders of the long spacing, whereas the nigre phase exhibits only two rather diffuse long spacing orders. This information and the microscopic observation that neat is anisotropic while nigre is isotropic, plus the great difference in fluidity (neat being relatively viscous while nigre is a mobile liquid), all contribute to the distinction of the neat phases from nigre.

Structurally the neat phases can be described as crystalline in the long spacing direction, and liquid or amorphous laterally. This description characterizes the smectic state and is in accord with the microscopic identification of anhydrous neat soap as smectic by means of the distinctive batonnets and focal conic texture. As in the waxy phases, the diffuse halo at 4.9A probably represents the average interchain distance in a loose hexagonally packed structure. However, since the neat phases exhibit only one short spacing

** In connection with the long spacings of the neat phases, several anomalous long spacings of weaker intensity and fewer orders than the main long spacing have been observed. These are plotted as filled circles in Fig. 2. No really satisfactory explanation for these spacings is known. It is thought that they might arise from planes of Miller indices other than 00*l*. Regardless of the origin of these weaker, anomalous long spacings, the experimental fact of the discontinuities in long spacing at the waxy-neat and neat-nigre transitions remains real. For the time being we have limited the interpretations in this paper to a consideration of the more intense, continuously variable, long spacing of the neat phases, as indicated by the straight line through the neat region in Fig. 2.

halo, the chains in the neat structure may be either rotating or in states of frozen rotation. This suggests a possible difference between the subneat and neat phases on the basis of frozen rotation in subneat and actual rotation in the less viscous neat.

The above structural descriptions of the waxy and the neat structures would account on a molecular basis for the greater fluidity of the neat phases over the waxy phases.

The Nigre Phase

The nigre pattern has already been described and discussed. Nigre is an isotropic liquid, and the long spacing diffractions which it exhibits probably arise from short range, one-dimensional order within particles or micelles too small to be detected with the light microscope. As in neat, the single diffuse short spacing ring probably arises from the lateral separation of the molecules.

Relation to Data from Other Methods

The x-ray data and structural interpretations just presented, while by no means invalidating the first-order transitions previously detected by dilatometer, microscope, and calorimeter, suggest that there is one basic waxy structure which embraces the three waxy phases and, similarly, that there is one basic neat structure which includes subneat and neat. This raises the question as to why the subwaxy-waxy, the waxy-superwaxy, and the subneat-neat discontinuities are not evident in the curves for x-ray spacing *versus* temperature. An explanation consistent with both x-ray and other evidence is that the phases within each basic structure are actually different and related by a first-order transition, as shown by the dilatometric and other discontinuities, but possess structures which lead to identical x-ray patterns. An example of such a situation is the frozen and free rotation postulated above for the subneat and neat phases. Alternatively, there is a real but relatively slight pattern difference which the present x-ray technique cannot detect. However, even if breaks should be revealed within the basic waxy and neat regions by more precise x-ray technique, they can be only minor compared with the break between these two regions.

III. CORRELATION WITH PREVIOUS X-RAY DATA

The data of Chesley[5] have been indicated in Table I. He reported all of the transition temperatures, except the waxy to superwaxy one, on

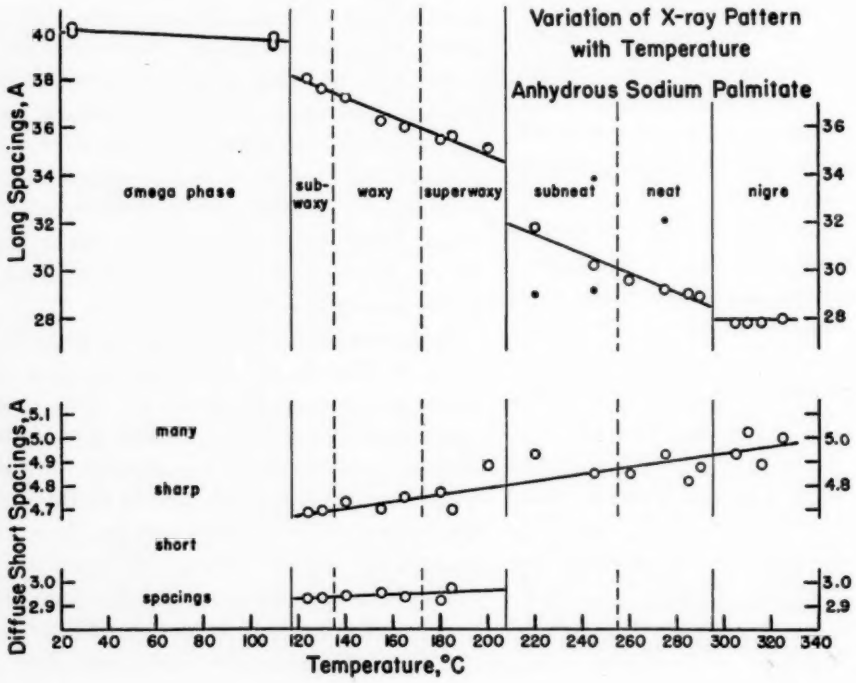

FIG. 2.

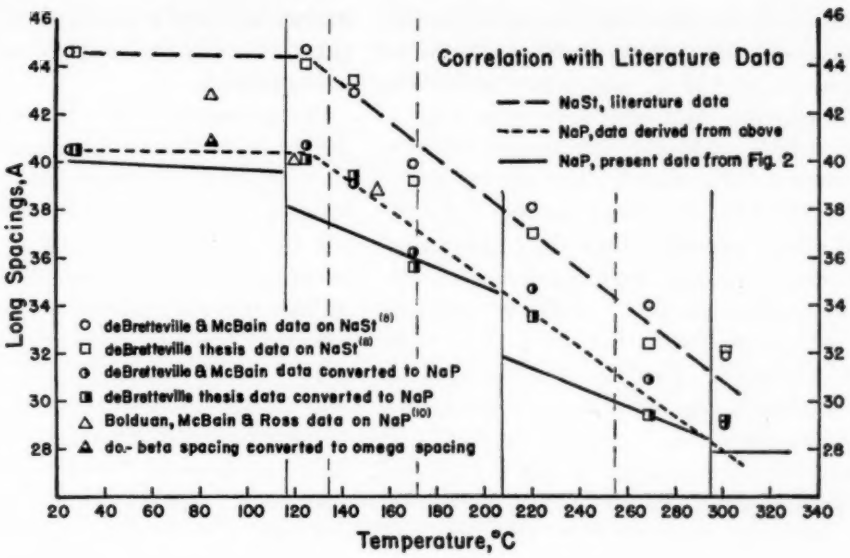
Correlation with Literature Data
NaSt, literature data
NaP, data derived from above
NaP, present data from Fig. 2
deBretteville & McBain data on NaSt(8)
deBretteville thesis data on NaSt(8)
deBretteville & McBain data converted to NaP
deBretteville thesis data converted to NaP
Bolduan, McBain & Ross data on NaP(10)
do.- beta spacing converted to omega spacing
Long Spacings, A
Temperature, °C

FIG. 3.

the basis of changes in x-ray pattern. The x-ray data of the present paper indicate that the transitions among the waxy phases and between the neat phases are accompanied by a continuous x-ray pattern variation, and therefore the x-ray method cannot be used to determine these transition temperatures. Unfortunately, there are not enough detailed x-ray data in either Chesley's publication or his thesis to make possible a comparison of his data with ours.

DeBretteville and McBain[8] presented x-ray data on the high temperature phases of anhydrous sodium stearate which can be compared with the present data on palmitate. To begin with, deBretteville and McBain did not find the differences in short spacing between the waxy phases and the neat phases which have just been presented. In fact, they concluded that the subwaxy and waxy phases were definitely crystalline and that the superwaxy phase more nearly resembled the neat phases. Neither of these conclusions is in accord with the data just presented.

A comparison of their long spacing data for anhydrous sodium stearate and the present data on palmitate is shown in Fig. 3. This figure is similar to Fig. 2 except that it shows long spacing data only. The solid lines are the data of this paper, reproduced from Fig. 2, and the dashed curve represents the data of deBretteville and McBain on sodium stearate. The half-filled squares and circles represent the sodium stearate data scaled down to sodium palmitate by assuming each long spacing quoted to equal $c \sin\beta$ and and substituting 44.6A, the experimentally determined c length of the sodium palmitate double molecule, instead of 51.4A, the c value for sodium stearate.[9] These derived data, through which the dotted curve has been drawn, should be directly comparable with the present data except for differences in transition temperatures between palmitate and stearate.

It will be seen that the long spacing data on sodium stearate cannot be grouped into separate straight lines for the three waxy phases and the two neat phases. There is need for more data on anhydrous sodium stearate because a minimum of two patterns is required for each phase to test the continuity or discontinuity of the long spacing variation. There is qualitative agreement with our data as regards the break at 117°C, which is the crystal-to-subwaxy transition, and at 170 and 270°C in the waxy and neat regions respectively. In the absence of further experimental data, the discrepancies at other temperatures may be accounted for by lack of complete conversion in their samples or by the differences between palmitate and stearate.

[8] Alexander deBretteville, Jr. and J. W. McBain, deBretteville Ph.D. Thesis, Stanford University (1941); J. Chem. Phys. **11**, 426 (1943).

[9] R. H. Ferguson and H. Nordsieck, Ind. Eng. Chem. **36**, 748 (1944).

Bolduan, McBain, and Ross[10] published x-ray fiber patterns of Na palmitate as supercurd at 85°C, subwaxy at 120°C, and waxy at 155°C. Their long spacing data also appear in Fig. 3. The point at 85°C probably corresponds to beta-phase because a correction for the known difference (42.1−40.2A)[9] in long spacing between beta- and omega-phases brings their value into fair agreement with ours. Incidentally, the existence of beta-phase at 85°C probably requires that the sample be partly hydrated. This is in keeping with the fact that the samples used by Bolduan, McBain, and Ross were fibers grown in a hydrous system.

Their subwaxy long spacing at 120°C indicates that the sample was incompletely converted and therefore contained some crystal. This interpretation is supported by the fact that Bolduan, McBain, and Ross found "definite crystallinity" at 120°C, contrary to the findings of this paper. Incomplete conversion is a real danger here because it takes about 2 hours for crystal to convert completely to subwaxy at 120°C even in a small, capillary x-ray sample. The discrepancy in long spacing at 155°C, together with the existence once more of "definite crystallinity," may again be the result of incomplete conversion.

IV. MATERIALS AND METHODS

The sodium palmitate used in this work was made by saponification of palmitic acid (Eastman Kodak Company) with reagent grade sodium hydroxide in alcohol solution followed by oven drying to constant weight at 150°C. This treatment results in omega-phase at room temperature. The palmitic acid had an acid value of 215.5 and saponification value of 216.2 from which the molecular weight is calculated to be 259.2 compared with the molecular weight of pure palmitic acid of 256.4.

X-ray patterns were recorded on flat film at 10 cm from the sample, using copper K_α radiation. By this technique the accuracy of the long spacing measurements is, on the average, ±0.5A for the various orders of a given spacing; the short spacings, even though diffuse, are accurate within ±0.1A (estimated). The sample was enclosed in a Pyrex glass capillary about 1 mm in diameter with a wall thickness of about 0.05 mm and heated in a small furnace attached to the catcher part of the x-ray collimating system. The heating furnace consists of a copper block, $1\frac{1}{4}\times\frac{1}{2}\times\frac{1}{8}''$, suitably wound with Nichrome resistance wire and insulated with mica and asbestos. The sample capillary is placed inside a longitudinal tunnel through the block, and the x-ray beam traverses the sample at right angles to the tunnel. Temperature is maintained by supplying electrical power to the resistance winding. Water cooling of the film is not necessary by this technique because the film is 10 cm from the sample. The sample temperature is measured by means of an iron-constantan thermocouple inside the block. No great precision in temperature was attempted, so that temperatures are accurate to about ±2 or 3°C. The time necessary for the sample to attain phase equilibrium differs for the various phases at the various temperatures so that, for each pattern reported here, a sufficient preheating time was used before x-raying to insure that the pattern would undergo no more change at each temperature. The preheating times were determined by recording successive x-ray patterns at $2\frac{1}{2}$ cm, after the sample attained temperature, until no further change in pattern was observed.

[10] O. E. A. Bolduan, J. W. McBain, and S. Ross, J. Phys. Chem. **47**, 528 (1943).

THE JOURNAL OF CHEMICAL PHYSICS VOLUME 16, NUMBER 3 MARCH, 1948

Statistical Mechanics of Multimolecular Adsorption. IV. The Statistical Analog of the BET Constant a_1b_2/b_1a_2. Hindered Rotation of a Symmetrical Diatomic Molecule Near a Surface

TERRELL L. HILL
Department of Chemistry, The University of Rochester, Rochester, New York
(Received October 30, 1947)

An approximate study is made of the restricted rotation of a symmetrical diatomic molecule near a surface. This makes possible some calculations concerning the BET constant $C=R\exp(\epsilon_1-\Lambda)/kT$, and especially the factor R (which is customarily set equal to unity). Cassie has pointed out that if this factor is set equal not to unity but to about 1/50 or even less, the low values of the heat of adsorption usually found on putting $R=1$ in the analysis of data are accounted for. The results obtained here indicate, unfortunately, that this factor is of the order of, say, 5–10, and that another explanation of the low heats of adsorption mentioned above will have to be found. An alternative method of estimating the area occupied per molecule in a completely filled monolayer is mentioned in an appendix.

The temperature dependence of the quantity R is of some experimental interest, and a brief discussion of this dependence as predicted by the present approximate treatment is included.

I. INTRODUCTION

WE are presenting in this series of papers[1–3] an approximate statistical theory of multimolecular adsorption. Statistical analogs of the BET constant C have appeared, expressed in terms of the energy of adsorption, the partition function and energy of molecules in the liquid state, the partition function of molecules in the gas phase, and the partition function of molecules in the first adsorbed layer.[4] There are available useful theoretical studies concerning all of these quantities except the last. Except for the very simplest cases, a really refined study of the degrees of freedom (and hence of the partition function) of molecules physically adsorbed on a surface seems out of the question at present because of mathematical difficulties. (The way to proceed in principle is quite clear.) The point of view of the present paper, therefore, is to try to get semiquantitative results which will be helpful at least in giving a general understanding of the essential features involved. As a start, we confine ourselves here, for the most part, to the adsorption of symmetrical diatomic molecules. Even for this case, as will be seen below, some fairly rough approximations are made in order to avoid excessive complications. We hope to consider more complicated molecules at a later time. One incidental question of interest in this connection is the extent to which a large molecule, for example, *n*-heptane, actually "lies flat" on a surface, and how this property varies with the temperature.

Degrees of Freedom

The three translational degrees of freedom of a monatomic molecule in the gas phase become (usually) two translational degrees (motion parallel to the surface) and one vibrational degree (motion perpendicular to the surface) on physical adsorption. In extreme cases (very low temperatures) the two translational degrees above may become[2] vibrational degrees.

The three translational, two rotational, and one internal vibrational degrees of freedom of a symmetrical diatomic molecule become, on physical adsorption, two translational, two rotational, one internal vibrational, and one vibrational degree (center of mass) perpendicular to the surface. However, the rotational motion will be seriously altered by the surface, the surface essentially introducing a potential barrier restricting the turning over of the molecule. In the extreme case of a very high barrier or low temperature the two rotational degrees will become effectively one degree of planar rotation (rotation of the mole-

[1] T. L. Hill, J. Chem. Phys. **14**, 263 (1946).
[2] T. L. Hill, J. Chem. Phys. **14**, 441 (1946).
[3] T. L. Hill, J. Chem. Phys. **15**, 767 (1947).
[4] A more refined theory must, of course, not assume that molecules in all layers save the first have liquid-like properties.

cule about an axis perpendicular to the surface, the molecular axis being parallel to the surface) and one degree of vibration (rocking of the molecular axis out of a plane parallel to the surface). The internal vibrational degree will, of course, also be perturbed by the surface, but much less strongly. This is because the forces introduced by the surface are generally rather small compared to the restoring force involved in the internal vibration.[5]

Model Adopted for Diatomic Molecules

We adopt the following admittedly approximate model in the calculations of this paper. It is felt, however, that the model resembles reality sufficiently to give results of semiquantitative significance from which some definite conclusions can be drawn. We ignore the perturbation resulting from the surface on the internal vibrational degree of freedom, since this should be a second-order effect in most cases. That is, we assume that the partition function for this degree of freedom is the same as in the gas phase, and that the two partition functions will cancel on taking ratios. The same assumption is made about the electronic partition function. We assume that the rotational and internal vibrational motions are separable, and we find the rotational properties from those of a rigid rotator with the equilibrium distance between atoms. In the absence of an alternative, we must assume that the van der Waals interaction of a diatomic molecule with an adsorbent molecule (or atom) can be obtained simply by adding the separate interaction caused by the two atoms of the diatomic molecule. In calculating the van der Waals interaction with the entire adsorbent, we integrate in the manner of London[6] instead of using the more refined procedure of summation.[7] Integration is used here because the considerable extra labor involved in summation is probably not justified at present in view of other approximations. In performing the integration the surface is assumed uniform. That is, we ignore here the (usually relatively small) periodic variation in energy of adsorption over the surface. For the two degrees of freedom parallel to the surface we assume free migration (localized adsorption is discussed in Section V). A more general partition function[2] for motion intermediate between free migration and localization could easily be substituted here (if one makes the implicit approximation that motion parallel to the surface is separable from other degrees of freedom), but free migration is the most important case.

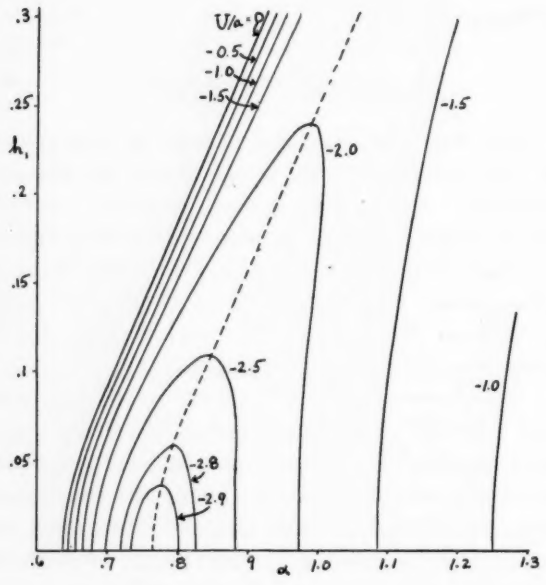

FIG. 1. Potential energy surface for U/a.

The above are approximations connected with the model. (Even with this model approximations must be made in the actual calculations. These will be mentioned as they arise.) The following are restrictions made in the generality of the calculations. We shall actually write down equations and make calculations only for symmetrical diatomic molecules. The corresponding equations for unsymmetrical diatomic molecules (and, in fact, for any linear molecule) will be obvious. We shall use for the van der Waals interaction energy only terms of the form r^{-6} and r^{-12}. Other terms could be introduced with-

[5] The frequency, ν, of internal vibration for most diatomic molecules is of the order of 4×10^{13} sec.$^{-1}$. The frequency of vibration of a molecule perpendicular to a surface (caused by surface forces) is of the order of 1×10^{12} sec.$^{-1}$. In localized adsorption, the frequencies of vibration parallel to the surface are of the order of 3×10^{11} sec.$^{-1}$. The latter frequencies are discussed in Section V.

[6] F. London, Zeits. f. physik Chemie **B11**, 222 (1930).

[7] S. Brunauer, *The Adsorption of Gases and Vapors* (Princeton University Press, Princeton, 1943). In Chapter VII there is a detailed discussion of integration *versus* summation for monatomic molecules.

out difficulty for interactions not properly represented by these expressions.

For purposes of comparison some calculations on monatomic molecules based on the above model (where it applies) are also discussed below.

II. THE POTENTIAL ENERGY FUNCTION

Let the surface be the xy plane, with z increasing in the direction away from the adsorbent. Consider an atom at a distance $z=\rho$ from the surface. Let the potential energy of interaction of this atom with a single molecule (or atom) of the adsorbent at a distance r be

$$u=u_0\left(\frac{r_0}{r}\right)^{12}-2u_0\left(\frac{r_0}{r}\right)^{6}. \tag{1}$$

We take infinite separation as the zero of energy throughout this paper. Suppose there are N_0 adsorbent molecules (or atoms) per cc. Then on straightforward integration over all values of x and y, and those values of z such that $z\leqslant 0$, one finds for the total interaction of the atom with the adsorbent

$$u_s=\frac{u_0r_0^{12}\pi N_0}{45\rho^9}-\frac{u_0r_0^{6}\pi N_0}{3\rho^3}. \tag{2}$$

The attractive term was given by London.[6] Now if we have a rigid symmetrical diatomic molecule of interatomic distance $2d$ whose center is a distance z ($z>d$) from the surface, the axis of the molecule making an angle θ ($0\leqslant\theta\leqslant\pi$) with the z axis, then the interaction of the molecule with the adsorbent is

$$U=a\left\{-\frac{1}{(\alpha+h_1)^3}-\frac{1}{(\alpha-h_1)^3}+\frac{1}{15}\left[\frac{1}{(\alpha+h_1)^9}+\frac{1}{(\alpha-h_1)^9}\right]\right\}, \tag{3}$$

where $a=u_0r_0^3\pi N_0/3$, $\alpha=z/r_0$, $h_1=h_0\cos\theta$, and $h_0=d/r_0$. Equation (3) follows from Eq. (2) on adding the separate energies of interaction of the two atoms in the diatomic molecule. It should be emphasized that u_0 and r_0 characterize the interaction of only *one* atom of the diatomic molecule with a molecule of the adsorbent.

The function U/a has been calculated and is shown in a contour diagram (potential energy surface) in Fig. 1. The maximum value of h_1 in any particular case is, of course, h_0 (at $\theta=0$). The figure is symmetrical about the line $h_1=0$ because of the symmetry of the molecule, so we have omitted negative values of h_1. The minimum value of U/a is -2.982 and occurs at $\alpha=\alpha_0=(1/5)^{1/6}=0.7647$ and $h_1=0$. The potential energy curve along the line $h_1=0$ ($\theta=\pi/2$) is shown in Fig. 2. The energy of adsorption (neglecting zero-point energy which is of the order of 100 cal./mole) is, according to this model, $\epsilon_1=2.982a$. For a typical numerical case (Section V) this turns out to be 2880 cal./mole, which is of the correct order of magnitude.

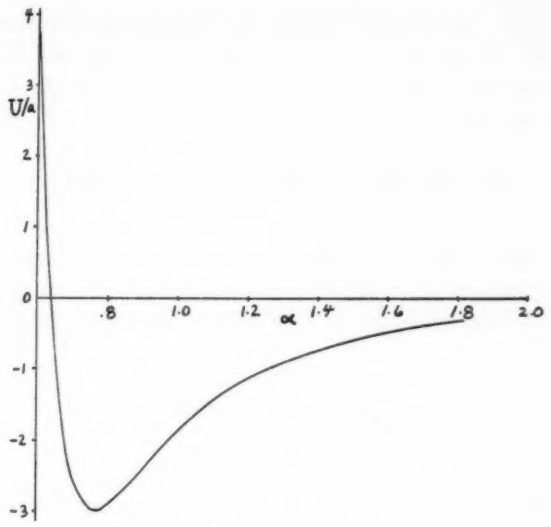

FIG. 2. U/a for $h_1=0$.

Using classical language, the physical situation associated with the potential energy surface, Fig. 1, is the following: the lowest energy occurs when the axis of the molecule is parallel ($\theta=\pi/2$) to the surface (the potential energy U is independent of the azimuthal angle φ in this model) and the molecule is at a distance $z=z_0=r_0\alpha_0=0.7647r_0$ from the surface. In order for the molecule to turn over, h_1 must increase from $h_1=0$ to $h_1=h_0$ (i.e., θ must decrease from $\theta=\pi/2$ to $\theta=0$). If the molecule turns over staying at the distance $\alpha=\alpha_0$ from the surface, the potential barrier involved is very large (56 kcal./mole in the numerical example of Section V). However, if the molecule moves away from the surface as it turns over, following the valley indicated by the dotted line in Fig. 1, the barrier

is the minimum barrier U_0 hindering rotation and is much smaller (1060 cal./mole in the example of Section V). This minimum barrier U_0 is plotted in Fig. 3 as a function of h_0.

III. THE PARTITION FUNCTION FOR AN ADSORBED MOLECULE

We desire the partition function for a rigid rotator near a surface, with a potential energy function given by $U(z, \theta)$ in Eq. (3). The Hamiltonian is

$$H=\frac{p_x^2}{2M}+\frac{p_y^2}{2M}+\frac{p_z^2}{2M}+\frac{p_\theta^2}{2I}+\frac{p_\varphi^2}{2I\sin^2\theta}+U(z,\theta), \quad (4)$$

where M is the mass of the molecule and I the moment of inertia ($I=Md^2$ here). The correct procedure is to find the energy levels for such a molecule confined to an area $\mathfrak{a}$ of the surface by solving Schrödinger's equation for the above Hamiltonian, and then form the partition function from these energy levels. This procedure appears to be impossible even for the present approximate model (the quantum-mechanical problem is discussed briefly in Appendix I). We must therefore turn to an approximate method. The approximation used here is the one suggested by Pitzer and Gwinn[8] for another type of problem. It is difficult to say what error is involved in using their approximation here. The error is no doubt greater than in the more restricted problem for which the approximation was originally designed, but certainly much smaller than the errors introduced by the model itself (compare the quantum-mechanical—using this approximation—and classical calculations of the partition function in the numerical example of Section V). The approximation is to write the partition function f as

$$f=f_{\text{classical}}\times\frac{f_{\text{harmonic osc—quantal}}}{f_{\text{harmonic osc—classical}}}, \quad (5)$$

where f_{class} is the classical partition function

$$f_{\text{class}}=\frac{1}{h^5}\int\cdots\int\exp(-H/kT)dxdydzd\theta d\varphi \times dp_x dp_y dp_z dp_\theta dp_\varphi, \quad (6)$$

and the other factors are partition functions calculated from the shape of the potential energy surface in the neighborhood of the minimum at $h_1=0$ and $\alpha=\alpha_0$.

Let us write down the harmonic oscillator expressions first. It may be helpful to refer to Appendix I in this connection. We expand U/a in a Taylor's series about $\alpha=\alpha_0$, $h_1=0$, and find

$$U/a=-2.982+68.82[(\alpha-\alpha_0)^2+h_1^2]+\cdots \quad (7)$$

with no cross product term of the form $h_1(\alpha-\alpha_0)$ (this is obvious from Fig. 1). Using Eq. (7) for U/a in Eq. (6), one obtains

$$f_{\text{har osc-class}}=\frac{2\pi MkT}{h^2}\mathfrak{a}\frac{2\pi(2\pi IkT)^{\frac{1}{2}}}{h}\frac{kT}{h\nu_z}\frac{kT}{h\nu_\theta}\times\exp(2.982\beta), \quad (8)$$

where

$$\beta=a/kT,$$

$$\frac{h\nu_z}{kT}=\frac{8.296\beta^{\frac{1}{2}}h}{(2\pi MkT)^{\frac{1}{2}}r_0\pi^{\frac{1}{2}}}, \quad (9)$$

$$\frac{h\nu_\theta}{kT}=\frac{8.296\beta^{\frac{1}{2}}hd}{(2\pi IkT)^{\frac{1}{2}}r_0\pi^{\frac{1}{2}}}. \quad (10)$$

Actually, since $I=Md^2$ here, $\nu_z=\nu_\theta$. From Eq. (8) one can write immediately

$$f_{\text{har osc—quant}}=\frac{2\pi MkT}{h^2}\mathfrak{a}\frac{2\pi(2\pi IkT)^{\frac{1}{2}}}{h}\times[1-\exp(-h\nu_z/kT)]^{-1}\times[1-\exp(-h\nu_\theta/kT)]^{-1}\times\exp(2.982\beta). \quad (11)$$

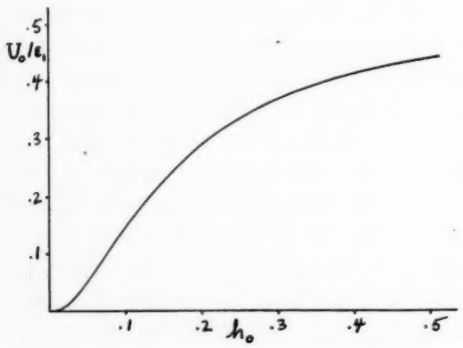

FIG. 3. Potential barrier hindering rotation as a fraction of the heat of adsorption.

[8] K. S. Pitzer and W. D. Gwinn, J. Chem. Phys. **10**, 428 (1942). It might be possible to use in problems of the sort being considered in this paper a new approximate method suggested by J. O. Halford, J. Chem. Phys. **15**, 645 (1947), based on the Wilson-Sommerfeld quantization rule.

TABLE I. Values of the function $q(\beta, h_1)$.

h_1 ↓ \ β →	0.1	1	2	4	8
0.000	1.259	8.51	74.8	17420.	17.78×10^8
0.025				14860.	12.82×10^8
0.050	1.240	7.86	58.8	9910.	5.53×10^8
0.100	1.202	6.81	38.0	3530.	0.67×10^8
0.200	1.144	5.55	20.4	712.	0.02×10^8
0.300	1.103	5.00	15.31	309.	
0.400	1.076	4.68	12.81	188.	
0.500	1.057	4.51	11.61	142.	

TABLE II. Values of the function $Q(\beta, h_0)$.

h_0 ↓ \ β →	0.1	1	2	4	8
0.1	0.1236	0.779	5.80	1036.	0.736×10^8
0.2	0.241	1.386	8.52	1193.	0.757×10^8
0.3	0.353	1.911	10.26	1240.	0.758×10^8
0.4	0.462	2.39	11.65	1264.	0.758×10^8
0.5	0.568	2.85	12.86	1280.	0.758×10^8

We now find f_{class}. Integration over x and y gives a factor $\mathfrak{A}$, over φ a factor 2π, over p_x and p_y a factor $2\pi MkT$, over p_θ a factor $(2\pi IkT)^{\frac{1}{2}}$, and over p_φ a factor $(2\pi IkT)^{\frac{1}{2}}\sin\theta$. So we have

$$f_{\text{class}}=\frac{2\pi MkT\mathfrak{A}4\pi^2IkT}{h^5}\iiint[\exp(-U/kT)\times\exp(-p_z^2/2MkT)\sin\theta d\theta dz dp_z]. \quad (12)$$

The question now arises as to what limits should be used for θ, z, and p_z. We are interested here in an "adsorbed" molecule. By an "adsorbed" molecule we mean one whose z motion is bound. That is, for any θ, the z motion is such that

$$U(z,\theta)+\frac{p_z^2}{2M}\leqslant 0, \quad (13)$$

or

$$p_z^2\leqslant -2MU(z,\theta). \quad (14)$$

The limits on p_z are, therefore, $\pm[-2MU(z,\theta)]^{\frac{1}{2}}$. The momenta p_x, p_y, p_θ, and p_φ have no such restriction. Further, since $p_z^2/2M\geqslant 0$ in any case, we integrate only over those values of θ and z such that $U(z,\theta)\leqslant 0$. There is, finally, the restriction that $0\leqslant\theta\leqslant\pi$. Referring to Fig. 1, we integrate between the $U=0$ contour and $z=\infty$ along the strip between $h_1=-h_0$ and $h_1=h_0$. The integral over p_z is

$$\int_{-(-2MU)^{\frac{1}{2}}}^{(-2MU)^{\frac{1}{2}}}\exp(-p_z^2/2MkT)dp_z=(2\pi MkT)^{\frac{1}{2}}\operatorname{erf}(-U/kT)^{\frac{1}{2}} \quad (15)$$

where erf$x$ is the error function

$$\operatorname{erf}x=\frac{2}{(\pi)^{\frac{1}{2}}}\int_0^x e^{-t^2}dt. \quad (16)$$

Equation (12) becomes

$$f_{\text{class}}=\left(\frac{2\pi MkT}{h^2}\right)^{\frac{1}{2}}\mathfrak{A}\frac{8\pi^2IkT}{h^2}\frac{r_0}{h_0}\iint_{\substack{0\leqslant h_1\leqslant h_0\\ U\leqslant 0}}\times\exp(-U/kT)\operatorname{erf}(-U/kT)^{\frac{1}{2}}d\alpha dh_1. \quad (17)$$

In this equation we shall refer to the integral over α for fixed h_1 as $q(\beta, h_1)$. Values of $q(\beta, h_1)$ were obtained by using numerical integration out to a sufficiently large value of α and then analytical integration to $\alpha=\infty$. The values of the double integral, which we shall call $Q(\beta, h_0)$, were found by interpolating and integrating (numerically) q from $h_1=0$ to $h_1=h_0$. The calculated values of q and Q are given in Tables I and II, respectively.

The asymptotic expressions for $q(\beta, 0)$ and $Q(\beta, h_0)$, for large β, are useful:

$$\lim_{\beta\to\infty}q(\beta,0)=\frac{\exp(2.982\beta)}{4.679\beta^{\frac{1}{2}}}, \quad (18)$$

$$\lim_{\beta\to\infty}Q(\beta,h_0)=\frac{\exp(2.982\beta)}{43.81\beta}. \quad (19)$$

These are found from Eqs. (7) and (8).

If these results are now substituted into Eq. (5), we have (we now include, for completeness: ρ, the nuclear spin weight; $\sigma=2$, the symmetry number; j_{el}, the electronic partition function; and j_{vib}, the partition function for internal vibration)

$$f=\frac{\rho^2}{2}j_{\text{el}}j_{\text{vib}}\frac{2\pi MkT}{h^2}\mathfrak{A}\left[\frac{43.81\beta Q(\beta,h_0)}{\exp(2.982\beta)}\right]\times\frac{2\pi(2\pi IkT)^{\frac{1}{2}}}{h}[1-\exp(-h\nu_z(kT)]^{-1}\times[1-\exp(-h\nu_\theta/kT)]^{-1}\exp(2.982\beta). \quad (20)$$

IV. THE BET CONSTANT C

The fundamental parameter in the BET adsorption isotherm[9] is

$$C=\frac{a_1b_2}{b_1a_2}\exp[(\epsilon_1-\epsilon_L)/kT], \tag{21}$$

where $-\epsilon_1$ is the energy of an isolated molecule in the first adsorbed layer, $-\epsilon_L$ is the energy of a molecule in the liquid state, and a_1b_2/b_1a_2 is a kinetic factor. In actual applications of Eq. (21) to experimental data it appears to be the custom to put Λ, the heat of vaporization of the liquid, in place of ϵ_L, without altering a_1b_2/b_1a_2. From the statistical derivations[10,1-3] of the BET equation it is clear that these two quantities should not be confused. The (theoretical) connection between them depends on which theory of liquids is referred to. $\Lambda=\epsilon_L-kT/2$ is probably approximately correct,[11] so $a_1b_2/b_1a_2\cong Re^{\frac{1}{2}}$ (see Eq. (22)). It is actually R and not a_1b_2/b_1a_2 which has been set equal to unity in applications, but the difference is perhaps not very important.

We can avoid the above uncertainty resulting from the lack of an adequate theory of liquids and also have C in the form actually used in analysis of experimental data by writing

$$C=R\exp[(\epsilon_1-\Lambda)/kT]. \tag{22}$$

The purpose of this section is to obtain expressions for R.

We consider for convenience adsorption at very low pressures, so that the adsorbed molecules form a two-dimensional perfect gas with no interactions between themselves. If N molecules are adsorbed on an area, $\mathcal{A}$, the partition function for the system is $f^N/N!$, where f is given by Eq. (20). The chemical potential of the adsorbed molecules is then

$$\frac{\mu_A}{kT}=-\frac{\partial\ln(f^N/N!)}{\partial N}=-\ln f+\ln N. \tag{23}$$

For molecules in the vapor phase at a pressure p

$$\frac{\mu_G}{kT}=\ln p+\ln\left[\left(\frac{h^2}{2\pi MkT}\right)^{\frac{3}{2}}\frac{1}{kTj_i}\right], \tag{24}$$

where

$$j_i=\frac{\rho^2}{2}j_{el}j_{vib}\frac{8\pi^2IkT}{h^2}. \tag{25}$$

At equilibrium,

$$\frac{\mu_A}{kT}=\frac{\mu_G}{kT},$$

so that

$$N=pf\left(\frac{h^2}{2\pi MkT}\right)^{\frac{3}{2}}\frac{1}{kTj_i}. \tag{26}$$

Let N^0 be the maximum number of molecules that can be adsorbed in the first layer, let p_0 be the vapor pressure at the temperature T of the gas being adsorbed, let $x=p/p_0$ and $\theta=N/N^0$. Then our low pressure isotherm can be written

$$\theta=Cx, \tag{27}$$

with

$$C=\frac{f}{N^0j_i}\frac{p_0}{kT}\left(\frac{h^2}{2\pi MkT}\right)^{\frac{3}{2}}. \tag{28}$$

This expression for C is rather general (for adsorption at higher pressures C is the same but the isotherm is more complicated[2]). It holds[2] for both localized and mobile adsorption and for any type of molecule. The appropriate f must, of course, be substituted. Equation (26) is even more general, since it has meaning for temperatures above the critical temperature of the gas being adsorbed.

For the particular case we are interested in here, we substitute Eqs. (20) and (25) into Eq. (28), and put $p_0=\delta\exp(-\Lambda/kT)$ and $2.982\beta=\epsilon_1/kT$. This gives C in the form of Eq. (22) with

$$R=\pi^{\frac{1}{2}}\left(\frac{h^2}{2\pi MkT}\right)^{\frac{1}{2}}\left(\frac{h^2}{8\pi^2IkT}\right)^{\frac{1}{2}}\frac{\mathcal{A}}{N^0}\frac{\delta}{kT}$$
$$\times\left[\frac{43.81\beta Q(\beta,h_0)}{\exp(2.982\beta)}\right][1-\exp(-h\nu_z/kT)]^{-1}$$
$$\times[1-\exp(-h\nu_0/kT)]^{-1}. \tag{29}$$

The substitution for p_0 is justified both experimentally and theoretically.[11] For non-polar molecules $\delta\cong2.7_4\times10^{10}$ ergs/cc.

We now consider certain special cases of Eq. (29). In a completely classical calculation we would use Eq. (17) instead of Eq. (5). This gives

$$R=\frac{\mathcal{A}}{N^0}\frac{\delta}{kT}\frac{Q(\beta,h_0)}{\exp(2.982\beta)}\frac{r_0}{h_0}. \tag{30}$$

[9] S. Brunauer, P. H. Emmett, and E. Teller, J. Am. Chem. Soc. 60, 309 (1938).
[10] A. B. D. Cassie, Trans. Faraday Soc. 41, 450 (1945).
[11] R. H. Fowler and E. A. Guggenheim, *Statistical Thermodynamics* (University Press, Cambridge, England, 1939), Chapter VIII.

If we assume that the rotation of the molecules is unaffected by the surface (i.e., that U is effectively independent of θ), the rotational partition functions for the gaseous and adsorbed phases will cancel. If we then use for the potential energy for all values of θ the function $U(z, \pi/2)$, and employ (for purposes of comparison) the approximation of Pitzer and Gwinn[8] for the z motion, the same argument as above for the more general problem leads here to (omitting j_{rot})

$$f_{\text{har osc–class}}=\frac{2\pi MkT}{h^2}\mathcal{A}\frac{kT}{h\nu_z}\exp(2.982\beta), \tag{31}$$

$$f_{\text{har osc–quant}}=\frac{2\pi MkT}{h^2}\mathcal{A}[1-\exp(-h\nu_z/kT)]^{-1}\times\exp(2.982\beta), \tag{32}$$

$$f_{\text{class}}=\left(\frac{2\pi MkT}{h^2}\right)^{\frac{1}{2}}\mathcal{A}r_0q(\beta, 0), \tag{33}$$

and

$$R=\left(\frac{h^2}{2\pi MkT}\right)^{\frac{1}{2}}\frac{\mathcal{A}}{N^0}\frac{\delta}{kT}\left[\frac{4.679\beta^{\frac{1}{2}}q(\beta, 0)}{\exp(2.982\beta)}\right]\times[1-\exp(-h\nu_z/kT)]^{-1}. \tag{34}$$

Equation (34) is also the expression for R for a monatomic molecule based on the methods of the present paper, but with one important alteration: when Eq. (34) is used for a monatomic molecule, $\beta=a/kT$ as before, but $a=u_0r_0^3\pi N_0/6$, where u_0 and r_0 refer to the interaction of the monatomic molecule with a molecule (or atom) of the adsorbent. This expression for a differs by a factor of two from the earlier one (Eq. (3)). In fact, Eq. (34) may be used for any mobile adsorbed molecule, however large, if one can neglect the effect of the surface on internal degrees of freedom (rotation, vibration, electronic) and uses

$$a=u_0r_0^3\pi N_0/6,$$

u_0 and r_0 referring to the interaction of an adsorbed *molecule* with a molecule (or atom) of the adsorbent.

For localized adsorption we must replace[2] the xy partition function

$$\frac{2\pi MkT}{h^2}\mathcal{A} \quad \text{by} \quad N^0[1-\exp(-h\nu/kT)]^{-2},$$

where $\nu=\nu_x=\nu_y$ is the frequency of vibration parallel to the surface:

$$\nu=(V_0/4Ms^2)^{\frac{1}{2}}. \tag{35}$$

In Eq. (35), V_0 is the maximum[2] potential barrier (of the order of, say, 0.3–1.0 kcal./mole), and s is the distance between potential minima along both x and y axes (the surface lattice being assumed simple cubic). Let R_l be the value of R for localized adsorption. Then, for any of the cases above, we can get R_l from R by using

$$R_l=\frac{h^2}{2\pi MkT}\frac{1}{s^2}[1-\exp(-h\nu/kT)]^{-2}R. \tag{36}$$

We have substituted $s^2=\mathcal{A}/N^0$ in writing Eq. (36).

The approximate temperature dependence of R is of some interest. It is easily seen from the above equations that for mobile adsorption R is roughly temperature independent for a symmetrical diatomic molecule (Eq. (29)), and R varies approximately at $T^{-\frac{1}{2}}$ for a monatomic molecule or for any molecule whose internal degrees of freedom are essentially unperturbed by the surface (Eq. (34)). For localized adsorption, the temperature dependence in the two cases above is approximately as T and $T^{\frac{1}{2}}$, respectively, (Eq. (36)).

V. A NUMERICAL EXAMPLE

It is desirable to get an idea of the orders of magnitude involved in the above equations. To do this, we give numerical results for a (hypothetical) case which is very average. Let us take $N_0=1\times10^{23}$ cc^{-1}, $u_0=15\times10^{-15}$ erg, $r_0=3.5$A, $T=244$°K, $M=50$ molecular weight units, $d=1.05$A, $\mathcal{A}/N^0=20$A^2 and $\delta=2.74\times10^{10}$ ergs/cc. Some derived quantities of interest for this example are then $\epsilon_1=2880$ cal./mole, $\beta=2$, $h_0=0.30$, $U_0=1060$ cal./mole (as compared to $kT=485$ cal./mole, so that rotation is restricted considerably), $Q=10.26$, $43.81\beta Q/\exp(2.982\beta)=2.31$, and $\nu_z=\nu_\theta=1.52\times10^{12}$ sec.$^{-1}$. The "correct" value of R obtained from Eq. (29) is 6.71. A completely classical calculation of R (Eq. (30)) gives $R=5.01$. This differs so little from the quantum-mechanical value that one can probably conclude that the use of the approximation of Pitzer and Gwinn is not very serious. If we

assume that the rotational partition function is unaffected by the surface, and use Eq. (34), we find $R=12.7$. The suppression of rotation in this example therefore decreases R by a factor of about two. If the adsorption is localized, taking $V_0=1000$ cal./mole (which is a rather large value), we find from Eq. (35) $\nu=\nu_x=\nu_y=3.24\times10^{11}$ sec.$^{-1}$ and $R_l=0.326R=0.326\times6.71=2.19$ from Eq. (36).

Cassie[10] has published some rather frequently quoted calculations in which he finds R, or rather R_l since he assumes localized adsorption, to be of the order of 1/50 or less. This is just the right order of magnitude to account for the extent to which the derived values of the heat of adsorption are found to be too low (on applying the BET equation assuming $R=1$). However, on the basis of the calculations outlined above,[12] the present writer is forced reluctantly to form the opinion that Cassie's explanation is not correct and that some other one will have to be found. The reasons Cassie found $R=1/50$ (or less) instead of $R=5-10$ are the following: (1) he assumed localized adsorption (which would actually cut the value of $R=5-10$ down only to about[13] $R_l=2$, even taking a rather large value for V_0), and (2) the remaining factor of 100 (or more) between 1/50 (or less) and two arises because Cassie used $\nu_x=\nu_y=\nu_z=4\times10^{12}$ sec.$^{-1}$, which would appear to be too high by a factor of about 10 for both ν_x and ν_y and perhaps another factor of two to four for ν_z. Several other frequencies may be mentioned for comparison: the value of $\nu_x=\nu_y$ for the adsorption of argon on potassium chloride is[2] 3.3×10^{11} sec.$^{-1}$, using $V_0=400$ cal./mole. Orr[14] found $\nu_z=1\times10^{12}$ sec.$^{-1}$ in his very refined calculations on the adsorption of argon by potassium chloride. In any case, as emphasized in the second paper of this series,[2] it is, in general, incorrect to consider physical adsorption as localized.

There will, of course, be a range in possible values of R calculated from the above equations. Most cases of interest will probably fall within a factor of five (larger or smaller) of the values given above for an average example. One can estimate this range by noting that the *approximate* dependence of R (mobile adsorption) on the fundamental parameters is given by (Eq. (29))

$$R\cong\text{const.}\times\left(\frac{\mathfrak{a}}{N^0}\right)\frac{1}{du_0r_0N_0}$$

for a symmetrical diatomic molecule, or by (Eq. (34))

$$R\cong\text{const.}\times\left(\frac{\mathfrak{a}}{N^0}\right)\frac{1}{T^{\frac{1}{2}}u_0^{\frac{1}{2}}r_0^{\frac{1}{2}}N_0^{\frac{1}{2}}}$$

for a monatomic molecule (or any molecule with rotation not much affected by the surface). We may note that the mass does not occur in either of these equations (the temperature has already been discussed).

One final remark on generality: it is fairly obvious that the general conclusions reached in this paper for symmetrical diatomic molecules will also hold for slightly unsymmetrical diatomic molecules. Also, the most favorable case for neglecting the effect of the surface on rotation of a complicated molecule is for a symmetrical molecule such as CH_4 or CCl_4. The behavior of a very unsymmetrical diatomic molecule (for example HCl) can be quite different in some respects. This case will be investigated.

APPENDIX I

On writing down the Schrödinger equation associated with Eq. (4), one can put $\psi=F(x, y)\Phi(\varphi)\chi(z, \theta)$, and then obtain the energy levels for a particle of mass M in a two-dimensional box from the F equation and, as usual, find

$$\Phi_m(\varphi)=\frac{1}{(2\pi)^{\frac{1}{2}}}\exp(im\varphi),\quad m=0, \pm1, \pm2, \cdots \quad (37)$$

from the Φ equation. The χ equation is

$$\frac{I}{M}\frac{\partial^2\chi}{\partial z^2}+\frac{1}{\sin\theta}\frac{\partial}{\partial\theta}\left(\sin\theta\frac{\partial\chi}{\partial\theta}\right)-\frac{m^2}{\sin^2\theta}\chi+\frac{8\pi^2I}{h^2}[E-U(z, \theta)]\chi=0, \quad (38)$$

where $E_{\text{total}}=E+E_{xy}$. There appears to be little hope of finding the energy eigenvalues of Eq. (38) for the $U(z, \theta)$ given by Eq. (3). However, in the limiting case of harmonic oscillations about the potential minimum, the solution is, of course, easy. We substitute in this case Eq. (7) into

[12] Even considering the roughness of the model the values of R given here ought to be accurate at least to within a factor of two. The heat of adsorption ϵ_1 from this model is probably accurate[7] to about a factor of two, and R should be much less sensitive than ϵ_1.

[13] It is interesting that R_l and hence a_1b_2/b_1a_2 is not far from unity here. This is just the assumption made in the original BET theory (*localized* adsorption).

[14] W. J. C. Orr, Trans. Faraday Soc. **35**, 1247 (1939).

Eq. (38), put $\chi=\Theta(\theta)Z(z)$, and find

$$Z''+\frac{8\pi^2M}{h^2}\left(E_z-\frac{68.82az^2}{r_0^2}\right)Z=0, \tag{39}$$

and

$$\Theta''+\frac{\cos\theta}{\sin\theta}\Theta'-\frac{m^2\Theta}{\sin^2\theta}+\frac{8\pi^2I}{h^2}\left(E_{\theta\varphi}-\frac{68.82ad^2\cos^2\theta}{r_0^2}\right)\Theta=0, \tag{40}$$

where $E+2.982a=E_z+E_{\theta\varphi}$. The energy levels E_z are

$$E_z=(n_z+\tfrac{1}{2})h\nu_z, \quad n_z=0, 1, 2, \cdots, \tag{41}$$

where ν_z is given by Eq. (9). For the limiting case of interest here put, in Eq. (40), $\theta-(\pi/2)=\xi$, $\Theta(\theta)=G(\xi)$, $\sin\theta=1$, and $\cos\theta=-\xi$. Then, dropping the term in Θ' (ξ small, a large), we have

$$G''+\frac{8\pi^2I}{h^2}\left(E_{\theta\varphi}-\frac{h^2m^2}{8\pi^2I}-\frac{68.82ad^2\xi^2}{r_0^2}\right)G=0. \tag{42}$$

The energy levels are $E_{\theta\varphi}=E_\theta+E_\varphi$ with

$$E_\theta=(n_\theta+\tfrac{1}{2})h\nu_\theta, \quad n_\theta=0, 1, 2, \cdots, \tag{43}$$

$$E_\varphi=\frac{m^2h^2}{8\pi^2I}, \quad m=0, \pm1, \pm2, \cdots, \tag{44}$$

in which ν_θ is given by Eq. (10). The lowest eigenvalue for the general Eq. (38) is given approximately by the lowest eigenvalue in the harmonic oscillator limiting case: $E\cong-2.982a+h\nu_z/2+h\nu_\theta/2\cong E_{\text{total}}$. This is the negative of the heat of adsorption (including properly the zero-point energy).

APPENDIX II

In calculating surface areas using the BET method, it is necessary to adopt a value for the area occupied per molecule when the surface is completely filled with one layer. This value is usually obtained from the density of the liquid. There is an alternative procedure that may be of interest. The values obtained do not differ much from the liquid density values.

TABLE III. Surface area per molecule in A^2.

	Liquid density value	b'
N_2	16.2	15.4
O_2	14.1	13.5
A	14.4	13.6
CO	16.8	15.6
CO_2	17.0	16.5
CH_4	18.1	16.4
n-C_4H_{10}	32.1	33.0
NH_3	12.9	15.0
NO	12.5	12.5
N_2O	16.8	16.9
n-C_7H_{16}	45.0	47.0
H_2O	10.5	13.1

If we use van der Waals' equation as the equation of state of the monolayer and also of the gas phase, it has been shown[2] that the surface area per molecule when the first layer is full is b', the two-dimensional van der Waals constant, and that b' is related to the three-dimensional van der Waals constant b by

$$b'=\frac{\pi}{2}\left(\frac{3b}{2\pi}\right)^{\frac{1}{3}}. \tag{45}$$

Now $b=kT_c/8P_c$, where T_c and P_c are the three-dimensional critical temperature and pressure, so one can write finally

$$b'=6.354\left(\frac{T_c}{P_c}\right)^{\frac{1}{3}} \text{ (in units of } A^2), \tag{46}$$

where P_c is in atmospheres. In Table III the values of b' for a number of gases, calculated from the critical temperatures and pressures, are compared with the commonly used liquid density values.

Low Temperature Transport Properties of Gases. II. Neon, Argon, Krypton, and Xenon

I. AMDUR
Department of Chemistry, Massachusetts Institute of Technology, Cambridge, Massachusetts

(Received November 5, 1947)

Values are computed for the viscosity, thermal conductivity, and coefficient of self-diffusion, as functions of temperature, for the following gases: neon (60°–200°K), argon (110°–290°K), krypton (150°–370°K), and xenon (210°–550°K). The method of calculation is the same as that previously developed for gaseous helium and involves the use of classical scattering theory within angular regions where diffraction effects are absent, to obtain appropriate classical transport cross sections for insertion into the exact formulas of Chapman and Enskog.

The average absolute deviations between calculated and experimental values are 5.5 percent for viscosity and 5.9 percent for thermal conductivity. In the case of self-diffusion, only two experimental values are available for comparison with calculated values, one each for krypton and xenon. The absolute deviations are 9.7 and 10.3 percent, respectively.

A procedure is suggested for obtaining approximate values of the mutual diffusion coefficient of a binary gas mixture from the self-diffusion coefficients of the constituents.

IN a recent publication[1] (hereafter referred to as the helium paper), the transport properties of gaseous helium were computed by a combination of classical scattering theory and the theory of transport properties as developed by Chapman[2] and Enskog.[3] The results agreed well with experiment in the temperature range for which the calculations were valid, 14°–200°K. Since the method should be of general applicability, it seemed advisable to extend the calculations to other rare gases to test further the generality of the method and to obtain calculated values of the transport properties in temperature regions where experimental values are unavailable. In the present paper, appropriate formulas will be given without derivation since the procedure and derivations were presented in detail in the helium paper.

TABLE I. Constants of potential energy functions.

	Neon	Argon	Krypton	Xenon
p	1.48	2.17	2.57	3.05
q	1.13	2.45	3.46	4.81
c (10^{-10} erg A^6)	0.140	0.874	1.48	3.54
A (10^{-10} erg)	0.966	8.30×10^3	2.18×10^4	1.84×10^5
a (A^{-1})	2.90	4.782	4.782	4.782
C (10^{-10} erg A^6)	0.121	0.755	1.26	3.01
D (10^{-10} erg A^8)	0.179	1.64	3.24	9.18
E (10^{-10} erg A^{10})	0.137	1.85	4.36	14.5

[1] I. Amdur, J. Chem. Phys. **15**, 482 (1947).
[2] S. Chapman, Phil. Trans. Roy. Soc. **A211**, 433 (1912); **A216**, 279 (1915); **A217**, 115 (1917).
[3] D. Enskog, "Kinetische Theorie der Vorgänge in massig verdünnten Gasen," Inaug. Diss., Upsala, 1917.

As indicated in the helium paper, the success of the calculations depends upon accurate knowledge of the interaction potential between two rare gas atoms. The potential functions used in the present case were obtained by combining expressions involving a single exponential repulsive term and a dipole-dipole interaction attractive term deduced by Kane[4] from properties of frozen inert gases, with ratios of the constants in the dipole-dipole, dipole-quadrupole, and quadrupole-quadrupole terms derived from calculations of Margenau.[5]

Kane used a potential energy function of the form

$$V(r)=Ae^{-ar}-(c/r^6), \tag{1}$$

where r is the separation distance between two atoms, and adjusted the constants to reproduce the total energy at the absolute zero at the observed lattice distance r_l, which, in every case, was very close to the potential minimum. It will be assumed that a more accurate function can be obtained by allowing for dipole-quadrupole and quadrupole-quadrupole interactions as follows:

At r_l the attractive energy may be written

$$-\frac{c}{r_l^6}=-\frac{C}{r_l^6}-\frac{D}{r_l^8}-\frac{E}{r_l^{10}}=-\frac{C}{r_l^6}\left(1+\frac{p}{r_l^2}+\frac{q}{r_l^4}\right), \tag{2}$$

[4] G. Kane, J. Chem. Phys. **7**, 603 (1939).
[5] H. Margenau, J. Chem. Phys. **6**, 896 (1938).

where p and q are the ratios computed from Margenau's results. Since Margenau's calculations are valid for distances near the minimum, the above method should correct satisfactorily for dipole-quadrupole and quadrupole-quadrupole interactions near the minimum, the region of interest in the present case, particularly since the inclusion of the higher order terms produced a *maximum* increase in the attractive energy of only 4.3 percent. Since Margenau[6] has shown that the effect of second-order exchange forces is negligible for all the inert gases except helium, the form of the complete potential function for neon, argon, krypton, and xenon will be taken as

$$V(r)=Ae^{-ar}-\frac{C}{r^6}-\frac{D}{r^8}-\frac{E}{r^{10}}. \tag{3}$$

Although most of the interaction potentials suggested in the literature were investigated, certain functions suggested by Kane and corrected as indicated gave the best results. Table I gives the Margenau ratios, the original constants of Kane, and the constants in the final potential function, Eq. (3).

Values of the classical total collision cross section, S, as a function of the relative velocity, v, are required for evaluation of the classical cross sections for viscosity and thermal conductivity, $Q_{\eta,K}$, and for self-diffusion, $Q_{D(1,1)}$, as functions of temperature. Now

$$S=\pi[b(\Theta_c)]^2, \tag{4}$$

where $b(\Theta_c)$, the impact parameter for the critical relative scattering angle sufficiently large to eliminate diffraction, is defined by

$$\left[1-\frac{V(r_0)}{\frac{1}{2}\mu v^2}\right]r_0^2=[b(\Theta_c)]^2, \tag{5}$$

in which μ is the reduced mass of the colliding system, and r_0, the distance of closest approach of the two particles. The velocity dependence of S results from the velocity dependence of r_0. For a potential function of the form of Eq. (3), this latter dependence, for the critical scattering angle, Θ_c, is given by

$$v=\left(\frac{\pi r_0}{8a}\right)^{\frac{1}{2}}\frac{A}{h}(8ar_0-1)e^{-ar_0}-\frac{11.78C}{h(r_0)^5}-\frac{13.74D}{h(r_0)^7}-\frac{15.46E}{h(r_0)^9}, \tag{6}$$

where h is Planck's constant. Results of classical total collision cross section calculations are summarized in Table II. The general equation

$$S=a'+\frac{b'}{v}+\frac{c'}{v^2} \tag{7}$$

was found capable of representing the velocity dependence of S in form suitable for evaluation of $Q_{\eta,K}$ and $Q_{D(1,1)}$. Values of S calculated from Eq. (7) using the constants in Table II show the following absolute deviations from the recorded values: neon-maximum, 0.84 percent; average, 0.60 percent: argon-maximum, 0.72 percent; average, 0.48 percent: krypton-maximum, 0.11 percent; average, 0.06 percent: xenon-maximum, 0.08 percent; average, 0.04 percent.

TABLE II. Classical total collision cross sections.

Gas	a' (A^2)	b' ($\frac{A^2\,cm}{sec.}$)	c' ($\frac{A^2\,cm^2}{sec.^2}$)	r_0 (A)	v ($\frac{10^5\,cm}{sec.}$)	$b(\Theta_c)$ (A)	S (A^2)
Ne	23.45	1.87×10^5	0.763×10^{10}	2.80	1.540	2.81	24.80
				2.83	1.242	2.85	25.51
				2.85	1.057	2.88	26.08
				2.88	0.793	2.94	27.25
				2.90	0.626	3.01	28.52
				2.93	0.392	3.24	33.01
A	39.85	2.05×10^5	3.40×10^{10}	3.6340	1.148	3.76	44.35
				3.6370	0.913	3.83	46.12
				3.6400	0.679	3.99	49.97
				3.6410	0.601	4.08	52.32
				3.6420	0.529	4.20	55.46
				3.6425	0.492	4.29	57.75
Kr	44.94	0.00	2.83×10^{10}	3.7860	0.716	4.01	50.42
				3.7865	0.662	4.04	51.36
				3.7870	0.612	4.09	52.54
				3.7875	0.557	4.14	54.02
				3.7880	0.504	4.23	56.08
				3.7890	0.397	4.47	62.91
Xe	55.14	0.00	3.05×10^{10}	4.1910	0.714	4.41	61.10
				4.1915	0.634	4.47	62.74
				4.1920	0.554	4.55	65.09
				4.1925	0.474	4.68	68.75
				4.1927	0.442	4.75	70.79
				4.1930	0.393	4.88	74.90
				4.1931	0.375	4.95	76.83

VISCOSITY AND THERMAL CONDUCTIVITY

The classical expression for the viscosity of a single gas is

$$\eta=\frac{5}{16}\frac{(1+\epsilon)(\pi MRT)^{\frac{1}{2}}}{NQ_{\eta,K}}, \tag{8}$$

[6] H. Margenau, Phys. Rev. 56, 1000 (1939).

TABLE III. Calculated and experimental† values of viscosity and thermal conductivity.

Gas	T (°K)	$Q_{\eta,K}$ (A^2)	$\eta_{exp.}\times10^5$ $\left(\frac{g}{sec.\ cm}\right)$	$\eta_{cal.}\times10^5$ $\left(\frac{g}{sec.\ cm}\right)$	$100\left\lvert\frac{\Delta\eta}{\eta_{exp.}}\right\rvert$ (%)	$K_{exp.}\times10^5$ $\left(\frac{cal.}{sec.\ cm\ deg.}\right)$	$K_{cal.}\times10^5$ $\left(\frac{cal.}{sec.\ cm\ deg.}\right)$	$100\left\lvert\frac{\Delta K}{K_{exp.}}\right\rvert$ (%)
Ne	200	26.03	23.755	20.85	12.2	8.82*	7.78	11.8
	180	26.21	22.040	19.62	11.0		7.32	
	160	26.44	20.255	18.33	9.4		6.84	
	140	26.71	18.405	16.97	7.8		6.33	
	120	27.07	16.460	15.50	5.8		5.78	
	100	27.55	14.345	13.91	3.0		5.19	
	90	27.86	13.200	13.04	1.2	4.93*	4.86	1.4
	80	28.24	11.980	12.14	1.3		4.53	
	70	28.71	11.17*	11.19	0.2		4.17	
	60	29.32	9.78*	10.15	3.8		3.79	
A	290	46.86	22.080	19.51	11.6		3.67	
	270	47.29	20.805	18.64	10.4	3.85*	3.50	9.1
	250	47.79	19.465	17.75	8.8		3.34	
	230	48.37	18.090	16.84	6.9		3.17	
	210	49.05	16.665	15.85	4.9		2.98	
	190	49.87	15.210	14.82	2.6	2.87*	2.79	2.8
	170	50.88	13.725	13.76	0.3		2.59	
	150	52.14	12.220	12.62	3.3		2.37	
	130	53.78	10.695	11.38	6.4		2.14	
	110	55.98	9.155	10.06	9.9		1.89	
Kr	370	51.29	30.49*	29.16	4.4		2.65	
	330	52.06		27.13			2.46	
	290	53.33	24.40*	24.96	2.3		2.27	
	270	53.64		23.81		2.10*	2.16	2.9
	250	54.34		22.62			2.05	
	230	55.16		21.39			1.94	
	210	56.13		20.06			1.82	
	190	57.31		18.69			1.70	
	170	58.76		17.25			1.57	
	150	60.61		15.72			1.43	
Xe	550	62.38	39.54	36.49	7.7		2.11	
	500	63.10	36.52	34.39	5.8		1.99	
	450	63.98	33.51	32.17	4.0		1.86	
	400	65.09	30.09	29.82	0.9		1.72	
	370	65.90	28.58*	28.33	0.9		1.64	
	340	66.85		26.77			1.55	
	310	67.98		25.13			1.45	
	290	68.86	22.52*	24.00	6.6		1.39	
	270	69.88		22.81		1.23*	1.32	7.3
	250	71.06		21.59			1.25	
	230	72.45		20.33			1.18	
	210	74.09		18.97			1.10	

† (a) Viscosity: neon (60° and 70°K), A. van Itterbeek and O. van Paemel, Physica **7**, 265 (1940); neon (80°–200°K) and argon, H. L. Johnston and E. R. Grilly, J. Phys. Chem. **46**, 948 (1942); krypton and xenon (290° and 370°K), A. G. Nasini and C. Rossi, Gazz. chim. ital. **58**, 433 (1928); xenon (400°–550°K), M. Trautz and R. Heberling, Ann. d. Physik **20**, 118 (1934). (b) Thermal conductivity: neon, S. Weber, Commun. Leiden Suppl. No. 42b (1918); argon, A. Eucken, Physik. Zeits. **12**, 110 (1911); krypton and xenon, M. Curie and A. Lepape, J. d. phys. et rad. [7] **2**, 392 (1931).

where ϵ is 0.016, M, the molecular weight, R, the gas constant per mole, N, Avagadro's number, and $Q_{\eta,K}$, the classical cross section for viscosity and thermal conductivity for a Maxwellian gas at temperature T. This cross section is defined by

$$Q_{\eta,K}=\frac{M^4}{512R^4T^4}\int_0^\infty v^7 S_{\eta,K}\exp[-Mv^2/(4RT)]dv, \tag{9}$$

where $S_{\eta,K}=2S/3$. For the functional form of S given in Eq. (7), Eq. (9) reduces to

$$Q_{\eta,K}=a'+3.04\times10^{-5}M^{\frac{1}{2}}b'/T^{\frac{1}{2}}+1.00\times10^{-9}Mc'/T\,A^2, \tag{10}$$

and Eq. (8) to

$$\eta=\frac{8.52\times10^{-5}M^{\frac{1}{2}}T^{\frac{1}{2}}}{a'+3.04\times10^{-5}M^{\frac{1}{2}}b'/T^{\frac{1}{2}}+1.00\times10^{-9}Mc'/T}\times\frac{g}{sec.\ cm}. \tag{11}$$

For a monatomic gas, the thermal conductivity may be written

$$K=2.5(1+\delta)\eta c_v, \tag{12}$$

where δ is 0.01 and c_v is the specific heat at constant volume which may be set equal to $1.5R/M$. If η is expressed in cgs units, Eq. (12) becomes

$$K=7.52\eta/M\frac{\text{cal.}}{\text{sec. cm deg.}}. \tag{13}$$

Values of $Q_{\eta,K}$ and η calculated from Eqs. (10) and (11), using the constants of Table II, and values of K calculated from Eq. (13) are shown in Table III as functions of temperature. Reliable experimental values have been included for comparison although viscosity determinations in the case of krypton and xenon, and thermal conductivity determinations in the case of all the gases, are relatively scarce. Starred values differ slightly from values cited in the literature because of correction to the rounded temperatures in the second column. As in the case of helium, the calculated values are terminated at the upper temperature limit because of decreasing accuracy of the potential energy functions at distances too far removed from the minimum, and at the lower temperature limit because the present development is demonstrably valid only for relatively small values of the critical scattering angle, Θ_c.

The average absolute deviation between calculated and experimental values is 5.5 percent in the case of viscosity and 5.9 percent in the case of thermal conductivity.

COEFFICIENT OF SELF-DIFFUSION

The classical expression for the coefficient of self-diffusion, $D(1, 1)$, is

$$D(1,1)=\frac{3\,(1+\epsilon)(\pi MRT)^{\frac{1}{2}}}{8\quad N\rho Q_{D(1,1)}}, \tag{14}$$

where ρ is the density in grams per unit volume and $Q_{D(1,1)}$, the classical cross section for self-diffusion in a Maxwellian gas at temperature T defined by

$$Q_{D(1,1)}=\frac{M^3}{32R^3T^3}\int_0^\infty v^5 S_{D(1,1)} \times\exp.[-Mv^2/(4RT)]dv, \tag{15}$$

where $S_{D(1,1)}=S/2$. For the form of S in Eq. (7), Eq. (15) reduces to

$$Q_{D(1,1)}=a'+3.65\times10^{-5}M^{\frac{1}{2}}b'/T^{\frac{1}{2}}+1.50\times10^{-9}Mc'/T\,A^2, \tag{16}$$

and Eq. (14) to

$$D(1,1)=\frac{1.02\times10^{-4}M^{\frac{1}{2}}T^{\frac{1}{2}}}{\rho(a'+3.65\times10^{-5}M^{\frac{1}{2}}b'/T^{\frac{1}{2}}+1.50\times10^{-9}Mc'/T)}\frac{\text{cm}^2}{\text{sec.}}, \tag{17}$$

where ρ is in g/cc, or

$$D(1,1)=\frac{8.50\times10^{3}T^{\frac{1}{2}}}{PM^{\frac{1}{2}}(a'+3.65\times10^{-5}M^{\frac{1}{2}}b'/T^{\frac{1}{2}}+1.50\times10^{-9}Mc'/T)}\frac{\text{cm}^2}{\text{sec.}}, \tag{18}$$

where P is in dynes/cm², since $\rho=PM/(RT)$.

Values of $Q_{D(1,1)}$ and $D(1, 1)$ for $P=1.01\times10^6$ dynes/cm² (1 atmosphere) have been computed from Eqs. (16) and (18) using the constants of Table II. The results appear in Table IV which does not include a column for experimental values since there are but two determinations at temperatures suitable for comparison with the calculated values. Groth and Harteck[7] find that at 1 atmosphere $D(1, 1)$ is 0.091 cm²/sec. for krypton at 293.96°K and 0.0443 cm²/sec. for xenon at an average temperature of 292.31°K. These values, which have a probable error of 5 percent, become 0.089 and 0.0437 when corrected to 290°K and differ by 9.7 percent and 10.3 percent respectively from the corresponding calculated values in Table IV.

Lord Kelvin[8] has outlined a method, which Chapman and Cowling[9] feel is somewhat justified

[7] W. Groth and P. Harteck, Zeits. f. Elektrochemie **47**, 167 (1941).

[8] Lord Kelvin, *Baltimore Lectures on Molecular Dynamics and the Wave Theory of Light* (C. J. Clay and Sons, London, England, 1904), p. 295.

[9] S. Chapman and T. G. Cowling, *Mathematical Theory of Non-Uniform Gases* (Cambridge University Press, Teddington, England, 1939), pp. 250 and 251.

TABLE IV. Calculated values of the self-diffusion coefficient at 1 atmosphere.

Gas	T (°K)	$Q_{D(1,1)}$ (A^2)	$D(1,1)$ (cm²/sec.)	Gas	T (°K)	$Q_{D(1,1)}$ (A^2)	$D(1,1)$ (cm²/sec.)
Ne	200	26.78	0.199	Kr	370	54.48	0.122
	180	27.02	0.167		330	55.64	0.100
	160	27.32	0.138		290	57.11	0.0804
	140	27.70	0.112		270	58.02	0.0711
	120	28.18	0.0874		250	59.06	0.0623
	100	28.83	0.0652		230	60.29	0.0538
	90	29.26	0.0549		210	61.75	0.0458
	80	29.77	0.0451		190	63.52	0.0384
	70	30.42	0.0362		170	65.70	0.0314
	60	31.27	0.0279		150	68.47	0.0250
A	290	49.66	0.133	Xe	550	66.01	0.144
	270	50.28	0.118		500	67.10	0.123
	250	51.00	0.104		450	68.43	0.103
	230	51.83	0.0902		400	70.09	0.0843
	210	52.82	0.0772		370	71.30	0.0738
	190	53.69	0.0650		340	72.73	0.0637
	170	55.47	0.0537		310	74.43	0.0542
	150	57.30	0.0430		290	75.76	0.0482
	130	59.68	0.0333		270	77.29	0.0424
	110	62.90	0.0246		250	79.06	0.0369
					230	81.14	0.0318
					210	83.62	0.0269

by the self-consistency of the results, for calculating self-diffusion coefficients from suitable combinations of experimental mutual diffusion coefficients of binary mixtures. Since it appears possible to calculate values of the self-diffusion coefficient, it seems desirable to point out that Lord Kelvin's method may be readily inverted.

At a given temperature, a pair of values of $Q_{D(1,1)}$ may be used to compute an approximate value of the mutual diffusion coefficient, $D(1,2)$, for a binary mixture from the formula

$$D(1,2)=\frac{3}{8}\frac{(RT)^{\frac{1}{2}}}{PNQ_{D(1,2)}}\left[\frac{\pi(M_1+M_2)}{2M_1M_2}\right]^{\frac{1}{2}}, \quad (19)$$

where M_1 and M_2 are the molecular weights of the gases, and $Q_{D(1,2)}$, the classical equivalent mutual cross section for diffusion for a Maxwellian binary gas mixture at temperature T. If the self-diffusion cross sections for the individual gases at the temperature T are represented by ${}^1Q_{D(1,1)}$ and ${}^2Q_{D(1,1)}$, $Q_{D(1,2)}$ is given by

$$Q_{D(1,2)}=\tfrac{1}{4}\{{}^1Q_{D(1,1)}+2[{}^1Q_{D(1,1)}{}^2Q_{D(1,1)}]^{\frac{1}{2}}+{}^2Q_{D(1,1)}\}, \quad (20)$$

which states that the equivalent hard sphere diameter for the two molecule system is the average of the equivalent hard sphere diameters of the two single molecule systems.

Eq. (19) does not take into account a small variation of $D(1,2)$ with composition and omits a small correction term, similar in character to the $(1+\epsilon)$ term in Eq. (14), which depends upon the law of force between the molecules. In spite of these limitations, the above method for estimating mutual diffusion coefficients may prove useful since, in most cases, insufficient information about interactions between unlike molecules is available for direct calculations of $D(1,2)$ by the methods outlined in the helium paper.

On the Nature of the Interaction between Starch and Iodine[1]

R. S. STEIN[2] AND R. E. RUNDLE[3]
Textile Foundation and Frick Chemical Laboratory, Princeton University, Princeton, New Jersey
(Received November 19, 1947)

(1) It is postulated that the interaction between starch and iodine in the amylose-iodine complex is of dipolar nature.

(2) A model for such dipolar interaction is proposed and the necessity for a cooperative effect is discussed.

(3) The interaction energy is calculated as a function of a parameter x and it is shown that this parameter possesses a critical value at which a "condensation" of iodine into the complex occurs.

(4) It is demonstrated that it is physically reasonable for this parameter to attain its critical value.

(5) It is shown that additional stabilization may occur as a result of the formation of a resonating "polyiodine" chain at high dipolar interaction having a I−I distance and heat of formation which compares favorably with experiment.

(6) Application of the theory is made in discussing the stability of the polyvinyl alcohol-iodine complex.

(7) The color of these complexes is discussed in terms of the theory.

INTRODUCTION

THE configuration of the starch-iodine complex has been the subject of several previous papers.[4–10] On the basis of x-ray diffraction measurements, studies of iodine activity, crystal birefringence and dichroism, flow dichroism, light absorption and chemical properties, a model for the complex has been proposed in which the iodine molecules are arranged in a linear array, enclosed within and parallel to the axis of an amylose helix (Fig. 1).

Several attempts have been made[10–13] to explain the nature of the interaction between the starch and the iodine on the basis of this structure. These explanations fall into two categories: (*a*) those which propose adsorption of iodine or solid solution formation, and (*b*) those which propose the formation of a new "compound" or phase of definite composition. However, potentiometric titrations of amylose with iodine[4] show that iodine activity remains essentially constant during the precipitation of the complex from amylose. Moreover, on adding half the amount of iodine necessary to precitate completely the amylose from a solution, it is found[10] that half of the amylose is precipitated completely while the remaining half is unaffected. These phenomena would be difficult to explain by any but the latter mechanism.

Also stoichiometric considerations (on the basis of steric requirements) of the displacement of other complexing agents (i.e., fatty acids) from amylose by iodine have strongly favored a complex of definite composition. It is the purpose of this paper to consider quantitatively the implications of a dipole interaction mechanism which would explain the type of forces involved in the formation of such a complex phase.

It has been pointed out[10] that many of the high molecular weight materials forming complexes with iodine of the starch-iodine type have

[1] Presented in part before the Division of Physical and Inorganic Chemistry, American Chemical Society, Atlantic City, N. J., April, 1946.
[2] Fellow of the Textile Research Institute, Inc.
[3] Present address: Department of Chemistry, Iowa State College, Ames, Iowa.
[4] F. Bates, D. French, and R. E. Rundle, J. Am. Chem. Soc. 65, 142 (1943).
[5] R. E. Rundle and R. R. Baldwin, J. Am. Chem. Soc. 65, 554 (1943).
[6] R. E. Rundle and D. French, J. Am. Chem. Soc. 65, 558 (1943).
[7] R. E. Rundle and D. French, J. Am. Chem. Soc. 65, 1707 (1943).
[8] R. E. Rundle and F. C. Edwards, J. Am. Chem. Soc. 65, 2200 (1943).
[9] R. R. Baldwin, R. S. Bear, and R. E. Rundle, J. Am. Chem. Soc. 66, 111 (1944).
[10] R. E. Rundle, J. F. Foster, and R. R. Baldwin, J. Am. Chem. Soc. 66, 2116 (1944).
[11] C. S. Hanes, *New Phytologist* 36, 101, 189 (1937).
[12] F. F. Mikus, R. M. Hixon, and R. E. Rundle, J. Am. Chem. Soc. 68, 1115 (1946).
[13] K. Freudenberg, E. Schaaf, G. Dumpert, and T. Ploetz, Naturwiss. 27, 850 (1939).

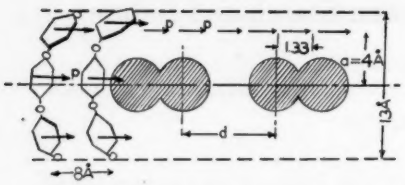

FIG. 1. The model of the iodine-filled amylose helix.

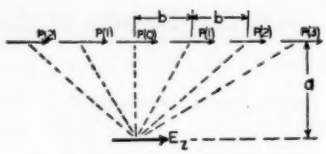

FIG. 2. The dipoles contributing to the field of the helix

two significant properties in common; that (a) the repeating unit of the structure has a residual component of dipole moment resulting in a linear array of dipoles in the polymer, and (b) a "channel" is available in the structure adjacent to and parallel to the array of dipoles of suitable dimensions to accommodate a chain of iodine molecules. Structural analysis has indicated that both the helical modification of amylose[7] and oriented polyvinyl alcohol[14,15] meet these qualifications.

In addition to iodine, alcohols, fatty acids, and nitro compounds may serve as complexing agents.[16,17] These all have in common either a high polarizability or a permanent dipole moment. This would indicate that the forces associated with complex stability are of dipolar origin.

If one considers the similarity of structure of the iodine, alcohol, and fatty acid complexes,[7,8,12] and the ease of replaceability without alteration of the basic amylose structure, it does not seem probable that any type of common valence force could be operative other than secondary binding.

Therefore, in the light of this evidence we shall consider only dipolar interaction between the iodine and the amylose helix.

It has been found that the iodine repeat distances along the helix, if it is regular, is probably incommensurate with the repeat distance of the helix itself.[7] West has found repeat distances for halogens in many halogen-polymer complexes[15b,35] which are incommensurate with the polymer spacings. This is added evidence that the influence of the polymers on the halogen molecules is not specific in nature and does not involve either direct chemical bonds or even hydrogen or dipolar bonds to the halogen in which the halogen molecule must be located in a specific position with respect to some polymer group.

Another experimental observation is useful in formulating an interaction theory. That is, one finds that the stability of the complex increases with helix length. Therefore, the origin of the attractive forces cannot be local but must be characteristic of the entire helix. They cannot be of the nature of a hydrogen bond which is local and capable of being saturated, but must be of a cooperative nature with the force on a particular iodine enhanced by the presence of other iodines. This, for example, could result from an "extended Silberstein Effect" due to the greater-than-additive polarizability of a chain of iodine molecules.

Similarly, a variation in intensity and wavelength of light absorption by the complex is observed with increasing helix strength[9,10] for the amylose complex. This also could be interpreted on the basis of increasing local field with increasing iodine chain length.

PROPOSED MODEL—THE FIELD OF THE HELIX

X-ray studies of the amylose helix have indicated that a turn of the amylose helix contains six glucose residues. Because of the helical structure, it is probable that the dipole moments of all the hydroxyl groups of the glucose residues will not cancel, and that there will be a residual component of dipole moment directed along the axis of the helix.[10] We have assumed, for purposes of calculation, that there is a residual moment of one hydroxyl group per glucose residue. The helix has an external van der Waals diameter of 13A and a hole down the center having an effective diameter of about 6A. Since the residual moment will represent an average between these radii which is weighted with

[14] R. C. L. Mooney, J. Am. Chem. Soc. **63**, 2828 (1941).
[15] (a) S. E. Sheppard and P. T. Newsome, J. Chem. Phys. **12**, 513 (1944). (b) C. D. West and E. H. Land in Alexander, *Advances in Colloid Chemistry* (Reinhold Publishing Corporation, New York, 1946).
[16] R. Bear, J. Am. Chem. Soc. **66**, 2122 (1944).
[17] R. Whistler and G. Hilbert, J. Am. Chem. Soc. **66**, 1721 (1944).

respect to an inverse high power of the radius, it would seem reasonable to assume that these average dipoles are located on the circumference of a cylinder of 8A diameter.

Because of the cylindrical symmetry, residual radial components of the dipole moments are neglected. It is possible that this radial field may be important in perturbing the iodine energy levels and thus influence the color of the complex. As a result of this symmetry property, one may consider these dipoles to be confined to a linear array rather than being distributed over the entire circumference of the cylinder. The resulting model is shown in Fig. 2, where $b = (8\text{A per loop}/6 \text{ glucose residues per loop}) = 1.33\text{A}$ and $a = 4\text{A}$.

The first stage of the calculation is the computation of the axial component of field at a particular point on the axis of the helix resulting from this array of dipoles. From elementary electrostatic field considerations, it may be shown that the component of field at a point on the axis originating from a dipole, **P**, located a distance, z, (along the axis) from the point is[18]

$$\mathbf{E}_z = \mathbf{P}\left[\frac{1}{(a^2+z^2)^{3/2}} - \frac{3z^2}{(a^2+z^2)^{5/2}}\right]. \qquad (1)$$

The total field from the entire array at point z' located a distance kb from the end of the helix of N glucose residues is

$$\mathbf{E}_z = \mathbf{P}\sum_{h=-k}^{N-k}\left(\frac{1}{(a^2+h^2b^2)^{3/2}} - \frac{3h^2b^2}{(a^2+h^2b^2)^{5/2}}\right). \qquad (2)$$

This field has been evaluated for helices of $N = 50$, 100, and 500, Fig. 3. It is seen that the field at the center is actually smaller for longer helices, as opposed to the observed variation of complex stability with chain length. However, it shall be seen that this tendency is more than overcome because of the greater enhancement of induced dipole moment in the longer helices.

INTERACTION OF THE IODINE MOLECULES WITH THE FIELD OF THE HELIX

If iodine molecules are now placed inside of these helices, they will become polarized by this field. Secondary polarization will result through interaction of the resulting induced dipoles. In an attempt to evaluate the resultant field, we shall make the following assumptions:

(a) The iodine molecule exists in the helix as a molecular entity having its usual polarizability, van der Waals' radius, and constant interatomic distance.

(b) The iodine molecules are linearly arranged along the axis of the helix which they completely fill, and may be assumed, for purposes of calculation, to be equidistant. The distance between iodine molecules may be determined by equating the van der Waals, electrostatic and resonance attractive forces to the usual van der Waals repulsive forces.

(c) The dipolar forces originate only with the helix with which the iodine is associated.

(d) The electrostatic forces arise from (1) the field of the helix and (2) the field of neighboring induced dipoles.

(e) The dipole interactions may be considered from a classical viewpoint, with the dipole considered as definite point charges, the magnitude and separation of which may be determined from consideration of polarizability and light absorption frequency.

(f) The effect on the field of the surrounding polarizable matter is neglected.

A set of equations for the field on a particular iodine molecule is set up. The field $\mathbf{E}_1$ on the first iodine molecule is

$$\mathbf{E}_1 = \mathbf{E}_1^0 + x_0\mathbf{E}_2 + x_0'\mathbf{E}_3 + \cdots \qquad (3)$$

where $\mathbf{E}_1^0$ is the axial field of the helix acting at the location of iodine molecule (1), $\mathbf{E}_2$, $\mathbf{E}_3$, etc. are the total fields at the location of iodine

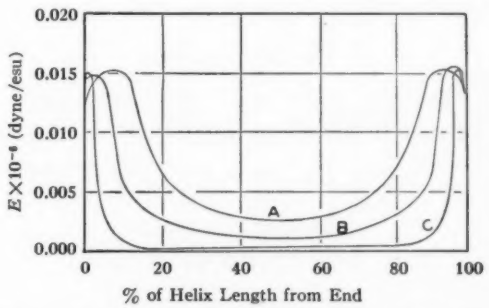

FIG. 3. The field of the amylose dipoles along the axis of the helix—*A*—50 glucose residues, *B*—100 glucose residues, *C*—500 glucose residues.

[18] See for example Frank, *Introduction to Electricity and Optics* (McGraw-Hill Book Company, Inc., New York and London, 1940), Chapter I.

molecules (2), (3), etc. and x_0, x_0', x_0'', etc. are the respective dipole interaction coefficients. The magnitudes of these coefficients depend upon the "coupling" of the respective dipoles which, in turn, is a function of the polarizability and the proximity of the particular iodine molecules. Therefore, they will not be constant but will vary with the field. However, it is convenient to write the equations in this form because of the ease in solving the resulting set of linear simultaneous equations, and because of the ease of determining the physical conditions requisite for a cooperative effect. These coefficients will be evaluated in terms of physical properties of the system in a later section.

Equation (3) may be simplified if it is noted that in the range of fields encountered, the ratio of the series of dipole interaction terms to the term representing nearest neighbor interaction is essentially constant. Therefore, if this ratio is called β, we may rewrite Eq. (3) as

$$\mathbf{E}_1=\mathbf{E}_1^0+\beta x_0\mathbf{E}_2, \tag{4}$$

where

$$\beta=(x_0\mathbf{E}_2+x_0'\mathbf{E}_3+\cdots)/x_0\mathbf{E}_2. \tag{5}$$

Similarly, for the second iodine molecule

$$\mathbf{E}_2=\mathbf{E}_2^0+x_0\mathbf{E}_1+\beta x_0\mathbf{E}_3. \tag{6}$$

Generally, further in the helix where end effects are negligible,

$$\mathbf{E}_n=\mathbf{E}_n^0+\beta x_0(\mathbf{E}_{n-1}+\mathbf{E}_{n+1}). \tag{7}$$

By solving this set of equations simultaneously (substituting Eq. (6) in (4), etc.), the following recursion formula may be derived:[19]

$$E_n=\left\{\mathbf{E}_n^0+x\mathbf{E}_{n+1}+\frac{x}{G_{n-1}}\left(\mathbf{E}_{n-1}^0+\frac{x}{G_{n-2}}\left[\mathbf{E}_{n-2}^0+\cdots+\mathbf{E}_1^0\right]\cdots\right)\right\}\Big/G_n, \tag{8}$$

where

$$x=\beta x_0 \tag{9}$$

$G_n=1-x^2$

$\quad\overline{1-x^2}$

$\qquad\overline{1-x^2}$, etc., for n "layers."

It is obvious from symmetry considerations that the resulting field must be symmetrical about the center of the helix. That is

$$\mathbf{E}_{(N/2)-1}=\mathbf{E}_{(N/2)+1},$$

so that

$$\mathbf{E}_{N/2}=\frac{\mathbf{E}_{N/2}^0+2\mathbf{Q}_{(N/2)-1}}{G_{N/2}[1-(x^2/G_{N/2}G_{(N/2)-1})]}, \tag{10}$$

where

$$\mathbf{Q}_N=\frac{x}{G_N}\left\{\mathbf{E}_N^0+\frac{x}{G_{N-1}}[(\mathbf{E}_{N-1}^0+\cdots+\mathbf{E}_1^0)\cdots]\right\}.$$

Also, $\mathbf{E}_1=\mathbf{E}_N$ so that

$$\mathbf{E}_N=\frac{\mathbf{E}_N^0+\mathbf{Q}_{N-1}}{G_N}.$$

The complete field distribution may then be obtained by application of Eq. (8).

The nature of x.—An examination of these equations reveals that the field at any point is an expansion in terms of successive powers of the parameter x. It is seen that in order for a cooperative effect to exist where an appreciable contribution is made by higher powered terms representing more distant dipoles, x/G must be close to unity. The function G is seen to converge rather rapidly (Fig. 4a) so that its properties will

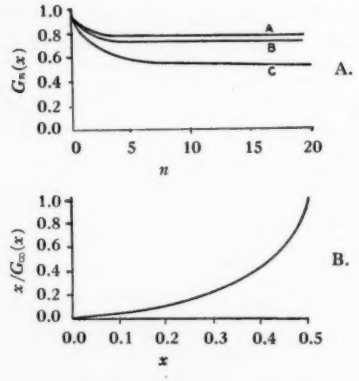

FIG. 4. Some properties of $G_n(x)$: 4A. the convergence of $G_n(x)$ A. $x=0.41$; B. $x=0.45$; C. $x=0.50$; 4B. the variation of $x/G_\infty(x)$ with x.

[19] This set of equations will be recognized as constituting a set of difference equations having variable coefficients. If the coefficients, x, are represented as an analytic function of the field, $\mathbf{E}$ (determined by the balancing of forces between iodines), a direct analytic solution of the problem should be possible.

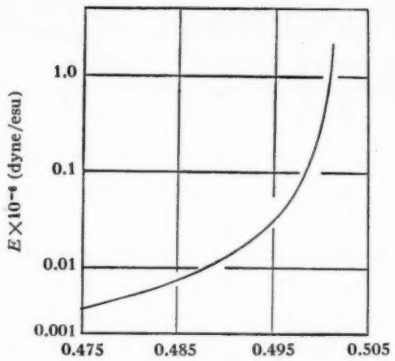

FIG. 5. The variation of the total field along the axis of a 200 glucose residue helix with the interaction coefficient x.

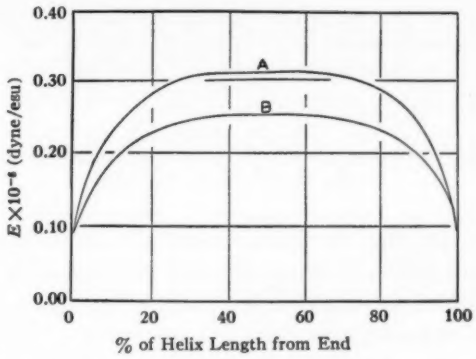

FIG. 6. The variation of the axial field of the completely filled helix with the helix length (assuming $x=0.5$): A—500 glucose residues; B—200 glucose residues.

be determined largely by its limiting value, G_∞. In Fig. 4b, x/G_∞ is plotted against x. It is seen that at a critical value of $x=0.5$, x/G_∞ rapidly increases, passing through unity. Therefore, we should expect that the physical restraints require x to lie in this region for the amylose-iodine configuration.

In Fig. 5 the total field at the center of the helix is plotted logarithmically against x. As expected, the field increases greatly at $x=0.5$. Actually, for an infinitely long helix, the field would become infinite at this point, while for a finite helix, x may slightly exceed the critical value. It shall be seen that the physical limitations on x keep the field within reasonable bounds.

It is interesting now to examine the variation of the field with helix length (Fig. 6). We have plotted the field variation along a 200 glucose helix (corn amylose) and a 500 glucose helix (potato amylose) for an arbitrarily chosen value of $x=0.5$. It is seen here that, as a result of the cooperative effect, the field now increases with helix length. This presumably would explain the experimentally observed decrease in iodine activity with helix length as well as the intensification of light absorption.

THE EVALUATION OF THE INTERACTION COEFFICIENT

The magnitude of the dipole moment induced in an iodine molecule residing in an electrostatic field may be expressed in terms of the polarizability tensor of the iodine. As a first approximation, the secondary force field originating from this dipole could then be expressed as a function of this dipole moment. Such an expression, however, involves the assumption that the separation of charges in the dipole is small as compared with the distance between the dipole and its point of action. As applied to this calculation, one finds that in the region where the cooperative effect becomes significant, this assumption is not valid. Therefore, a refinement is required.

We have chosen to represent the dipole as two equal finite point charges located symmetrically on the principle axis of the iodine molecule. The, polarizability is no longer adequate in characterizing this system since both the magnitude and the displacement of the charges must be specified. A possible means of very roughly specifying the charge displacement independently of its magnitude is to relate it to the light absorption. If it is assumed that the absorption of light by the iodine results from the natural harmonic vibration of the same electrons involved in polarization, then the frequency of maximum absorption may be related to the force constant for the electronic displacement by the usual relationship,

$$\nu_0=1/2\pi(k/m)^{\frac{1}{2}}.$$

The displacement of the electrons l may then be related to the field strength and the electronic charge e, since

$$\mathbf{E}e=k\mathbf{l},$$

so that

$$l=e/(4\pi^2\nu_0^2m)\mathbf{E}=K\mathbf{E}. \qquad (12)$$

One finds from the absorption spectra of iodine in the helix that $K=5.55\times10^{-4}$A/unit field.

Obviously, the assumption of a linear restoring

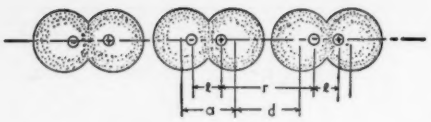

FIG. 7. Arrangement of the induced dipoles of the iodine molecules in the helix.

force on the electrons cannot be applicable at higher fields. It actually must become more difficult to separate the charges further as the separation becomes large. However, there appears to be no simple way to characterize completely this restoring force, and it must be realized that our solutions in regions of high fields may be in error as a result of this approximation.

Thus, it is seen that the solution of the problem involves the evaluation of the field of a system of displaceable point charges (Fig. 7), the spacing of which is determined by the balancing of the associated forces. In considering the separation of charges caused by the polarization of an iodine molecule, one is confronted with the problem of assigning a point in the molecule at which an effective average polarizing field acts. However, we may safely assume that such a point is on the axis of the molecule, not too far from its center, and closest to the polarizing dipole. Its location also will vary with the extent of polarization. As a working assumption, we have assumed that this point is located at a distance $r+l/3$ from the closest charge of the polarizing dipole.

We then may set up an equation for the total field at the nth iodine molecule,

$$\begin{aligned}E_n&=E_n^0+\sum_i \frac{q_i}{r_{in}^2}\\&=E_n^0+q\left\{\left(\frac{1}{(r_n')^2}-\frac{1}{(r_n'+l_{n-1})^2}\right)\right.\\&\quad+\left(\frac{1}{(r_{n+1}')^2}-\frac{1}{(r_n'+l_{n+1})^2}\right)\\&\quad+\left(\frac{1}{(r_n'+r_{n+1}'+l_{n+1})^2}-\frac{1}{(r_n'+r_{n+1}'+l_{n+2})^2}\right)\\&\quad+\left(\frac{1}{(r_n'+r_{n-1}'+l_{n-1})^2}\right.\\&\quad\left.\left.-\frac{1}{(r_n'+r_{n-1}'+l_{n-1}+l_{n-2})^2}\right)+\cdots\right\}\end{aligned}\tag{13}$$

where $r'=r+l/3$. Then

$$E_n=E_n^0+\frac{\alpha\beta}{K}\left\{\left(\frac{1}{(r_n')^2}-\frac{1}{(r_n'+l_{n-1})^2}\right)+\left(\frac{1}{(r_{n+1}')^2}-\frac{1}{(r_n'+l_{n+1})^2}\right)\right\},\tag{14}$$

where β is defined by Eq. (5) and $q=(\alpha l/E)/(l/E)=\alpha/K$. Since the variation in l will be much greater than the variation in r, we may assume that all of the r's are equal in this equation. Expanding:

$$\begin{aligned}E_n&=E_n^0+\frac{\alpha\beta}{K}\left\{\left(\frac{1}{(r')^2}\right)-\left(\frac{1}{(r')^2}-\frac{2l_{n-1}}{(r')^3}\right.\right.\\&\quad\left.+\frac{3l_{n-1}^2}{(r')^4}+\cdots\right)+\left(\frac{1}{(r')^2}\right)-\left(\frac{1}{(r')^2}\right.\\&\quad\left.\left.-\frac{2l_{n+1}}{(r')^3}+\frac{3l_{n+1}^2}{(r')^4}+\cdots\right)\right\}\\&=E_n^0+\frac{2\alpha\beta}{(r')^3}\left\{\left(E_{n+1}-\frac{3}{2}\frac{KE_{n+1}^2}{r'}\right.\right.\\&\quad\left.+\frac{2K^2E_{n+1}^3}{(r')^2}-\frac{5}{2}\frac{K^3E_{n+1}^4}{(r')^3}+\cdots\right)\\&\quad+\left(E_{n-1}-\frac{3}{2}\frac{KE_{n-1}^2}{r'}+\frac{2K^2E_{n-1}^3}{(r')^2}\right.\\&\quad\left.\left.-\frac{5}{2}\frac{K^3E_{n-1}^4}{(r')^3}+\cdots\right)\right\}\\&=E_n^0+x(E_{n-1}+E_{n+1}),\end{aligned}\tag{15}$$

where

$$x_n\cong\frac{2\alpha\beta}{(r')^3}\left\{1-\frac{3}{2}\left(\frac{KE_n}{r'}\right)+2\left(\frac{KE_n}{r'}\right)^2-\frac{5}{2}\left(\frac{KE_n}{r'}\right)^3+\cdots\right\}.\tag{16}$$

It has been assumed in writing down the expression for x that (in this factor) it is permissible to set $E_{n-1}=E_n=E_{n+1}$. This assumption is probably not too serious since, over most of the length of the helix, E varies rather slowly, and since E enters into this series only into the relatively negligible higher powered terms.

Evaluation of β.—β is defined in Eq. (5) and may be numerically evaluated in terms of the above theory. The complete equation (including further neighbor fields) for the field is given by Eq. (13). For purposes of evaluating β, it is sufficiently accurate to consider all of the l's and r's to be identical in this equation. Therefore, β may be given by

$$\beta=\frac{\left(\begin{array}{r}[1/(r+(l/3))^2+1/(2r+(4/3)l)^2+1/(3r+(7/3)l)^2+\cdots] \\ -[1/(r+(4l/3))^2+1/(2r+(7/3)l)^2+1/(3r+(10/3)l)^2+\cdots]\end{array}\right)}{\{1/(r+(l/3))^2-1/(r+(4/3)l)^2\}}.$$

The numerator of this equation may be expressed as

$$\sum_{n=1}^{N/2}[(an-\tfrac{2}{3}l)^{-2}-(an+\tfrac{1}{3}l)^{-2}]$$

where $a=r+l$. Expanding these terms, this becomes

$$\sum_{n=1}^{N/2}\{[(an)^{-2}+(4/3)l(an)^{-3}+(4/3)l^2(an)^{-4}+(32/27)l^3(an)^{-5}+(80/81)l^4(an)^{-6}+\cdots]$$
$$-[(an)^{-2}-(2/3)l(an)^{-3}+(1/3)l^2(an)^{-4}-(4/27)l^3(an)^{-5}+(5/81)l^4(an)^{-6}+\cdots]\}$$
$$=(1/l^2)\left\{2(l/a)^3\sum_1^{N/2}(1/n^3)+(l/a)^4\sum_1^{N/2}(1/n^4)+(4/3)(l/a)^5\sum_1^{N/2}(1/n^5)+(25/27)(l/a)^6\sum_1^{N/2}(1/n^6)+\cdots\right\}.$$

Therefore,

$$\beta=\frac{\{[1/l^2][2.404(l/a)^3+1.082(l/a)^4+1.382(l/a)^5+0.941(l/a)^6+\cdots]\}}{\{1/(r+(1/3)l)^2-1/(r+(4/3)l)^2\}}.$$

In Table I we have evaluated β for several values of the field.

It is seen that β does not vary significantly and that its application as an approximation is very well justified.

The solution for x.—It is seen from Eq. (16) that x is a function of the field $\mathbf{E}$ and the distance between dipoles r. Also, from the solution from the set of cooperative effect equations we have shown that the field is a function of x. In order to obtain a solution for the three variables, a third relationship is necessary.

An examination of these variables reveals that we may interrelate r and $\mathbf{E}$ by considerations of the force equilibrium. In the absence of a field, the distance between iodine molecules is determined by the van der Waals distance, d_0, which results from the balancing of the van der Waals (dispersion) attractive force against the repulsive forces. In the presence of a field, there is an additional attractive force resulting from electrostatic attraction of the induced dipoles. This will reduce the van der Waals distance to a new value, d. If d is reduced sufficiently so as to become comparable with the interatomic distance a it is possible that the interatomic and intermolecular bonds characterizing particular iodine molecules lose their identities and that additional stabilization may result from the resonance energy. In these processes, a also will presumably change but to a lesser extent than does d.

A relationship then may be obtained between the reduced van der Waals radius and the field. It is obvious from Fig. (7) that r is given by

$$r=d(E)+a-l=d(E)+a-KE. \qquad (17)$$

We have, then, our desired third relationship among the three variables, x, r, and E. These

TABLE I.

$E\times10^{-6}$	β
0.568	1.17
0.360	1.16
0.050	1.18

may be solved simultaneously to give the solution for the state of the system.

THE FORCE BALANCE

The repulsive force.—The repulsive force function may be estimated from the Morse curve by a method due to Eyring.[20] The force between two iodine atoms united in a molecule may be obtained by differentiating the Morse function[21] with respect to the distance between them, d. This gives

$$F=2D\alpha(e^{-2\alpha(d-a)}-e^{-\alpha(d-a)}).$$

For I_2, the constants are given[22] as $D=2.47\times10^{-12}$ erg, $\alpha=1.85\text{A}^{-1}$, and $a=2.67$A. The first term in the expression represents a repulsive force while the second represents attraction. The attractive force, if considered quantum mechanically from the point of view of the London theory,[23] may be expressed as a sum of Coulombic integrals and exchange integrals. If the two iodine atoms are not bound in a molecule, it is found that the exchange integrals no longer contribute to the attractive force but represent a repulsion equal in magnitude to $\frac{1}{2}$ of their former attraction. Then, the force will be

$$F_{\text{repulsive}}=2D\alpha\left(e^{-2\alpha(d-a)}-\left(\%\text{ Coulombic}-\frac{\%\text{ Exchange}}{2}\right)e^{-\alpha(d-a)}\right). \quad (18)$$

For the purposes of this calculation, it was assumed that the I—I bond is 86 percent Coulombic.

The van der Waals attractive force.—The van der Waals attractive force has been shown[24] theoretically to vary inversely with the seventh power of the distance between centers of the attracting atoms. If an expression of this type is equated to the above type equation for the repulsive force for the case of $d=d_0$, the unperturbed van der Waals distance (4.3A for iodine),

$$F_{\text{repulsive}}=F_{\text{attractive}}=(A/d_0^7), \quad (19)$$

the proportionality constant A may be evaluated. For iodine, A was found to be equal to 4104×10^{-4} dyne/A^7.[24a]

Resonance stabilization.—The possibility of resonance between structures of the type.

(I) I—I I—I I—I,

(II) I I—I I—I I,

must also be considered.

If d is the unperturbed van der Waals distance, the exchange integrals between the atoms separated by this distance will be small, and the contribution of structures of type (II) will be negligible. However, as d is reduced through operation of electrostatic attraction, these integrals become increasingly more important, and an increasing resonance energy exists due to interaction between types (I) and (II) structures. The variation of resonance energy with d results in an attractive force which serves to reduce d further.

The secular equation for a set of resonating structures of this type is identical to that arising from the description of the π electrons of a long conjugated hydrocarbon. These have been treated by means of the valence bond method by Pauling and Wheland,[25] Wheland,[26–29] and Pauling and Sherman,[30] and by the molecular orbital method by Huckel[31] and Lennard-Jones.[32] For our purposes the treatment of Lennard-Jones appeared most useful.

He considers the general problem of a conjugated hydrocarbon where the bond lengths alternate and is successful in obtaining a general solution for the associated secular equation. He

[20] Henry Eyring, J. Am. Chem. Soc. **54**, 3191 (1932).
[21] P. Morse, Phys. Rev. **34**, 57 (1929).
[22] G. Hertzberg, *Molecular Spectra and Molecular Structure*, I. *Diatomic Molecules* (Prentice-Hall, Inc. New York, 1939), p. 488.
[23] F. London, Zeits. f. Elektrochemie **35**, 552 (1929).
[24] R. Eisenschitz and F. London, Zeits. f. Physik **60**, 491 (1930).

[24a] An alternate method for calculating the van der Waals and repulsive forces would be to calculate explicitly the absolute attractive force between iodines from the London formula and using an empirical inverse twelfth power or exponential repulsive force.
[25] L. Pauling and G. W. Wheland, J. Chem. Phys. **1**, 362 (1933).
[26] G. W. Wheland, J. Chem. Phys. **2**, 356 (1934).
[27] G. W. Wheland, J. Chem. Phys. **2**, 474 (1934).
[28] G. W. Wheland, J. Chem. Phys. **2**, 230, 365 (1935).
[29] G. W. Wheland, J. Am. Chem. Soc. **63**, 2025 (1941).
[30] L. Pauling and J. Sherman, J. Chem. Phys. **1**, 679 (1933).
[31] Huckel, Zeits. f. Physik **70**, 204 (1931); **72**, 310 (1931); **76**, 628 (1932).
[32] J. E. Lennard-Jones, Proc. Roy. Soc. **158A**, 280, 297 (1937).

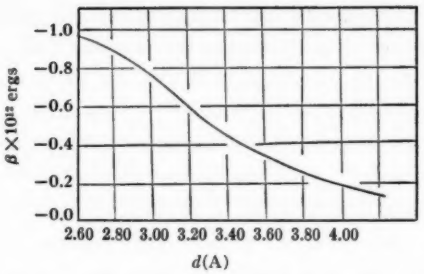

FIG. 8. The variation of the molecular orbital exchange integral with the intermolecular distance (for constant a=2.67A).

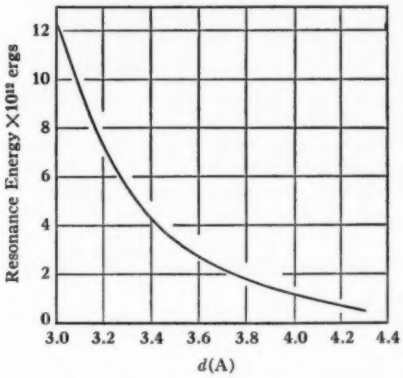

FIG. 9. Variation of resonance energy with intermolecular distance (keeping a constant=2.67A).

obtains the following equation for the orbital energy for a chain having 2ν atoms:

$$\delta=2\beta_a\sum_{r=1}^{\nu}\{1+2(\beta_d/\beta_a)\cos\theta r+(\beta_d/\beta_a)^2\}^{\frac{1}{2}}, \qquad (20)$$

where

$$\theta_r=\frac{2r\pi}{2\nu+1}-\frac{1}{2\nu+1}\left(1-\frac{\beta_d}{\beta_a}\right)\tan\frac{r\pi}{2\nu+1}.$$

β_d and β_a are the molecular orbital exchange integrals across the distances d and a, respectively. It is assumed that exchange integrals between other than adjacent atoms are negligible, and that there are sufficient atoms in the chain so that all of the diagonal terms in the secular determinant may be considered identical (end effects are negligible). The expression given for θ_r is a first approximation and is only accurate if a and d are not too different.

The exchange integrals cannot be directly evaluated as no thermochemical or spectroscopic data is available for polyiodine type compounds. However, comparison reveals[24] that the results of the molecular orbital and valence orbital methods are surprisingly consistent. The ratio of the molecular orbital exchange integral β to the valence orbital exchange integral α is fairly constant and approximately equals 0.45 for long conjugated chains. α may be evaluated rather readily as it is approximately a constant fraction (0.86) of the energy (given by the Morse function) which may be obtained from the exact treatment of simpler molecules. Therefore, a plot of β as a function of d calculated in this way is given in Fig. 8.

The resonance energy is obtained by subtracting from the orbital energy, the orbital energy of the static, unexcited structure, $2\nu\beta_a$. We have calculated this resonance energy as a function of d (with a held constant at 2.67A) for a chain of 40 iodine molecules (Fig. 9). This would roughly correspond to a filled helix of 200 glucose residues. The slope of this curve is equal to the force caused by the resonance energy.

Electrostatic attractive force.—The electrostatic attractive force is a result of (1) the Coulombic potential resulting from the attraction and repulsion of the charges representing the dipoles and (2) the potential energy expended in separating the charges in forming the dipole. That is

$$F_{\text{electrostatic}}=\sum_i\sum_i\frac{q^2}{r_{ij}^2}-\sum_i\frac{\partial}{\partial d}\left(\frac{p_i^2}{2\alpha}\right)$$

where p_i is the dipole moment of the ith dipole. It has been shown[33] (to the approximation that the forces may be represented by interactions between dipoles) that the charge separation term is opposite in sign and equal in magnitude to half of the first (Coulombic attraction) term. Therefore,

$$F_{\text{electrostatic}}=\frac{1}{2}\sum_i\sum_i\frac{q^2}{r_{ij}^2}$$

$$=\frac{\beta q^2}{2}\left(\frac{1}{r^2}+\frac{1}{(r+2l)^2}-\frac{2}{(r+l)^2}\right), \qquad (22)$$

where β, as before, corrects for further neighbor interaction.

[33] See, for example, O. K. Rice, *Electronic Structure and Chemical Binding* (McGraw-Hill Book Company, Inc., New York, 1940), Appendix III.

TABLE II.

	Energy (kcal./mole of I_2)
Repulsive	15.5
van der Waals attraction	−10.6
Electrostatic attraction	−28.7
Resonance attraction	− 3.12
Total energy	−26.9

To solve for the relationship between d and E, the equation,

$$F(d)=\frac{\beta\alpha^2}{2K^2}\left(\frac{1}{(a+d-KE)^2}+\frac{1}{(a+d+KE)^2}-\frac{2}{(a+d)^2}\right), \quad (23)$$

where

$$F(d)=F_{\text{repulsive}}-F_{\text{van der Waals}}-F_{\text{resonance}},$$

was solved graphically. The resulting plot of d against E is given in Fig. 10.

THE SOLUTION OF THE SIMULTANEOUS EQUATIONS

The following procedure was followed in obtaining the solution of the three simultaneous equations: (a) For a given value of x, E was obtained from Eq. (10); (b) using the value of x and E, Eq. (16) was solved graphically for r; (c) d was then calculated using Eq. (17), and d was plotted against x. (See, for example, curve A of Fig. 11); (d) another plot of d against x was obtained from the solution of Eq. (23) (curve B of Fig. 11). The intersection of these two curves is the desired solution.

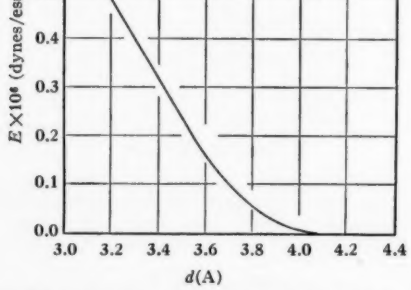

FIG. 10. The force balance—Variation of interatomic distance with field strength.

The curves of Fig. 11 represent a solution for the center of a 200 glucose residue helix. It is seen that the intersection occurs at $x=0.5005$, $d=3.13$A, and $E=0.50\times10^6$ dynes/unit charge. One observes that another intersection occurs at about $x=0.2$. This, however, represents a negligibly small field with d at the unperturbed van der Waals distance. This would correspond to a state having much higher free energy than the high field solution and would be unstable with respect to it.

The stabilization energy corresponding to this solution may be readily computed. The contributions of the interactions making up this energy are tabulated in Table II.

While the configurational stabilization energy appears rather high, its order of magnitude is not too unreasonable. Qualitative observations indicate that the stability of the iodine in the complex is comparable with that of iodine held by weak primary valence bonds. The heat of formation of the complex indicated by the electrode potential is −19.6 kcal. per mole of iodine at 25°C.[34] It is expected that this value should be lower than that of the dry complex because it has formed in solution, and there is the possibility of ion or solvent inclusion which would interrupt the iodine chain.

It should be noted that while the ordinary van der Waals distance for I_2 is 4.3A, the intermolecular distance is as short as 3.54A in the I_2 crystal. In view of this, the shortening of the van der Waals distances in the iodine complexes predicted by our theory is not as unreasonable as it might appear.

In this treatment, changes in a resulting from resonance and from unequal electrostatic forces on the two iodine atoms of the molecule have been neglected. This change is probably rather small because of the "stiffness" of the primary bond and is probably no more than a few hundredths of an angstrom unit. It presumably would affect the solution because of the following effects: (a) increasing a would decrease the polarizability, (b) increasing a would decrease K, (c) increasing a would affect the location of the average dipole. As the atoms become separated, the electrons spend less of their time between

[34] Harvey Dube, Thesis, Iowa State College (1947), p. 81.

the two atoms and it probably would not be correct to locate the dipole in the center of the molecule, but it should be considered to reside in the individual atoms. This is especially true if d and a are close together and resonance results in loss of molecular identity.

The absolute value of this stabilization energy should not be taken too seriously because of the uncertainty of the many assumptions necessary for solution. However, we believe that we have shown that it is possible by this mechanism to obtain a solution having the correct order of magnitude to account for the stability and qualitative behavior of the complex.

It is interesting to discuss the formation of a complex of definite composition in terms of this mechanism. It is seen that a long uninterrupted iodine chain is necessary for the manifestation of a cooperative effect. The enhancement of the interaction energy is a function of this chain length. Therefore, the decrease in energy per iodine molecule added will be greater, the more iodine already in the helix. There will then be a greater tendency for iodine to keep going into a helix once it has started than for it to start filling an empty helix. This process would be more energetically favorable as it proceeds until the helix is filled.

OTHER HALOGEN-POLYMER COMPLEXES

Recently, West[15,35] has found that many hydrophilic, organic polymers form complexes with iodine, bromine, and iodine-bromide. Aside from the amylose-iodine complex, the most notable iodine complex is probably that of polyvinyl alcohol.

Polyvinyl alcohol is known to form a complex with iodine which is similar in appearance and behavior to the starch-iodine complex. This complex appears to be very stable—it is not possible to measure the vapor pressure of iodine above it by ordinary methods.[15] Preliminary evidence indicates that the complex is also a *molecular compound* rather than a result of ordinary adsorption or solid solution formation.

The structure of crystalline polyvinyl alcohol has been determined by Mooney[13] and has been recently criticized by Bunn.[36] Mooney has

[35] C. D. West, J. Chem. Phys. 15, 689 (1947).
[36] Bunn, in *Advances in Colloid Science* (Interscience Publishers, New York, 1946), Vol. II, pp. 121–3.

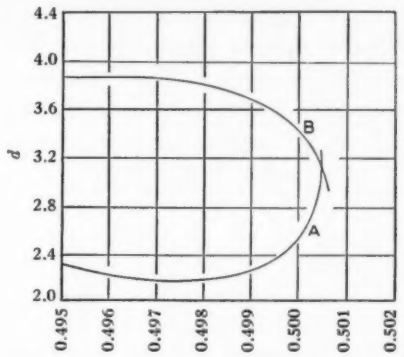

FIG. 11. The solution of the simultaneous equations.

postulated a structure consisting of parallel hydrocarbon chains interlinked by hydrogen bonds between the hydroxyl groups (Fig. 12). From considerations of complex forming ability, the most striking feature of this structure is that the hydroxyl groups are held in such a way that each contributes a re-enforcing component of dipole moment along the fiber axis. This would give rise to a field similar to that of the amylose helix. Also, there are channels parallel to this array of dipoles. Preliminary x-ray studies indicate that the iodine actually does reside in these channels.

West has found that the polymer halogen complexes studied produce x-ray reflections characteristic of a one-dimensional lattice with periods 3.10 (iodine), 2.70 (bromine) and 2.90A (iodine bromide) essentially independent of the polymer. He has interpreted these spacings as interatomic distances in linear polyhalogen chains.

As we have seen, equally spaced iodines are allowed by our theory only if there is complete resonance of the bond between nearest neighbors in the linear array. In this case each bond would have an electronic density of half an electron pair (bond number $\frac{1}{2}$ in Pauling's nomenclature)[37] and the expected bond distance is 2.85A (calculated in accordance with Pauling's rule, $R(1)-R(n)=0.300 \log n$, where n is the bond number and R the radius of the atom).[37] This is far shorter than West's spacing, which corresponds to a bond number of only 0.17 (again by Pauling's rule).

It seems very difficult to understand how the iodine—iodine bond in a polyiodine chain could have so low a bond number. Indeed, the bond

[37] Pauling, J. Am. Chem. Soc. 69, 542 (1947).

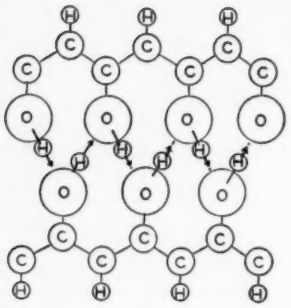

FIG. 12. The structure of polyvinyl alcohol (Mooney).

number is so low that halogen-halogen bonding appears to have nearly disappeared if West's interpretation is accepted. There is no chemical evidence to indicate that bonding to the polymer has replaced the original I—I bond in I_2 and, in fact, since the x-ray spacing of the halogen is unrelated to the fiber spacing of the polymer, polymer-iodine bonding is hardly possible.

Actually, the x-ray data are not sufficient to assure that the iodine atoms are equally spaced in the linear array. Only three orders of the spacing are observed even in "favorable circumstances," and it may well be that these are the even orders of a spacing twice as great (6.2A). (The fact that West has not observed a doubling of the spacing for the iodine-bromide complexes is further evidence that the data cannot be accepted as evidence for equally spaced, equivalent halogens.)

If we allow unequal spacings between iodine molecules, then a shortened van der Waals distance (our calculated value for the particular field assumed for the starch helix goes as low as 3.2A), and a normal, or more probably a somewhat lengthened, single bond distance could easily account for a 6.2A spacing. Of the first few x-ray reflections, only even orders could be visible. Indeed, the observed spacing is near enough to that which our calculations would predict as to tend to confirm the general validity of our procedure.

The observed spacings in bromine and iodine bromide complexes also correspond roughly to bond numbers of 0.17. Again, it appears more probable that the halogen atoms are unequally spaced, corresponding to halogen molecules separated by rather short van der Waals distances. It appears from the observed spacings that no known complexes have reached the limiting value of equally spaced halogens, though we should again emphasize that this possibility is not excluded.

Both the helical form of amylose and the usual form of polyvinyl alcohol provide polymer dipole fields in accord with the demands of the present proposal. It seems not unreasonable to suppose that these demands are met by other polymers forming halogen complexes, and that the mechanism, proposed here, aside from the very particular points peculiar to amylose structure can be carried over to explain the halogen complexing powers of other polymers.

It should be noted that the theory only strictly applies to the formation of the complex with dry amylose or polyvinyl alcohol and iodine in the vapor phase. In solution several additional complications arise. A consideration of the effect of the dielectric constant of an imbibing medium has been neglected. This approximation will be serious in aqueous solution where the fields may be materially reduced by polarization of the water. Also ions will enter the helix in solution and, as has been experimentally demonstrated,[4] will affect the stability of the complex.

It is somewhat disturbing that water which has a higher (macroscopic) dielectric constant than iodine does not preferentially enter the helix. Possibly water in the helix would exhibit a different structure from its macroscopic structure and would not orient to give a high polarization necessary for complex formation. It seems quite possible that through hydrogen bonding for specific hydroxyl groups, its action could be entirely local.

This model for the complex offers an explanation for the enhancement of the color of the iodine. It has been pointed out that the color of iodine in solution varies with the nature of the solvent. This probably results from the perturbation of the energy levels of the iodine molecule by the field of the solvent molecules in such a manner as to allow previously forbidden transitions. The same effect could obviously result from the action of the strong fields in the helix. Also, the resonance energy contribution may lower the energy levels sufficiently so as to shift the wave-length of absorption. While we calculate that resonance energy is only about 10

percent of the total binding energy, it should be noted that the resonance energy is a very sensitive function of inter-iodine distance in this region so that a slight error in calculation may materially change the resonance contribution.

ACKNOWLEDGMENT

The authors wish to express their appreciation to Professors Henry Eyring and Walter Kauzmann for discussions which have been of help in the preparation of this paper.

THE JOURNAL OF CHEMICAL PHYSICS VOLUME 16, NUMBER 3 MARCH, 1948

The Molecular Structure of Nitrogen Dioxide. A Reinvestigation by Electron Diffraction*

STIG CLAESSON, JERRY DONOHUE, AND VERNER SCHOMAKER
Department of Chemistry, California Institute of Technology, Pasadena, California

(Received November 18, 1947)

An investigation of the structure of the nitrogen dioxide molecule has been made by the electron diffraction method. The interpretation of the photographs, which showed rings extending to values of q of nearly $100(q=40/\lambda \sin\vartheta/2)$, leads to the following structural parameter values: $N-O=1.20\pm0.02A$, $<O-N-O=132\pm3°$. These values are discussed briefly and compared with those obtained by other methods.

INTRODUCTION

IN recent years the molecular structure of nitrogen dioxide has been the subject of numerous investigations but, aside from general agreement on a non-linear symmetrical structure with a wide bond angle and a multiplicity corresponding to only the odd electron, the conclusions have been surprisingly divergent. This is true of the dielectric constant measurements on the $NO_2-N_2O_4$ system, which have lead variously to the conclusions that both nitrogen dioxide and nitrogen tetroxide have small constant dipole moments of the order of 0.4×10^{-18} e.s.u., that of nitrogen tetroxide being the greater,[1,2] and that nitrogen dioxide has a moment of this magnitude which decreases with increasing temperature while nitrogen tetroxide has a zero moment.[3] It is especially true of the bond angle and bond distance estimates and determinations, which naturally concern us directly. However, Giauque and Kemp's[4] comprehensive considerations of the equilibrium measurements[5] on the dissociation of nitrogen dioxide in connection with spectroscopic data for nitric oxide,[6] oxygen,[7] and nitrogen dioxide rule out the suggestion of Zeise[8] that the molecule has a multiplicity of 4. This suggestion is likewise ruled out by the results of the magnetic susceptibility measurements of Havens,[9] as was pointed out by Harris and King.[10]

From consideration of an assumed electronic structure Pauling[11] predicted 1.18A for the nitrogen-oxygen distance and 140° for the angle O−N−O. On the assumption of a valence potential function and a frequency assignment suggested by the infrared spectrum Penney and Sutherland[12] obtained the value 114° for the bond angle. With a similar assumption but a slightly

* Contribution from the Gates and Crellin Laboratories of Chemistry, California Institute of Technology, No. 1156.
[1] C. T. Zahn, Physik. Zeits. **34**, 461 (1933).
[2] R. W. Schultz, Zeits. f. Physik **109**, 517 (1938).
[3] J. W. Williams, G. H. Schwingel, and C. H. Winning, J. Am. Chem. Soc. **58**, 197 (1936).
[4] W. F. Giauque and J. D. Kemp, J. Chem. Phys. **6**, 40 (1938).
[5] Especially those of M. Bodenstein and Lindner, Zeits. f. physik. Chemie **100**, 82 (1922).
[6] H. L. Johnston and A. T. Chapman, J. Am. Chem. Soc. **55**, 153 (1933).
[7] H. L. Johnston and M. K. Walker, J. Am. Chem. Soc., **55**, 172 (1933).
[8] H. W. Zeise, Zeits. f. Elektrochemie **42**, 785 (1936).
[9] G. G. Havens, Phys. Rev. **41**, 337 (1932).
[10] L. Harris and G. W. King, J. Chem. Phys. **8**, 775 (1940).
[11] L. Pauling, *The Nature of the Chemical Bond* (Cornell University Press, Ithaca, New York, 1940), second edition, p. 270.
[12] W. Penney and G. B. B. M. Sutherland, Proc. Roy. Soc. **A156**, 654 (1936).

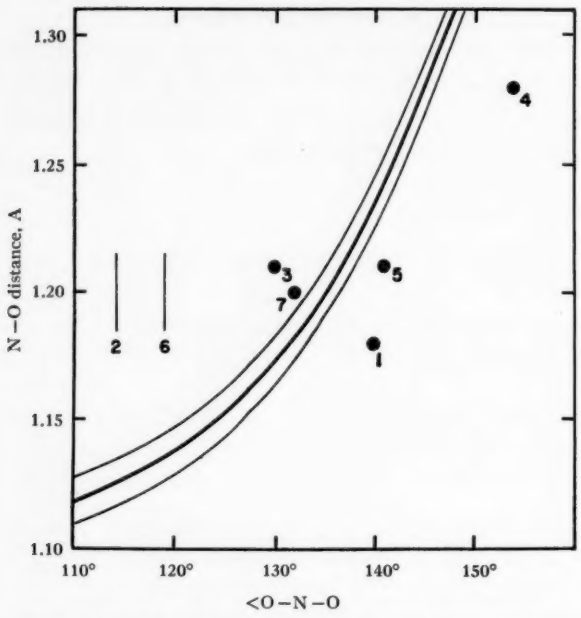

FIG. 1. Results of various estimates and determinations of the structure of nitrogen dioxide. 1: Pauling; 2: Penney and Sutherland; 3: Maxwell and Mosley; 4: Harris and King; 5: Spurr; 6: Herzberg; 7: This work. The curves show values consistent with the revised product of the moments of inertia and its limit of error.

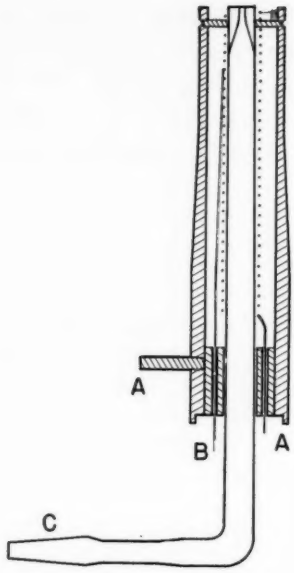

FIG. 2. High temperature nozzle used in this investigation. *A*: leads to heating coil; *B*: leads to thermocouple; *C*: standard taper joint to fit the tube containing the sample.

different assignment of frequencies Herzberg[13] obtained the value 119° for the bond angle. An early electron-diffraction study by Maxwell, Mosley, and Deming[14] was unable to give reliable structural information, but a subsequent investigation of Maxwell and Mosley[15] gave the values 1.21A and 130° for the two structural parameters; however a subsequent treatment of the data of Maxwell and Mosley by Spurr[16] gave the same value for the bond distance but the much higher value of 141° for the bond angle. On the other hand, after a partial analysis of the ultraviolet spectrum, Harris and King[10] reported 1.28A for the bond distance and 154° for the bond angle.

The calculations of Giauque and Kemp,[4] which were based on spectroscopic data[6,7] and equilibrium measurements of the dissociation of nitrogen dioxide,[5] gave a reliable value for the product of the moments of inertia, from which may be obtained an equation giving corresponding values of the bond distance and bond angle. Since the accepted values for natural constants have changed significantly since Giauque and Kemp made their calculations, we have calculated the change in the value of the product of the moments of inertia which results when the revised constants[13] are used.[17] We find that the value of $I_1I_2I_3$ must be revised upwards by 4.3 percent to 1.50×10^{-116} g^3 cm^6 if the vibrational assignment for nitrogen dioxide used by Penney and Sutherland[12]—the one used by Giauque and Kemp—is used; if the vibrational assignment of Herzberg[13] is used the value of $I_1I_2I_3$ must be revised upwards 3.0 percent. (An upward revision of $I_1I_2I_3$ of 2.6 percent is required by the changes in the rotational and translational parts of the calculation alone.) The value of $I_1I_2I_3$

[13] G. W. Herzberg, *Infrared and Raman Spectra* (D. Van Nostrand Company, Inc., New York, New York, 1945), p. 170.

[14] L. R. Maxwell, V. Mosley, and L. Deming, J. Chem. Phys. **2**, 331 (1934).

[15] L. R. Maxwell and V. Mosley, J. Chem. Phys. **8**, 738 (1940).

[16] R. Spurr, quoted in Yost and Russell, *Systematic Inorganic Chemistry* (Prentice-Hall, New York, New York, 1944), p. 27.

[17] In calculating the changes in the values of the thermodynamic quantities $(F°-H_0°)/T$ of nitric oxide and oxygen it was assumed that whatever change in these values would result from changing the constants is identical with the change in the calculated result for a rigid rotator harmonic oscillator approximation, plus a 120 cm^{-1} doubling of all levels of nitric oxide, since the original calculations (see references 7 and 8) made use of the spectroscopically observed levels and a recalculation on that basis would be somewhat complicated.

$=1.50\times10^{-116}$ g^3 cm^6 is probably known to about 5 percent.

We have reinvestigated the structure of nitrogen dioxide by the electron diffraction method; we find 1.20 ± 0.02A for the nitrogen-oxygen distance and $132\pm3°$ for the bond angle. This result together with the various results mentioned above are shown in Fig. 1.

EXPERIMENTAL

Nitrogen dioxide was prepared by heating lead nitrate in a stream of oxygen. The gas was condensed with dry ice and then twice distilled in an atmosphere of oxygen in an all-glass apparatus.

Electron diffraction photographs were taken with the apparatus described by Brockway.[18] An all-glass high-temperature nozzle of special design shown in Fig. 2, was used to heat the gas sample before the photographs were taken. The length of the chimney, which was heated to 140° before each exposure, was sufficient to insure that the dissociation of nitrogen tetroxide to nitrogen dioxide was complete before the gas entered the diffraction chamber.

The photographs were examined on a viewing box equipped with a lamp of adjustable intensity, and, for the outer rings, two or more good photographs were superimposed. Measurements of the diffraction features were made in the usual way.

Because of the simplicity of the problem the customary radial distribution treatment was omitted and only the correlation method[19] was used in interpreting the photographs. The formula

$$I(q)=\sum_{ij}\frac{Z_iZ_j}{r_{ij}}\sin\left(\frac{\pi}{10}r_{ij}q\right),$$

was used to calculate simplified theoretical intensity curves, shown in Fig. 3, for six models with N−O=1.20A and ∠O−N−O=125°, 130°, 132½°, 135°, 140°, and 145° respectively. These calculations were made on International Business Machines with punched cards.[20]

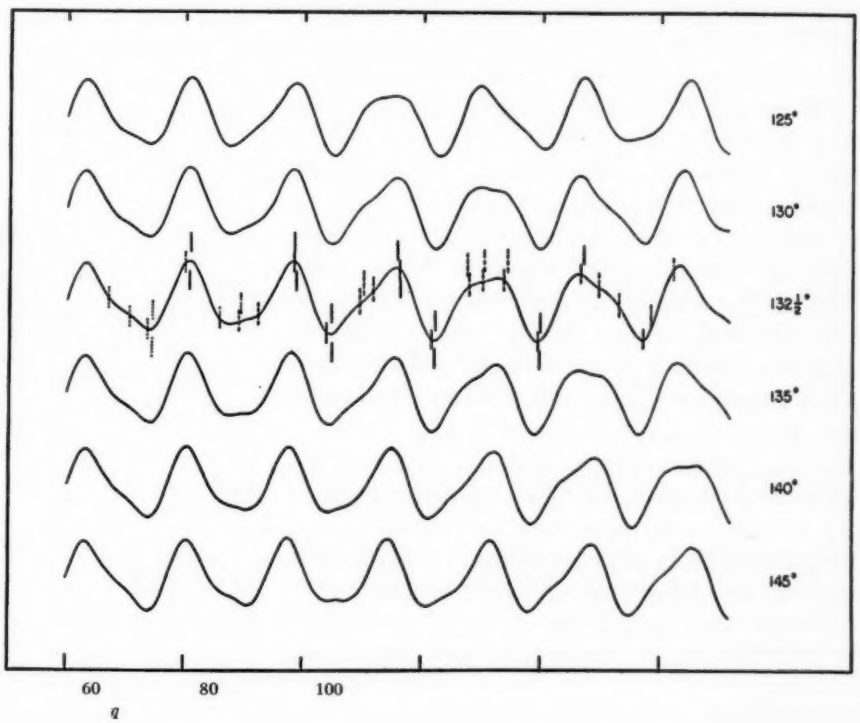

FIG. 3. Electron diffraction curves for nitrogen dioxide. Nitrogen-oxygen distance 1.20 A for all models, O−N−O angles as indicated. The three sets of lines with the curve for the 132½° model represent the measurements of the three observers: those below the curve: S. C.; on the curve: V. S.; above the curve: J. D.

[18] L. O. Brockway, Rev. Mod. Phys. **6**, 234 (1936). Wave length calibration: C. S. Lu and E. W. Malmberg, Rev. Sci. Inst. **14**, 2181 (1937). The lattice constants of zinc oxide given by them in *kX* units were converted to angstrom units.

[19] L. Pauling and L. O. Brockway, J. Chem. Phys. **2**, 867 (1934).

[20] P. A. Schaffer, Jr., V. Schomaker, and L. Pauling, J. Chem. Phys. **14**, 659 (1946).

TABLE I. Results of measurements of electron diffraction photographs of nitrogen dioxide.

Observer	Average value of $q_{132°}/q_{obs.}$	Average deviation	Number of features included in average
S. C.	0.996	0.006	6
J. D.	0.999	0.004	7
	0.999	0.008	12
V. S.	1.003	0.007	7
	1.002	0.008	16

RESULTS

As may be seen in Fig. 3, the character of the features of the theoretical intensity curves changes rapidly with change in bond angle. Comparison of these curves with the appearance of the photographs fixes the bond angle at $132\pm3°$. The features at $q\cong55$, 70, and 85 were particularly useful in fixing the bond angle. The relative heights of the components which comprise these three doublet maxima are in best agreement with the appearance of the photographs at 132°. At larger bond angles the outer components of the rings at $q\cong70$ and 85 are too strong; at smaller bond angles the inner components of the rings at $q\cong55$ and 70 are too strong, and the outer component of the ring at $q\cong85$ disappears.

Between seven and twenty-five measurements were made on each of the features measured by the three observers. The average values of $q_{132°}$ (obtained by interpolation) divided by $q_{obs.}$ are presented in Table I. We consider those obtained from the measurements indicated by the solid lines in Fig. 3 to be the most reliable. The averages obtained from these measurements together with those indicated by the dashed lines in Fig. 3 include features which are more difficult to measure; it is interesting that the average values of $q_{132°}/q_{obs.}$ are not changed appreciably by including these measurements. The averages $q/q_{obs.}$ and the average deviations were calculated for the measurements of the smaller sets of features of each of the three observers for the 125°, 130°, 135°, and 140° models also. In each case there is a convincing minimum in the average deviations very near 132°, substantiating the value of the bond angle determined by the correlation treatment. Measurements on the extreme inner and outer features, indicated by dotted lines in Fig. 3, were considered by the respective observers to be unreliable, and were not included in any averages. The averaged results of the three observers give for the nitrogen-oxygen distance 1.20A. In consideration of the average deviations shown in Table I and the uncertainty in the bond distance arising from the uncertainty in the bond angle obtained by the correlation treatment, we estimate the limit of error of the nitrogen-oxygen distance to be ±0.02A.

DISCUSSION

Our results are in fairly good agreement with the previous electron diffraction results of Maxwell and Mosley;[15] we feel that ours are somewhat more accurate because we observed features at larger q values than did the previous investigators. Moreover, our results are in better agreement with the product of the moments of inertia. It is apparent that the structures derived from the spectroscopic considerations[10,12,13] are considerably in error.

The structure found for the nitrogen dioxide molecule is in good qualitative agreement with the discussion of Pauling,[11] who predicted a bond distance slightly larger than that of a nitrogen-oxygen double bond, and a bond angle intermediate between 125°16′, the double bond value, and 180°, corresponding to the following resonating structure for the molecule:

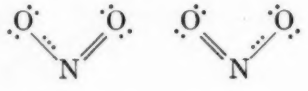

ACKNOWLEDGMENT

We wish to thank Mr. Kenneth Hedberg for his assistance in preparing the photographs.

Indirect Measurement of Spectral Line Breadth in the Infra-Red*

A. M. THORNDIKE**
Mallinckrodt Chemical Laboratory, Harvard University, Cambridge, Massachusetts

(Received November 18, 1947)

If infra-red absorption by a sample gas is measured at low resolution in the presence and absence of pressure broadening by a non-absorbing gas, information may be obtained concerning breadth and fine structure of individual rotational lines. Data on 590-cm^{-1} and 1285-cm^{-1} bands of N_2O indicate self-broadening coefficients of about 0.21 and 0.13 cm^{-1} per atmosphere, respectively. These values may be compared with 0.20 cm^{-1} per atmosphere obtained by Adel and Barker by direct measurement on the 590-cm^{-1} band.

IT is very difficult to construct an infra-red spectrograph of sufficiently high resolving power that line breadths can be measured directly for molecular vibration spectra. By using the following indirect method one can obtain an estimate of line breadth in some cases on the basis of measurements made with a spectrograph of low resolution, provided the line spacing is known. Since spacings have been measured for many molecules the method may be of interest, although the author has not had an opportunity to conduct a detailed investigation of its possibilities.

An infra-red band is composed of a large number of lines, each of which absorbs strongly, with regions of slight absorption often lying between the lines. A spectrograph of low resolution measures an average value of the absorption over several lines. This average value depends on the extent of the "gaps" between the lines, and hence on the line breadth. If the individual lines are adequately pressure broadened, it is possible to measure the true intensity of absorption.[1] If the individual lines are pressure-broadened to a lesser extent, the observed absorption depends on both true intensity and line width, and may be used to measure the line width.[2] In particular, we may compare the absorption of pure sample gas with that obtained when an inert (non-absorbing) gas is added for pressure broadening.

Such a comparison was made in a qualitative way during an investigation of the effect of the addition of inert gas upon measurements of absolute intensities. In the case of the N_2O 1285-cm^{-1} band, which was studied, addition of inert gas caused a very marked increase in the observed absorption.[3]

In order to carry out this procedure quantitatively a number of simplifying restrictions must be introduced.[4] We assume that in the frequency range transmitted by the spectrograph at any setting: (a) the lines are equally spaced, equally intense, and sufficiently widely spaced that they do not overlap, (b) that their shape is given by the Lorentz formula, and (c) that the incident intensity does not depend on frequency. Experimental conditions can be found which satisfy these requirements fairly well for many bands. Then the fraction, g, of light absorbed *by pure gas* is given by

$$g=\frac{1}{s}\int_{\nu_0-(s/2)}^{\nu_0+(s/2)}\left\{1-\exp\left[\frac{-A\delta pL}{\pi(\delta^2+(\nu-\nu_0)^2)}\right]\right\}d\nu. \quad (1)$$

Here s = spacing between lines, ν_0 = frequency of line center, A = intensity of a line, δ = half-width of line, p = gas pressure, and L = length of absorption cell. Since lines do not overlap, we

* Most of the material of this paper is taken from a thesis submitted to the Faculty of Arts and Sciences of Harvard University for the degree of Doctor of Philosophy in Chemical Physics on May 1, 1947.

** National Research Council Predoctoral Fellow; now at Brookhaven National Laboratory, Upton, New York.

[1] E. Bright Wilson, Jr. and A. J. Wells, J. Chem. Phys. 14, 578 (1946). See also, A. M. Thorndike, A. J. Wells, and E. Bright Wilson, Jr., J. Chem. Phys. 15, 157 (1947), and A. M. Thorndike, J. Chem. Phys. 15, 868 (1947).

[2] The use of techniques of this sort was first suggested by Summerfield and Strong, Phys. Rev. 59, 217 (1941). A general discussion of factors influencing the observed absorption of infra-red bands has been given by Nielsen, Thornton, and Dale, Rev. Mod. Phys. 16, 307 (1944).

[3] This effect has been studied by many investigators, for example: E. von Bahr, Ann. d. Physik 29, 780 (1909); 33, 585 (1910). P. C. Cross and F. Daniels, J. Chem. Phys. 2, 6 (1934); N. D. Coggeshall and E. L. Saier, J. Chem. Phys. 15, 65 (1947).

[4] Very similar assumptions were used by Grasse (Zeits. f. Physik 89, 261 (1934)) in calculating line breadths for HCl by a somewhat different method.

may extend the integration to infinity and introduce a change of variables to obtain

$$g=\frac{ApL}{s}f(k),$$

where

$$f(k)=\int_{-\infty}^{\infty}\left\{1-\exp\left[\frac{-k}{\pi(k^2+x^2)}\right]\right\}dx, \qquad (2)$$

$$\delta=ALkp, \quad \nu-\nu_0=ALpx.$$

We have used the fact that line width, δ, is proportional to pressure, with the result that the fraction absorbed, g, is a linear function of the path length, (pL), having slope $G=g/(pL)\equiv(A/s)f(k)$. Such a linear function was, in fact, observed experimentally, and the above argument developed to account for the observation.

If, on the other hand, a non-absorbing gas is added to give pressure broadening, it is possible to estimate the line intensity, A. We measure the "apparent absorption coefficient," given by

$$\lim_{pL\to 0}\left(-\frac{1}{pL}\ln\frac{T}{T_0}\right),$$

where T is the light transmitted through the absorbing gas and T_0 is the incident light.[1] Then, since we are dealing with a series of identical lines:

$$A=s\left[\lim_{pL\to 0}\left(\frac{1}{pL}\ln\frac{T_0}{T}\right)\right]. \qquad (3)$$

That is, $A/s\equiv A'$ is the slope of $\ln(T_0/T)$ (plotted as a function of path length) for zero path length.

From calculated values of $f(k)$, therefore, and an experimental value of G/A, we determine k using Eq. (2). This determines δ/p, that is, the line breadth per unit of pressure.

The method is applicable only to bands with simple structure and fairly wide spacing between lines, such as those of diatomic or linear molecules. The data used to evaluate G should be at pressures substantially less than one atmosphere, and the fraction of light absorbed should be less than 50 percent to approximate the non-overlapping requirement.

With this procedure, line breadths, or rather self-broadening coefficients, have been determined for parts of the N_2O bands at 1285 cm^{-1} and 590 cm^{-1}. In each case the region selected was that of a branch maximum where the lines are most nearly equal in intensity. The actual frequencies selected were about 1270 cm^{-1} and 600 cm^{-1}.

In Fig. 1 the experimental data are plotted for the 590-cm^{-1} band. Those for the 1285-cm^{-1} band show an even greater difference between absorptions with and without added inert gas. In both cases the curve for absorption by pure gas is straight in the middle with portions at both ends which are concave downwards. At high pressures this is due to overlapping of the lines, at low pressures to Doppler line breadth which introduces a constant line width rather than one proportional to pressure.[5]

If we assume that each band consists of a series of single lines spaced about 0.86 cm^{-1} apart,[6] the results are as given in Table I.

As far as order of magnitude goes the two results are in agreement with each other and with expectations. Direct measurements by Adel and Barker on the 590-cm^{-1} band gave a half-width of 0.08 cm^{-1} at a pressure of 30-cm Hg, corresponding to 0.20 cm^{-1} per atmosphere.[7] The excellent agreement between our value for the 590-cm^{-1} band and that of Adel and Barker is

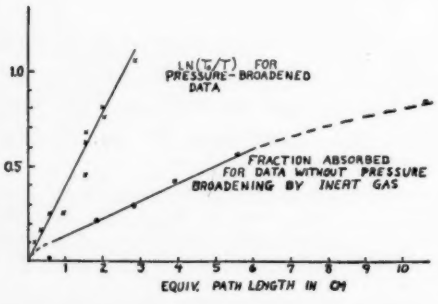

FIG. 1. Experimental data on absorption by 590-cm^{-1} band of N_2O at a frequency of about 600 cm^{-1}.

[5] At room temperature the velocity of an N_2O molecule is about 3×10^4 cm per sec., so that the line breadth attributable to Doppler effect is about $(3\times10^4/3\times10^{10})\times600=.0006$ cm^{-1}. The self-broadening resulting from collisions is here estimated to be about 0.2 cm^{-1} per atmosphere; a pressure of 0.003 atmosphere would therefore lead to a line breadth comparable to the Doppler line breadth. The cell length is 30 cm, so that this pressure corresponds to a path length of about 0.1 cm. For such path lengths, therefore, Doppler line breadth becomes important.

[6] E. K. Plyler and E. F. Barker, Phys. Rev. **38**, 1827 (1931).

[7] A. Adel and E. F. Barker, Rev. Mod. Phys. **16**, 236 (1944) as corrected by A. Adel, Phys. Rev. **71**, 806 (1947).

TABLE I.

Data on N_2O line breadths.

	1285-cm^{-1} band	590-cm^{-1} band
Slope, G	0.28	0.090
Slope, A'	5.75	0.40
$f(k)$	0.049	0.225
k	0.00090	0.015
δ/p, in cm^{-1} per atmos.	0.13	0.21

probably fortuitous. A possible explanation of the discrepancy between our results for the two bands is that weak lines from difference bands which overlap the 590-cm^{-1} band contribute to the absorption in this case and lead to the higher value for the line width. If so, the result for the 1285-cm^{-1} band is the more significant. Here our value is lower than that of Adel and Barker.

A further application of this sort of procedure which would lead to information concerning unresolved fine structure should be possible. It would be necessary to carry out measurements over a wide range of pressures of the pure gas, so that at the lower pressures the lines would be separate, whereas at the higher they would merge because of increased line breadth. Different values for the slope, G, should be observed in the two regions, and from them information could be deduced concerning the fine structure splitting provided it was considerably greater than the Doppler line breadth of about 0.001 cm^{-1}. No experiments of this type were carried out, however.

In many cases information of this type may be gained with much greater accuracy from the very high resolution of microwave spectroscopy. Microwave techniques are, however, not in general applicable at present to molecules of small, or vanishing, dipole moment. The indirect method described above may be valuable in such cases.

THE JOURNAL OF CHEMICAL PHYSICS VOLUME 16, NUMBER 3 MARCH, 1948

Force Constants for Some Halomethanes*

J. C. DECIUS**
Mallinckrodt Chemical Laboratory, Harvard University, Cambridge, Massachusetts
(Received November 25, 1947)

Valence-type force constants, including several interaction terms, have been deduced from some of the experimentally observed fundamental vibration frequencies of the molecular sequence CX_4, CX_3Y, CX_2Y_2, CXY_3, and CY_4 in which X may be chlorine or bromine, Y hydrogen or deuterium. By assuming that the force constants are invariant for the different molecules and by neglecting several interaction constants associated with two bending motions, the number of distinct constants was reduced to 28, from which, after slight adjustment, 100 vibration frequencies were calculated. The quality of the fit with the experimental frequencies is indicated by a reasonably low root mean square deviation between calculation and observation (1.1 percent for 82 frequencies) and by the success of the constants in predicting 22 of the frequencies which were not used in the initial numerical evaluation of the constants.

I. INTRODUCTION

IN the study of the vibrational spectra of polyatomic molecules it is at present not feasible to calculate the vibrational frequencies *a priori*, even in the harmonic oscillator approximation, since the quantum mechanical problem of deducing internuclear potential functions, solved in principle by Born and Oppenheimer[1] has not in practice been developed sufficiently to allow explicit representations of the potential energy associated with small displacements of the nuclei from their equilibrium configuration, except for very simple molecules. In order, therefore, to facilitate the interpretation of the structure of increasingly complex molecules from their vibrational spectra, it has proved worth while to calculate empirically the values of force constants for various types of quadratic potential functions. Two types of such functions have been principally used: central and valence force systems. In either system, the number of constants in the most general quadratic form, even after consideration of symmetry, generally exceeds the number of independent data, i.e., the observed frequencies. The situation may, of course, be improved if isotopically substituted molecules have been studied experimentally. On the other hand, most attempts to fit the observed spectra with the minimum number of parameters, as with a diagonal potential function (no interaction constants), are less and less successful as the size of the molecule increases.

It is the purpose of this paper to continue the attempt, initiated by Crawford and Brinkley[2] and others, to obtain a set of force constants, including some interaction terms, which can be used without change for a variety of molecules to predict the vibration frequencies with reasonable precision. The molecules involved constitute the sequence CX_4, CX_3Y, CX_2Y_2, CXY_3, and CY_4 in which X may be either Cl or Br and Y either H or D.

II. COORDINATE BASIS AND KINETIC ENERGY MATRIX ELEMENTS

A coordinate basis of the valence type has been chosen and the following nomenclature adopted:

$$R=\Delta(C-X),$$
$$r=\Delta(C-Y),$$
$$\alpha=\Delta(X-C-Y),$$
$$\beta=\Delta(X-C-X),$$
$$\eta=\Delta(Y-C-Y).$$

I.e., the Roman letters are used to denote bond stretches and Greek letters designate bond bendings.

The potential and inverse kinetic energy matrix elements relative to such a basis are identified by the following scheme of notation. The f or g

* From a thesis submitted to the Faculty of Arts and Science, Harvard University, in partial fulfillment of the requirements for the degree of Doctor of Philosophy.
** Present address: Metcalf Research Laboratory, Brown University, Providence, Rhode Island.
[1] M. Born and J. R. Oppenheimer, Ann. d. Physik **84**, 457 (1927).
[2] B. L. Crawford, Jr. and S. R. Brinkley, Jr., J. Chem. Phys. **9**, 64 (1941).

identifying a potential energy or inverse kinetic energy matrix element respectively is followed by literal subscripts designating which types of valence coordinates are involved. When this much is specified there remain several possibilities in most cases: these are distinguished by the use of numerical superscripts. As an example, consider the matrix element corresponding to a combination of H−C stretching and H−C−Cl bending. Since the H may or may not be common to the pair of coordinates, f_{ra}^{1} if used in case the H is common and f_{ra}^{2} is used when different H atoms are involved. All such combinations will be identified below by figures giving the numbering of coordinates and tables in which the individual f matrix elements are defined relative to the numbered coordinates.

The individual g matrix elements have not been tabulated here, since it is planned to present an extensive tabulation of these quantities, both algebraically and numerically, in a forthcoming paper. They have been computed by the vector method of Wilson.[3]

The molecular parameters which enter the calculations of the inverse kinetic energy matrix elements are the reciprocal masses of the individual atoms, the reciprocals of the interatomic distances, and trigonometric functions of the bond angles. The following numerical values have been adopted in these calculations:

Mass (atomic wt. units)		Distance (A)	
C	12.01	C−Cl	1.75
Cl	35.457	C−Br	1.88
Br	79.916	C−H	1.093
H	1.008	C−D	1.093
D	2.0147		

All bond angles have been assumed tetrahedral, i.e., 109°28′.

Refined studies of rotational spectra and electron diffraction may indicate small variations of bond lengths in different molecules, but the present assumption of constancy is consistent with that of the invariance of the force constants.

III. SYMMETRY FACTORING

A. General Procedure

Once the matrix elements have been set up in a valence coordinate basis, it is still necessary to transform them to a symmetry coordinate basis in order to realize the fullest factoring of the secular determinant possible by group theory. Previously, this has been accomplished by forming, more or less by inspection, linear combinations of the valence coordinates which exhibit the transformation properties characteristic of the irreducible representations of the point group of the molecule. In the following treatment, use is made of a more systematic method developed by Lippman[4] in an unpublished work. According to Lippman's method, there exist transformation formulas of the form

$$f_{ip,\,jq}^{(k)} = \sum_{m=1}^{v_{ij}} \gamma_{ij}^{m} a_{ip,\,jq}^{(k)m} f_{ij}^{m} \qquad (1)$$

Here $f_{ip,\,jq}^{(k)}$ is a potential energy matrix element in a symmetry coordinate basis, (fully factored) formed from valence coordinates of the ith and jth classes (corresponding to particular bond stretches and/or deformations as described above, such as H−C stretching and H−C−Cl bending). The summation index, m, refers to the various possible valence coordinate matrix elements of this particular pair of coordinate types, with v_{ij} the number of such different matrix elements, f_{ij}^{m}. The indices p and q in the general case may have a maximum range of 3, but for the sequence of molecules presently to be considered, the maximum number of symmetry coordinates which are formed from any given valence coordinate type appearing in a given irreducible representation (identified by the index k) is only one, and the indices p and q which are associated with this possible multiplicity, assume only the value of unity and will henceforth be omitted. Under these conditions, the "symmetry coefficients," $a_{ij}^{(k)m}$, and the "multiplicities," γ_{ij}^{m}, can be determined as follows. Let u_i denote the number of valence coordinates in the ith set and let β_{ij}^{m} denote the number of times f_{ij}^{m} occurs in the first row of F_{ij}, the submatrix of F which corresponds to all rows of coordinates of type i and all columns of coordinates of type j. Then

$$\gamma_{ij}^{m} = \beta_{ij}^{m} \left(\frac{u_i}{u_j}\right)^{\frac{1}{2}} \qquad (2)$$

[3] E. B. Wilson, Jr., J. Chem. Phys. **9**, 76 (1941).

[4] Caro Lippman, private communication, Harvard University.

TABLE I. Characters and frequency distribution for CX_4.

T_d	E	$8C_3$	$6\sigma_d$	$6S_4$	$3S_4^2=3C_2$	n_R	n_β	n'	n	Selection rule
A_1	1	1	1	1	1	1	1	1	1	$R(p)$
A_2	1	1	−1	−1	1	0	0	0	0	I
E	2	−1	0	0	2	0	1	0	1	$R(d)$
F_1	3	0	−1	1	−1	0	0	0	0	I
F_2	3	0	1	−1	−1	1	1	0	2	IR, $R(d)$
χ^R	4	1	2	0	0					
χ^β	6	0	2	0	2					
χ'	1	1	1	1	1					
χ	9	0	3	−1	1					

and, when $i=j$

$$a_{ii}^{(k)m}=\frac{u_i}{h}\sum_{r\epsilon H_{im}}\chi_r^{(k)}, \tag{3}$$

where h is the order of the group, $\chi_r^{(k)}$ is the character of the rth group element in the kth irreducible representation, and the summation is to be extended over the set of those group elements, H_{im},† which have the property of sending the first coordinate of the ith type into one whose order number is m, which is in turn defined as the order number of any column in the first row of F_{ii} occupied by f_{ii}^m. When $i\neq j$

$$a_{ij}^{(k)m}=\frac{\pm(\beta_{ij}^1)^{\frac{1}{2}}\sum_{t(m)}a_{jj}^{(k)t(m)}}{\beta_{ij}^m\left(\sum_{t(1)}a_{jj}^{(k)t(1)}\right)^{\frac{1}{2}}}, \tag{4}$$

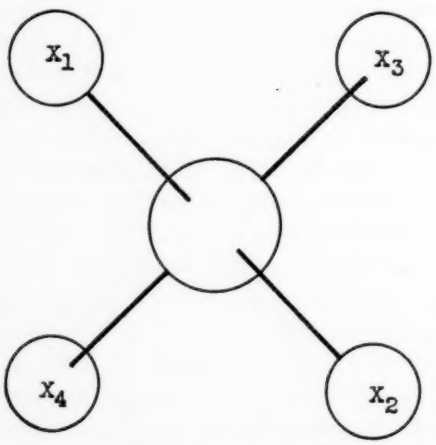

FIG. 1. Coordinates for CX_4. $R_i=\Delta CX_i$, $\beta_1=\Delta X_1CX_2$, $\beta_2=\Delta X_1CX_3$, $\beta_3=\Delta X_1CX_4$, $\beta_4=\Delta X_2CX_3$, $\beta_5=\Delta X_3CX_4$, $\beta_6=\Delta X_4CX_2$.

† H_{im} is one of the cosets determined by H_{i1}, the subgroup which leaves the first coordinate of the ith set invariant.

where

$$a_{jj}^{(k)t(m)}=a_{jj}^{(k)m}, \tag{5}$$

and the summations over $t(m)$ and $t(1)$, respectively, are extended over those columns in which f_{ij}^m and f_{ij}^1 appear in the first row of F_{ij}.

These expressions become especially simple when $\chi_1^{(k)}=1$ (dimension of the irreducible representation equals unity). They are then

$$a_{ij}^{(k)m}=\chi_r^{(k)}, \quad r\epsilon H_{im}, \tag{6}$$

and, in particular, for the totally symmetric representation

$$a_{ij}^{(1)m}=1. \tag{7}$$

The transformation scheme for the inverse kinetic energy matrix elements is identical with that for the potential energy matrix just described.

B. The CX_4 and CY_4 Molecules

The initial assumption of tetrahedral angles compels consideration of T_d symmetry for these molecules. The coordinates are numbered as in Fig. 1. The symmetry factoring is illustrated by Table I.

The first six rows and columns in Table I define the irreducible representations and their characters. The columns headed n_R and n_β give, respectively, the number of times symmetry coordinates formed from each of these valence coordinates appear in the factored secular equation. In general, $n_i^{(k)}$ is found from the character relation,

$$n_i^{(k)}=\frac{1}{h}\sum_j\rho_j\chi_j^{(k)}\chi_j^{i}\dagger\dagger \tag{8}$$

$$n_i^{(k)}=\frac{u_i}{h}\sum_{r\epsilon H_{i1}}\chi_r^{(k)}.$$

where ρ_j is the number of elements in the jth class, $\chi_j^{(k)}$ the character of the jth class in the kth irreducible representation, and χ_j^i the character of the jth class in the representation afforded by the ith set of valence coordinates; this latter quantity is merely the number of coordinates of the ith set taken into themselves by a given group element of the jth class.

In this scheme, in general, there may exist redundant coordinates: the column headed n'

†† Lippman (reference 4) has shown that this expression can be contracted to

TABLE II. Force constants for the CX_4 molecule.

	R				β					
	1	2	3	4	1	2	3	4	5	6
R	f_R^1	f_R^2	f_R^2	f_R^2	$f_{R\beta}^1$	$f_{R\beta}^1$	$f_{R\beta}^1$	$f_{R\beta}^2$	$f_{R\beta}^2$	$f_{R\beta}$
β					f_β^1	f_β^2	f_β^2	f_β^2	f_β^3	f_β^2

gives the number of redundancies in each factor, while the last column represents the net order of each factor. The entries of the last column are readily determined by equations similar to (8) with χ_j^i replaced by χ_j, where χ_j is to be determined, for example, by the method of Rosenthal and Murphy,[5] and is merely the character of the complete set of genuine vibrations (internal displacements involving no displacement of the center of mass and no rotation) of the molecule.

The selection rules are given in the last column, where R means Raman active, IR means infrared active, I means inactive in both spectra, p and d mean polarized and depolarized, respectively.

Table II defines the potential energy matrix elements relative to the valence coordinate basis.

Note that the terms of the type f_{ii}^m are abbreviated as f_i^m. Finally, the symmetry analysis of the CX_4 molecule is completed by tabulating the multiplicities and symmetry coefficients (Table III).

Thus, by the use of Eq. (2), the symmetry factored $\mathfrak{F}$‡ matrices become

$$\begin{aligned} A_1:&\quad f_R^1+3f_R^2 \quad (6)^{\frac{1}{2}}(f_{R\beta}^1+f_{R\beta}^2)\\ &\qquad\qquad\quad f_\beta^1+4f_\beta^2+f_\beta^3\\ E:&\qquad\qquad\quad f_\beta^1-2f_\beta^2+f_\beta^3\\ F_2:&\quad f_R^1-f_R^2 \quad (2)^{\frac{1}{2}}(f_{R\beta}^1-f_{R\beta}^2)\\ &\qquad\qquad\quad f_\beta^1-f_\beta^3 \end{aligned}$$

in which the elements below the principal diagonal have been omitted on account of the symmetry of the matrices.

The corresponding $\mathcal{G}$ matrices are:

	CCl_4		CBr_4	
	R	β	R	β
A_1:	.02820	0	.01251	0
		0		0
E:		.02763		.01062
F_2:	.13922	−.12688	.12354	−.11811
		.16342		.13272

[5] J. Rosenthal and G. M. Murphy, Rev. Mod. Phys. **8**, 317 (1936).

‡ Roman symbols stand for matrices relative to the valence coordinates and script symbols for matrices relative to symmetry coordinates.

TABLE III. Multiplicities and symmetry coefficients for CX_4.

	R		$R\beta$		β		
f_{ij}^m	f_R^1	f_R^2	$f_{R\beta}^1$	$f_{R\beta}^2$	f_β^1	f_β^2	f_β^3
γ_{ij}^m	1	3	$(6)^{\frac{1}{2}}$	$(6)^{\frac{1}{2}}$	1	4	1
A_1	1	1	1	1	1	1	1
E	0	0	0	0	1	$-\frac{1}{2}$	1
F_2	1	$-\frac{1}{3}$	$(3)^{-\frac{1}{2}}$	$-(3)^{-\frac{1}{2}}$	1	0	−1

In this case, the redundancy in the A_1 factor is revealed directly by the vanishing column; this corresponds, of course, to the condition:

$$\sum_{l=1}^{6}\beta_l=0. \tag{9}$$

In the general case, the redundancy may appear in the $\mathcal{G}$ matrix only as a linear dependence between the columns.

In the analysis of the remaining molecules, the $\mathfrak{F}$ matrices will not be given explicitly, since they can be constructed immediately once a table corresponding to Table III has been given.

The treatment of the CY_4 molecule is formally identical with that just given for CX_4, requiring only the substitution of coordinates r for R and η for β. The $\mathcal{G}$ matrices are:

	CH_4		CD_4	
	r	η	r	η
A_1:	0.99206	0	0.49634	0
		0		0
E:		2.4912		1.2464
F:	1.1031	−0.20314	0.60736	−0.20314
		2.0325		1.2027

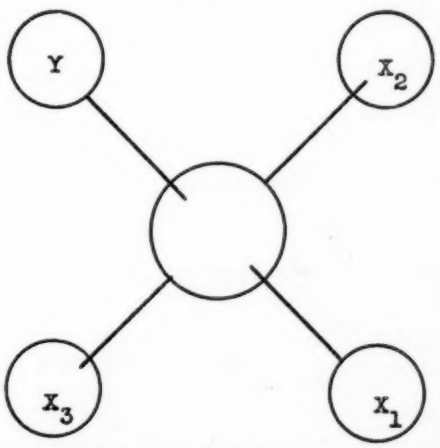

FIG. 2. Coordinates for CX_3Y: for CXY_3, permute X and Y, R and r, substitute η for β. $R_i=\Delta CX_i$, $r=\Delta CY$, $\alpha_i=\Delta X_iCY$, $\beta_1=\Delta X_2CX_3$, $\beta_2=\Delta X_1CX_2$, $\beta_3=\Delta X_1CX_2$.

TABLE IV. Characters and frequency distribution for CX_3Y.

C_{3v}	E	$2C_3$	$3\sigma v$	n_R	n_r	n_α	n_β	n'	n	Selection rule
A_1	1	1	1	1	1	1	1	1	3	$IR, R(p)$
A_2	1	1	−1	0	0	0	0	0	0	I
E	2	−1	0	1	0	1	1	0	3	$IR, R(d)$
χ^R	3	0	1							
χ^r	1	1	1							
χ^α	3	0	1							
χ^β	3	0	1							
χ'	1	1	1							
χ	9	0	3							

TABLE V. Force constants for the CX_3Y molecule.

	R			r	α			β		
	1	2	3		1	2	3	1	2	3
R	f_R^1	f_R^2	f_R^2	f_{Rr}^1	$f_{R\alpha}^1$	$f_{R\alpha}^2$	$f_{R\alpha}^2$	$f_{R\beta}^2$	$f_{R\beta}^1$	$f_{R\beta}^1$
r				f_r^1	$f_{r\alpha}^1$	$f_{r\alpha}^1$	$f_{r\alpha}^1$	$f_{r\beta}^1$	$f_{r\beta}^1$	$f_{r\beta}^1$
α					f_α^1	f_α^2	f_α^2	$f_{\alpha\beta}^2$	$f_{\alpha\beta}^1$	$f_{\alpha\beta}^1$
β								f_β^1	f_β^2	f_β^2

C. The CX_3Y and CXY_3 Molecules

These molecules possess the point group symmetry C_{3v}. The coordinates are numbered in accordance with Fig. 2. Tables IV to VI give the details of the symmetry factoring.

The nine fundamental frequencies are accounted for by two third-order determinants, one of which is doubly degenerate. The redundancy anticipated in the totally symmetric factor is obviously associated with the α- and β-coordinates.

The table of multiplicities and symmetry coefficients is considerably condensed by noting the identical symmetry properties of the coordinates R, α, and β.

The symmetry treatment of the CXY_3 molecule is almost identical when the substitutions r for R and η for β are performed. In addition, however, the matrix element f_α^2 must be replaced by f_α^3, the former involving two $X-C-Y$ bendings with a common Y and the latter, two such coordinates with a common X.

The $\mathcal{G}$ matrices for the different factors of the molecules of this class are now given in numerical form:

	A_1			E		
	R	r	α	R	α	β
CCl_3H:	0.05596	−0.04807	0.04486	0.13922	−0.13016	0.08972
		1.07532	−0.07770		1.40744	−0.10058
			0.08170			0.09553
CCl_3D:	0.05596	−0.04807	0.04486	0.13922	−0.13016	0.08972
		0.57960	−0.07770		0.78502	−0.10058
			0.08170			0.09553
CBr_3H:	0.04027	−0.04807	0.04176	0.12354	−0.12861	0.08352
		1.07532	−0.07233		1.39815	−0.09498
			0.06636			0.07167
CBr_3D:	0.04027	−0.04807	0.04176	0.12354	−0.12861	0.08352
		0.57960	−0.07233		0.77574	−0.09498
			0.06636			0.07167
	r	R	α	r	α	η
$CClH_3$:	1.01981	−0.04807	0.07182	1.10308	−0.10320	0.14364
		0.11147	−0.12346		0.94016	0.28168
			1.01627			2.26190
$CClD_3$:	0.52409	−0.04807	0.07182	0.60736	−0.10320	0.14364
		0.11147	−0.12346		0.52521	0.07421
			0.60133			1.22452
$CBrH_3$:	1.01981	−0.04807	0.07182	1.10308	−0.09855	0.14364
		0.09578	−0.12346		0.92319	0.29770
			1.01627			2.26190
$CBrD_3$:	0.52409	−0.04807	0.07182	0.60736	−0.09855	0.14364
		0.09578	−0.12346		0.50825	0.08023
			0.60133			1.22452

In tabulating these matrices, columns in the A_1 factor corresponding to a symmetry coordinate of type β in the case of CX_3Y and η in the case of CXY_3 have been omitted since they are exactly the negatives of the columns headed by α. This is evidence of the redundancies

$$\sum_{l=1}^{3}(\alpha_l+\beta_l)=0 \qquad (10)$$

and

$$\sum_{l=1}^{3}(\alpha_l+\eta_l)=0 \qquad (11)$$

in CX_3Y and CXY_3, respectively. In such cases it has been shown[3] that a column (and row) of $\mathfrak{G}$ involved in the linear dependence may be ignored, provided an appropriate transformation is made upon $\mathfrak{F}$, resulting in a reduction of its order by unity.

D. The CX_2Y_2 Molecule

Coordinates are numbered in accordance with Fig. 3. Tables VII to IX give the symmetry factoring, based on the assumption of C_{2v} symmetry.

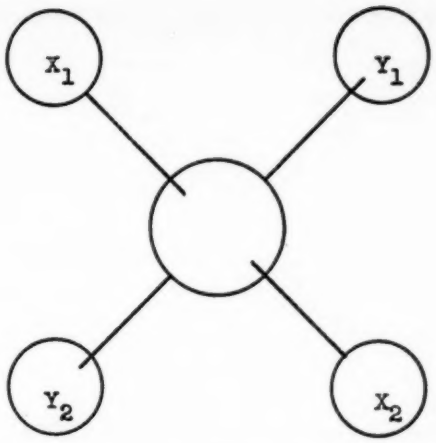

FIG. 3. Coordinates for CX_2Y_2. $R_i=\Delta CX_i$, $r_i=\Delta CY_i$, $\alpha_1=\Delta X_1CY_1$, $\alpha_2=\Delta X_1CY_2$, $\alpha_3=\Delta X_2CY_2$, $\alpha_4=\Delta X_2CY_1$, $\beta=\Delta X_1CX_2$, $\eta=\Delta Y_1CY_2$.

The A_1 factors for these molecules contain redundancies involving symmetry coordinates of types α, β, and η. In this case, the α-column has been omitted in the tabulation:

CCl_2H_2:

A_1:	R	r	β	η	B_2:	r	α
	0.08371	−0.05551	−0.06344	0.10157		1.10308	−0.06798
		1.04757	0.06344	−0.10157			0.62088
			0.09092	−0.11608	B_1:	R	α
A_2:	α			1.84669		0.13922	−0.18407
	1.25944						1.55544

CCl_2D_2:

A_1:	R	r	β	η	B_2:	r	α
	0.08371	−0.05551	−0.06344	0.10157		0.60736	−0.06798
		0.55185	0.06344	−0.10157			0.41340
			0.09092	−0.11608	B_1:	R	α
A_2:	α			1.01679		0.13922	−0.18407
	0.63702						0.93302

CBr_2H_2:

A_1:	R	r	β	η	B_2:	r	α
	0.06803	−0.05551	−0.05906	0.10157		1.10308	−0.14595
		1.04757	0.05906	−0.10157			0.59546
			0.06990	−0.10805	B_1:	R	α
A_2:	α			1.84669		0.12354	−0.18188
	1.25092						1.54538

CBr_2D_2:

A_1:	R	r	β	η	B_2:	r	α
	0.06803	−0.05551	−0.05906	0.10157		0.60736	−0.14595
		0.55185	0.05906	−0.10157			0.38799
			0.06990	−0.10805	B_1:	R	α
A_2:	α			1.01679		0.12354	−0.18188
	0.62851						0.92297

TABLE VI. Multiplicities and symmetry coefficients for the CX_3Y molecule.

	(R, α, β)		$(R, \alpha, \beta)r$	r
	f_R^1	f_R^2	f_{Rr}^1	f_r^1
	$f_{R\alpha}^1$	$f_{R\alpha}^2$		
	$f_{R\beta}^2$	$f_{R\beta}^1$	$f_{r\alpha}^1$	
	f_α^1	f_α^2		
	$f_{\alpha\beta}^2$	$f_{\alpha\beta}^1$	$f_{r\beta}^1$	
	f_β^1	f_β^2		
γ_{ij}^m	1	2	$(3)^{\frac{1}{2}}$	1
A_1	1	1	1	1
E	1	$-\frac{1}{2}$	0	0

IV. CALCULATION OF FORCE CONSTANTS

At this point it becomes essential to simplify the calculations by making some reasonable assumptions which will eliminate many of the 53 force constants which have been defined in Part III. The remarkable constancy of hydrogen-carbon stretching frequencies suggests putting all interaction constants involving this coordinate (r) equal to zero. Moreover, the large separation of such frequencies ($\sim$3000 cm^{-1}) from the remaining ones ($<$1500 cm^{-1}) justifies an approximation of practical importance; such frequencies may be factored using the method described by Wilson.[3] A further approximation is made by similarly assuming that all interaction constants involving the hydrogen-carbon-hydrogen coordinate (η) vanish. Finally, it has been quite arbitrarily assumed that all interactions between the angular coordinates α and β (hydrogen-carbon-halogen and halogen-carbon-halogen) can be put equal to zero, although a few small interaction terms of the types $\alpha\alpha$ and $\beta\beta$ have been retained.

After making these assumptions, only 28 nonvanishing constants are left to be dealt with; 100 distinct fundamental vibration frequencies are to be calculated, of which 82 have actually been observed. The actual process used in determining the force constants consisted first in selecting numerical values for combinations of the constants appearing in secular determinants of order unity which fit the corresponding observed frequencies.‡‡ Utilization of the approximate factoring of the $(C-Y)$ stretching frequency gives, in all, 32 separate relations from which the force constants given in Table X have been determined.

Following these calculations, the second order determinants of the CXY_3 molecule were next investigated, and the resulting constants, which differ only very slightly, owing to a slight change in the inverse kinetic energy matrix elements, from a similar treatment previously given by Noether[6] are given in Table XI.

TABLE VII. Characters and frequency distribution for CX_2Y_2.

C_{2v}	E	C_2	σ_v	$\sigma_{v'}$	n_R	n_r	n_α	n_β	n_η	n'	n	Selection rule
A_1	1	1	1	1	1	1	1	1	1	1	4	IR, $R(p)$
B_2	1	−1	−1	1	0	1	1	0	0	0	2	IR, $R(d)$
A_2	1	1	−1	−1	0	0	1	0	0	0	1	$R(d)$
B_1	1	−1	1	−1	1	0	1	0	0	0	2	IR, $R(d)$
χ^R	2	0	2	0								
χ^r	2	0	0	2								
χ^α	4	0	0	0								
χ^β	1	1	1	1								
χ^η	1	1	1	1								
χ'	1	1	1	1								
χ	9	1	3	3								

TABLE VIII. Force constants for the CX_2Y_2 molecule.

	R		r		α				β	η
	1	2	1	2	1	2	3	4		
R	f_R^1	f_R^2	f_{Rr}^1	f_{Rr}^1	$f_{R\alpha}^1$	$f_{R\alpha}^1$	$f_{R\alpha}^2$	$f_{R\alpha}^2$	$f_{R\beta}^1$	$f_{R\eta}^1$
r			f_r^1	f_r^2	$f_{r\alpha}^1$	$f_{r\alpha}^2$	$f_{r\alpha}^2$	$f_{r\alpha}^1$	$f_{r\beta}^1$	$f_{r\eta}^1$
α					f_α^1	f_α^3	f_α^4	f_α^2	$f_{\alpha\beta}^1$	$f_{\alpha\eta}^1$
β									f_β^1	$f_{\beta\eta}^1$
η										f_η^1

The values of $f_\alpha^1 - f_\alpha^3$ and f_η^1 are in reasonable agreement with the values given in parentheses which may be obtained from Table X.

There are now sufficient data to compute the individual values of the following force constants: f_R^1, f_R^2, $f_{R\alpha}^1$, f_r^1, f_α^1, f_α^2, f_α^3, f_α^4, and f_η^1. By inserting numerical values of f_R^1, f_R^2 in the F_2 factor for CX_4, the A_1 factor of CX_3Y, and the B_1 factor of CX_2Y_2, six additional linear combinations of constants may be computed for each value of $X=$Cl and $X=$Br. After such a calculation, all the force constants assumed to be nonvanishing can be individually determined. As a matter of fact, there exist at this point several

‡‡ The experimental frequencies used for these calculations are given later in Table XIII.

[6] H. D. Noether, J. Chem. Phys. **10**, 664 (1942).

TABLE IX. Multiplicities and symmetry coefficients for CX_2Y_2.

	R		Rr	$R\alpha$		$R(\beta,\eta)$	r		$r\alpha$	
	f_R^1	f_R^2	f_{Rr}^1	$f_{R\alpha}^1$	$f_{R\alpha}^2$	$f_{R\beta}^1$ $f_{R\eta}^1$	f_r^1	f_r^2	$f_{r\alpha}^1$	$f_{r\alpha}^2$
γ_{ij}^m	1	1	2	$(2)^{\frac{1}{2}}$	$(2)^{\frac{1}{2}}$	$(2)^{\frac{1}{2}}$	1	1	$(2)^{\frac{1}{2}}$	$(2)^{\frac{1}{2}}$
A_1	1	1	1	1	1	1	1	1	1	1
B_2	0	0	0	0	0	0	1	−1	1	−1
A_2	0	0	0	0	0	0	0	0	0	0
B_1	1	−1	0	1	−1	0	0	0	0	0

	$r(\beta,\eta)$ $f_{r\beta}^1$ $f_{r\eta}^1$	α f_α^1	f_α^3	f_α^4	f_α^2	$\alpha(\beta,\eta)$ $f_{\alpha\beta}^1$ $f_{\alpha\eta}^1$	β,η f_β^1 f_η^1	$f_{\beta\eta}^1$
γ_{ij}^m	$(2)^{\frac{1}{2}}$	1	1	1	1	2	1	
A_1	1	1	1	1	1	1	1	
B_2	0	1	−1	−1	1	0	0	
A_2	0	1	−1	1	−1	0	0	
B_1	0	1	1	−1	−1	0	0	

checks involving the constants which do not give quite consistent results, but by taking slightly adjusted values, the final numerical results are obtained in Table XII.

The following constants have been put equal to zero: f_{Rr}^1, $f_{R\eta}^1$; f_r^2, $f_{r\alpha}^1$, $f_{r\alpha}^2$, $f_{r\beta}^1$, $f_{r\eta}^1$, and $f_{r\eta}^2$; $f_{\alpha\beta}^1$, $f_{\alpha\beta}^2$, $f_{\alpha\eta}^1$, $f_{\alpha\eta}^2$; $f_{\beta\eta}^2$; f_η^2, and f_η^3.

The relative smallness of the interaction constants involving two bending coordinates suggests that most such constants could have been omitted without impairing the quality of the fit and helps to justify the arbitrary omission of many constants of similar type. On the other hand, the interaction constants between carbon-halogen stretching and the lower frequency bending coordinates ($R\alpha$ and $R\beta$) are relatively large and undoubtedly have real physical significance.

TABLE X. Force constants calculated from one-dimensional factors of the methane derivatives.

	$X=$Cl	$X=$Br
f_r^{1}[a]	5.04±0.02[b]	
f_η^1	0.523±0.01[c]	
$f_R^1+3f_R^2$	4.379	3.397
$f_\beta^1-2f_\beta^3+f_\beta^2$	1.013	0.8324
$f_\alpha^1-f_\alpha^3-f_\alpha^4+f_\alpha^2$	0.7719	0.6707
$f_\alpha^1-f_\alpha^3+f_\alpha^4-f_\alpha^2$	0.6239	0.5594

[a] Here and throughout this paper the units of the force constants are 10^5 dyne cm^{-1}, for two stretching coordinates, 10^{-2} dyne for one stretching and one bending coordinate, and 10^{-11} dyne cm for two bending coordinates.
[b] Average and standard deviation for 20 separate calculations; C−H and C−D results, which show a real difference due to anharmonicity, have been averaged together.
[c] Average and standard deviation for 4 separate calculations.

TABLE XI. Force constants for the CXY_2 molecule.

	$X=$Cl		$X=$Br	
f_R^1	3.383		2.840	
$f_{R\alpha}^1$	0.3401		0.3045	
$f_\alpha^1+f_\eta^1+2f_\alpha^3$	1.156		1.0711	
$f_\alpha^1-f_\alpha^3$	0.721	(0.698)	0.6393	(0.615)
f_η^1	0.538	(0.523)	0.5351	(0.523)

Table XII shows comparable force constants computed by Stepanov[6a] who reported values not only for the bromine and chlorine derivatives, but also for the fluorine derivatives of this same series. It is noteworthy that these values are, on the whole, in good agreement, the present author having been unaware of the work of Stepanov at the time he undertook these calculations. In particular, the calculations are based upon the same assignments for the CX_2Y_2 molecule, about which there has been some controversy. The principal differences in the numerical values are to be attributed to varying assumptions about negligible constants, Stepanov having chosen to ignore the class of interaction constants involving:

(i) Bond stretching with a bending having neither bond in common with the stretching.
(ii) Bond bendings having no bonds in common. This accounts for Stepanov's zeros for $f_{R\alpha}^2$, $f_{R\beta}^2$, f_α^4, and f_β^3.

On the other hand, Stepanov found finite, although, for the most part, relatively small values

TABLE XII. Force constants for chloro- and bromomethanes.

	$X=$Cl		$X=$Br	
f_R^1	3.383	3.533[a]	2.840	2.856[a]
f_R^2	0.332	0.265	0.186	0.147
$f_{R\alpha}^1$	0.340	0.588	0.305	0.492
$f_{R\alpha}^2$	−0.164	0	−0.152	0
$f_{R\beta}^1$	0.338	0.661	0.342	0.568
$f_{R\beta}^2$	−0.249	0	−0.190	0
f_r^1	5.04	5.023	5.04	5.023
f_α^1	0.687	0.777	0.589	0.673
f_α^2	0.009	0.115	−0.005	0.084
f_α^3	−0.034	0.056	−0.026	0.042
f_α^4	−0.065	0	−0.060	0
f_β^1	1.136	1.133	1.061	0.937
f_β^2	0.092	0.098	0.134	0.067
f_β^3	−0.037	0	0.039	0
f_η^1	0.530	0.525	0.530	0.525

[a] These values have been obtained by averaging the results in reference 6a.

[6a] B. Stepanov, Acta Physicochimica **20**, 174 (1945).

TABLE XIII. Comparison of calculated and observed frequencies: chloro- and bromomethanes; methane and deuteromethane.

Molecule	Irr. Rep.	Type of Coord.	$X=Cl$ $\tilde{\nu}_{calc.}$ (cm^{-1})	$X=Cl$ $\tilde{\nu}_{exp.}$ (cm^{-1})	$X=Cl$ Δ (%)	$X=Br$ $\tilde{\nu}_{calc.}$ (cm^{-1})	$X=Br$ $\tilde{\nu}_{exp.}$ (cm^{-1})	$X=Br$ Δ (%)
CX_4	A_1	R	458	458	0.0	269	269	0.0
	E	β	218	218	0.0	123	123	0.0
	F_2	R	785	785	0.0	672	672	0.0
		β	314	314	0.0	183	183	0.0

Molecule	Irr. Rep.	Type of Coord.	$Y=H$ $\tilde{\nu}_{calc.}$	$Y=H$ $\tilde{\nu}_{exp.}$	$Y=H$ Δ (%)	$Y=D$ $\tilde{\nu}_{calc.}$	$Y=D$ $\tilde{\nu}_{exp.}$	$Y=D$ Δ (%)	$Y=H$ $\tilde{\nu}_{calc.}$	$Y=H$ $\tilde{\nu}_{exp.}$	$Y=H$ Δ (%)	$Y=D$ $\tilde{\nu}_{calc.}$	$Y=D$ $\tilde{\nu}_{exp.}$	$Y=D$ Δ (%)
CX_3Y	A_1	r	3040	3030	+0.3	2240	2257	−0.7	3037	3023	+0.5	2237	2247	−0.4
		R	677	672	+0.7	656	655	+0.2	541	539	+0.4	522	519	+0.6
		$\beta(\alpha)$	354	363	−2.5	352	364	−3.3	223	222	+0.5	223	222	+0.5
	E	α	1221	1217	+0.3	887	908	−2.3	1137	1142	−0.4	820	848	−3.3
		R	744	760	−2.1	736	738	−0.3	645	656	−0.7	637	629	+1.3
		β	258	261	−1.1	257	262	−1.9	154	154	0.0	154	153	+0.6
CX_2Y_2	A_1	r	2993	2984	+0.3	2174			2993	2988	+0.2	2174		
		$\eta(\alpha)$	1437	1423	+1.0	1064			1413	1388	+1.8	1043		
		R	710	702	+1.1	674			578	576	+0.3	545		
		$\beta(\alpha)$	288	283	+1.8	286			180	174	+3.4	179		
	B_2	r	3073	3048	+0.8	2283			3078	3061	+0.6	2281		
		α	902	899	+0.3	731			809	810	−0.1	665		
	A_2	α	1177	1155	+1.9	836			1091	1090	+0.1	773		
	B_1	α	1267	1266	+0.1	936			1183	1183	0.0	870		
		R	737	737	0.0	723			638	637	+0.2	621		
CXY_3	A_1	r	2958	2928	+1.0	2127	2136	−0.4	2958	2932	+0.9	2126	2134	−0.4
		$\eta(\alpha)$	1350	1355	−0.4	1024	1029	−0.5	1301	1305	−0.3	984	987	−0.3
		R	733	732	+0.1	693	695	−0.3	613	610	+0.5	573	577	−0.7
	E	r	3078	3047	+1.0	2294	2287	+0.3	3080	3061	+0.6	2293	2294	0.0
		η	1455	1460	−0.3	1044	1058	−1.3	1446	1450	−0.3	1041	1053	−1.1
		α	1020	1020	0.0	771	775	−0.5	938	957	−2.0	703	717	−2.0

Molecule	Irr. Rep.	Type of Coord.	$Y=H$ $\tilde{\nu}_{calc.}$ (cm^{-1})	$Y=H$ $\tilde{\nu}_{exp.}$ (cm^{-1})	$Y=H$ Δ (%)	$Y=D$ $\tilde{\nu}_{calc.}$ (cm^{-1})	$Y=D$ $\tilde{\nu}_{exp.}$ (cm^{-1})	$Y=D$ Δ (%)
CY_4	A_1	r	2914	2914	0.0	2062	2085	−1.1
	E	η	1498	1499	−0.1	1059	1054	+0.4
	F_2	r	3080	3020	+2.0	2297	2258	+1.7
		η	1337	1306	+2.4	1003	996	+0.7

for some of the constants which have been ignored by the present author, namely: $f_{Rr}{}^1=0.088$, 0.059; $f_r{}^2=0.029$, 0.029; $f_{r\alpha}{}^1=0.364$, 0.310; $f_{r\eta}{}^1=0.225$, 0.225; $f_{\alpha\beta}{}^1=0.063$, 0.056; $f_{\alpha\eta}{}^1=0.042$, 0.042; $f_\eta{}^2=-0.024$, -0.024; the numerical values being cited for chlorides and bromides in that order.

There seems to be little physical ground for a choice between these sets of parameters at present, because the wider range of Stepanov's calculations, including the other halides (and references to a notable series of calculations for various hydrocarbons) are in part compensated by the application of the present calculations to the deuterium analogues which were not considered in Stepanov's paper.

Finally, Table XIII gives a direct comparison between calculated and experimental frequencies.

The authors from whose work the experimental frequencies have been taken are as follows: CCl_4, CBr_4, CH_4, and CD_4, Langseth[7] and data cited

[7] A. Langseth, Zeits. f. Physik **72**, 350 (1931).

by Herzberg;[8] CCl_3H, Nielsen and Ward;[9] CCl_3D, Wood and Rank;[10] CBr_3H and CBr_3D, Redlich and Stricks,[11] Barchewitz and Parodi;[12] $CClH_3$, Bennett and Meyer;[13] $CClD_3$, Noether;[6] $CBrH_3$, Barker and Plyler;[14] $CBrD_3$, Noether;[6] CCl_2H_2, Corin and Sutherland,[15] Wagner;[16] CBr_2H_2, Wagner,[16] Delwaulle.[17]

All the frequencies were recalculated using the slightly adjusted values of the constants given in Table XII, the approximate factoring of the $C-Y$ stretching modes not being used except in the case of the A_1 factor of CX_2Y_2. Naturally, the fit is somewhat better in the simpler factors, such as those of CX_4, from which the constants were more or less directly determined. Good confirmation of the assumed potential functions is found, however, in the comparison of the calculations with observed values for the E factor of CX_3Y and the A_1 factor of CX_2Y_2 which were not used in obtaining the force constants; these frequencies are underlined in the table. For the 82 frequencies for which experimental data were available, the root mean square difference between calculation and observation is 1.1 percent.

It must be remembered, however, that the assignment of the fundamentals for the methylene halides is not certain. Spectroscopic data for the deutero-methylene halides would provide an interesting test of the potential functions which have been developed here.

ACKNOWLEDGMENT

The author gratefully acknowledges the cordial and illuminating assistance given him by Professor E. Bright Wilson, Jr., of Harvard University.

[8] G. Herzberg, *Infra-Red and Raman Spectra of Polyatomic Molecules* (D. Van Nostrand Company, Inc., New York, 1945).
[9] J. R. Nielsen and N. E. Ward, J. Chem. Phys. **10**, 81 (1942).
[10] R. W. Wood and D. H. Rank, Phys. Rev. **48**, 63 (1935).
[11] O. Redlich and W. Stricks, Monats. F. Chem. **67**, 328 (1936).
[12] P. Barchewitz and M. Parodi, J. de phys. et rad. **10**, 143 (1939).
[13] W. H. Bennett and C. G. Meyer, Phys. Rev. **32**, 888 (1928).
[14] E. F. Barker and E. K. Plyler, J. Chem. Phys. **3**, 367 (1935).
[15] C. Corin and G. B. B. M. Sutherland, Proc. Roy. Soc. **165**, 43 (1938).
[16] J. Wagner, Zeits. f. physik. Chemie **B45**, 69 (1939).
[17] M. Delwaulle, Comptes rendus **217**, 172 (1944).

THE JOURNAL OF CHEMICAL PHYSICS VOLUME 16, NUMBER 3 MARCH, 1948

The Fluorescence of Solid Acetone*

W. E. KASKAN AND A. B. F. DUNCAN
University of Rochester, Rochester, New York

(Received December 23, 1947)

IT has been known for some time that acetone vapor, illuminated by wave-length 3130A, shows a weak blue fluorescence spectrum.[1,2] It occurred to us that the fluorescence should be intensified in the solid state at 83°K, both because of increased density and reduced number of collisions. This intensification has been found. We find this fluorescence also in a rigid solvent (isopentane, ether, and ethyl alcohol) at 83°K.[3]

The fluorescence spectrum consists of a broad band, beginning at about 4000A and extending to about 5000A, with a broad maximum at approximately 4556A. The spectrum shows no resolved structure at dispersions of 150A per mm and at 16A per mm. Methyl ethyl and diethyl ketones were examined under the same conditions, and show similar short- and long-wave limits, with intensity maxima at 4675 and 4707, respectively. The latter ketones were photographed only at the lower dispersion. No indication of the well-known fluorescence of biacetyl was obtained in any of these cases.

The absorption level of acetone[4] in the vapor

* This work has been supported by the Office of Naval Research, U. S. Navy, under Contract N6onr-241.
[1] G. H. Damon and F. Daniels, J. Am. Chem. Soc. **55**, 2363 (1933).
[2] R. E. Hunt and W. A. Noyes, Jr., J. Am. Chem. Soc. (in press).
[3] G. N. Lewis and M. Kasha, J. Am. Chem. Soc. **66**, 2100 (1944).
[4] W. A. Noyes, Jr., A. B. F. Duncan, and W. M. Manning, J. Chem. Phys. **2**, 717 (1934).

TABLE I.

Substance	Mean lifetime
Acetone	10×10^{-4} sec.
Biacetyl	12×10^{-4}
Diethyl ketone	8×10^{-4}

state is believed to be 30800 cm^{-1} above the ground state. Excitation by 3130A corresponds to about 31900 cm^{-1}, whereas the short-wave limit of the fluorescence corresponds to about 25000 cm^{-1}. A five-hour exposure with solid acetone failed to show any fluorescence in the ultraviolet between 3130 and 4000A. We conclude that fluorescence from the level reached by absorption directly back to the ground state (resonance fluorescence) is effectively absent under these conditions. If the absorption level were actually lower in a condensed phase than in the gas, the blue fluorescence might still come from the level reached by absorption. The absorption spectrum of a one-meter column of liquid acetone was photographed. Under these conditions acetone appears to be completely transparent above 3440A, which puts the upper level in absorption at least 29100 cm^{-1} above the ground level. Assuming that this is true in the solid also, the difference between the fluorescence maximum and the lowest part of the absorption level is about 6500 cm^{-1}. If it were assumed that fluorescence takes place from the lowest vibrational level of the absorption level, then the highest frequency observed in fluorescence corresponds to a transition which ends on a vibrational level 3600 cm^{-1} above the zero level.

Potential energy surfaces of two electronic states could be drawn to fit this situation, so that two minima in the upper surface relative to the lower surface were in the proper places for absorption and fluorescence. While this somewhat artificial process avoids the assumption of a separate excited electronic level for fluorescence, the transition probabilities of absorption and fluorescence are not easily explained. The mean lifetime of acetone in the absorption level was estimated from the integrated absorption coefficient to that level,[5] using the data of Rice,[6] to be 2.9×10^{-6} sec. This estimate implies the absence of quenching collisions, which might reduce the experimental lifetime.

The lifetime of the blue fluorescence of acetone at 83°K was measured directly with a photomultiplier tube, oscillograph combination.[7] Light from a single condenser discharge through a gas-filled tube was filtered to give radiation in the neighborhood of 3130A. The single flash had a mean life of about 5×10^{-6} sec. The light was focused on the sample contained in a quartz tube, immersed in liquid nitrogen in a quartz Dewar flask. The fluorescent light fell on the photo-multiplier tube, and its output was fed to the vertical deflection terminals of the oscillograph. Timing marks were obtained from a calibrated square-wave oscillator and the oscillograph beam was blanked until the trace was to appear on the screen. The resulting intensity-time curve was photographed and the mean lifetime determined in the usual way.

With this method, some of the preliminary results obtained are summarized in Table I, all at 83°K. The data on biacetyl may be compared with the mean lifetime of the fluorescence of biacetyl vapor, determined as 1.65×10^{-3} sec. by Almy and Anderson[8] and 1.4×10^{-3} sec. by Rawcliffe.[9] The error in our data is believed to be about 15 percent, which can be lowered by refinement of experimental details.

If any quenching occurs in the solid at 83°K, the true lifetime may be longer than the experimental value of 1×10^{-3} sec. for acetone. On the same basis the lifetime for the absorption level should not be longer than 2.9×10^{-6} sec. We conclude from this that the fluorescence originates on a level with a probability of emission of not more than 0.0029 times that of the absorption level. It appears more natural to assume in this case that there are two different upper electronic levels, rather than two parts of the same electronic level which differ only in nuclear configurations.

The experimental measurements are being extended in the hope of providing some explanation of the nature of the fluorescence level, and will be reported in detail at a later date.

[5] R. S. Mulliken, J. Chem. Phys. **7**, 14 (1939).
[6] F. O. Rice, Proc. Roy. Soc. (London) **A91**, 76 (1914).
[7] G. H. Dieke, H. Y. Loh, and H. M. Crosswhite, J. Opt. Soc. Am. **36**, 185 (1946).
[8] G. M. Almy and S. Anderson, J. Chem. Phys. **8**, 805 (1940).
[9] R. D. Rawcliffe, Rev. Sci. Inst. **13**, 413 (1942).

THE JOURNAL OF CHEMICAL PHYSICS VOLUME 16, NUMBER 3 MARCH, 1948

Ultraviolet Absorption Spectrum of Hydrogen Peroxide

R. B. Holt, C. K. McLane, and O. Oldenberg
Lyman Physical Laboratory, Harvard University, Cambridge, Massachusetts

(Received November 25, 1947)

The absorption coefficient for hydrogen peroxide vapor in the wave-length range 1850–2200A was determined. A careful redetermination of the absorption coefficients for the vapor and for aqueous solutions at 2537A was also made.

I. PROBLEM

In connection with an investigation (to be reported in a subsequent paper) of the thermal reaction between hydrogen and oxygen, it was desired to use absorption spectroscopy as an analytical tool for the qualitative and quantitative determination of hydrogen peroxide. In order to accomplish this, it was necessary to make measurements of the absorption coefficient of hydrogen peroxide over a considerable wave-length range (1850-2200A) and to determine the absorption coefficient at a single wave-length (2537A) with greater accuracy than had been achieved previously.

Concordant results for the absorption coefficient of hydrogen peroxide solutions have been obtained by several investigators,[1] especially in the wave-length range above 2500A. All of the results indicate a continuous absorption beginning in the visible (probably around 4000A) and increasing steadily toward the ultraviolet as far as the observations were carried (about 2200A).

Less work has been done on the absorption by the vapor. The most extensive investigation was that of Urey, Dawsey, and Rice,[2] in which they measured the absorption coefficients for the solution and the vapor down to 2150A. A similar investigation[3] made somewhat later confirmed the results down to 2200A, but showed an easily measurable, although small, difference between the absorption coefficients for the vapor and for aqueous solutions, which had not been noted by the previous investigators.

No quantitative data below 2150A have come to our attention. Two qualitative statements regarding the nature of the absorption have been published. Urey, Dawsey, and Rice state that ". . . the spectrum is continuous throughout the range from 2000A to 3100A . . . with no indication of a maximum in this region." Later, Sharma[4] reported that the absorption spectrum showed a "sharp cut" at 2055A. This observation reported by Sharma is of considerable interest because it was used recently[5] in an indirect way to set a limit on the value for the energy of dissociation of water molecules into H atoms and OH radicals.

The present investigation was undertaken to yield quantitative data on the absorption below 2200A, to clear up the discrepancy between Sharma's observation and that of Urey and co-workers, and to investigate the reported difference in the absorption coefficients of the vapor and of aqueous solutions at one wave-length at least.

II. METHOD

More or less conventional techniques were used for the measurement of absorption coefficients. For the 1850–2200A range, the experimental set-up consisted of a hydrogen discharge tube which emitted a continuous spectrum, a quartz lens to render the light nearly parallel, an absorption cell fitted with quartz windows, a second quartz lens for refocusing the transmitted light, and a quartz spectrograph.

The discharge tube[6] employed large aluminum electrodes to insure low current density. The two tubes containing the electrodes were connected by means of a capillary tube of rectangular

[1] A. J. Allmand and D. W. G. Style, J. Chem. Soc. 606 (1930); V. Henri and H. Wurmser, Comptes rendus **156**, 1012 (1913); E. Lederle and A. Rieche, Ber. Chem. Ges. 62, 2573 (1929).
[2] H. C. Urey, L. H. Dawsey, and F. O. Rice, J. Am. Chem. Soc. **51**, 1371 (1929).
[3] W. C. Furgusson, L. Sotin, and D. W. G. Style, Trans. Faraday Soc. **32**, 956 (1936).
[4] R. S. Sharma, Proc. Acad. Sci. United Provinces Agra Oudh India **4**, 51 (1934).
[5] G. Damköhler and R. Edse, Naturwiss. **31**, 310 (1943).
[6] N. D. Smith, J. Opt. Soc. Am. **28**, 40 (1938).

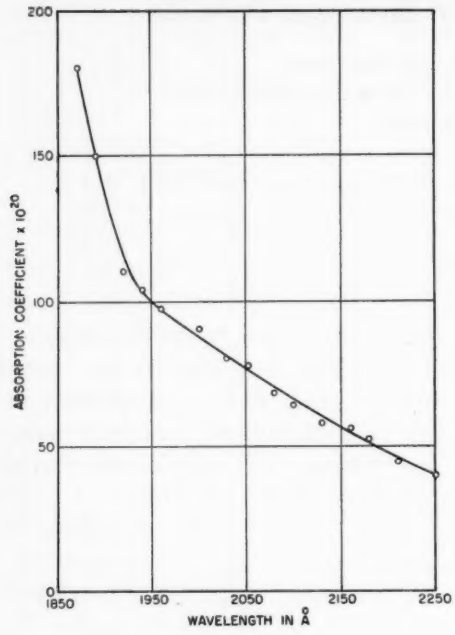

FIG. 1. Absorption coefficient for hydrogen peroxide vapor (average values).

cross section, which was viewed end-on through a quartz window attached to a side arm on one of the electrode tubes. This side arm projected through the water jacket which surrounded the entire discharge tube. A somewhat similar glass window system was provided on the other electrode tube in order to facilitate lining-up of the source with the rest of the optical system. The capillary was coated on the inside with a thin layer of platinum for the purpose of causing recombination of any atomic hydrogen formed in the discharge. This source gave a very intense continuous spectrum characteristic of molecular hydrogen when operated in series with a high resistance from a 2200 volts a.c. source at a current of one-half ampere. It was found that no noticeable change in intensity could be observed by means of photographs taken at intervals of one-half hour during the operation of this discharge tube.

The absorption cell used for hydrogen peroxide vapor was a 3.8-cm diameter Pyrex tube 183 cm long, fitted with quartz windows. Hydrogen peroxide vapor was introduced by bubbling nitrogen through several saturators containing hydrogen peroxide[7] and causing the nitrogen containing the vapor to flow at a constant rate through the absorption cell. The concentration of the vapor in the cell was determined by observing the rate of flow of nitrogen by means of a calibrated capillary-type flow meter and analyzing the exit gas for hydrogen peroxide by titration with potassium permanganate. The hydrogen peroxide was separated from the nitrogen in the exit gas by use of a warm and cold wall trap of recent design.[8] This type of trap, which employs one wall kept at liquid-air temperature and the other near room temperature, with a spacing of about two millimeters between the two walls, is superior to conventional traps in that it avoids loss of condensable material through fog formation. The concentration of hydrogen peroxide in the cell could be varied by changing the concentration of the solution in the saturators.

Chemical analyses of the exit gas, with and without the light source on and under otherwise identical conditions, showed that no appreciable photo-chemical decomposition of hydrogen peroxide took place. A Hilger quartz spectrograph (focal length 20 cm), which had been modified for this spectral range, was employed. The instrument was equipped with means for circulating nitrogen through the light path, thus avoiding difficulty with the oxygen absorption bands between 1800 and 2000A. Eastman Type II-0 ultraviolet sensitized plates were used. Wire mesh screens of known transmission were inserted between the lenses (region of nearly parallel light) with the empty absorption tube in place in order to allow comparison on a given photographic plate of the blackening produced by various intensities at a given wave-length during equal exposures. Comparisons of blackening were made on a microphotometer. This method avoids dependence on the reciprocity law for photographic emulsions, since only the fact that equal blackening is produced by equal exposure to the same intensity on the same plate is used. As a matter of practical manipulation, in

[7] The hydrogen peroxide used in the investigation was a commercial 90 percent solution of very high purity and exceptional stability kindly supplied by the Buffalo Electrochemical Company, Buffalo, New York.

[8] D. H. Volman, J. Chem. Phys. **14**, 707 (1946).

order to determine the percentage transmission of the vapor at a given wave-length, the photographic density (given by the microphotometer reading) for a given time of exposure was plotted against the logarithm of the known transmission for the various screens and for the empty tube; this, as would be expected, yielded a nearly straight line. The unknown transmission could then be found from photographic density of the exposure taken with hydrogen peroxide vapor in the light path by interpolation. Although this was a laborious process, it was necessary, especially in the transmission range above about 70 percent, since no screens with transmission larger than about 65 percent were available.

A short absorption cell of conventional design was used in the study of the absorption of aqueous solutions in this wave-length range. Otherwise, the experimental procedure was the same as for the vapor.

For the measurements at 2537A, the experimental set-up consisted of a quartz mercury arc, the same lens system and absorption cell arrangements as described above, and a photo-cell for a detector.

The quartz mercury arc, of conventional design, was operated on high voltage a.c. with a large series resistor to limit the current to a few milliamperes. Under these conditions, more than 99 percent of the radiant energy below 3100A was found to be concentrated in the line 2537A.

An argon-filled photo-cell with a cadmium cathode was employed. Since the photoelectric threshold of cadmium is about 3100A, this arrangement made the system essentially monochromatic. An amplifier of standard design,[9] employing an electrometer tube (type FP-54), was used with the photo-cell.

III. EXPERIMENTAL RESULTS

The absorption of the *vapor* in the range 2200 to 1850A was found to increase steadily toward the shorter wave-lengths. In particular, there was no evidence at all to indicate a "sharp cut" in the spectrum at 2055A as reported by Sharma in his previously discussed paper. Figure 1 shows the average values of the absorption coefficients found over this wave-length range. The absorption coefficient plotted here is defined by the equation $\alpha=(1/cd)\ln(I_0/I)$, where c is the concentration in molecules/cc, d is the length of the light path in cm, I_0 is the intensity of the incident light, and I is the intensity of the transmitted light. This is the convention used by Urey, Dawsey, and Rice;[2] other values cited have been converted to this basis. In constructing this curve, the average of the absorption coefficient calculated from each of six plates (each of which contained three sets of exposures) was taken. Individual values from the various plates are in good agreement, so there is no reason to believe that the average given is in error (except possibly at the extreme short wave-length end of the range) by more than 10 percent at most. Absolute accuracy greater than this would have been very difficult to obtain in this region, since the sensitivity of the photographic plate varies somewhat (due to irregularities in the fluorescent coating, probably) and the intensity of the source decreases rapidly toward the shorter wave-lengths.

Comparison of the values of the absorption coefficient of the vapor which our results yielded with those in the two previously discussed papers in the wave-length region in which the measurements overlapped gives reasonably good agreement. For example, at 2200A, Urey, Dawsey, and Rice got 29×10^{-20} for the absorption coefficient, Furgusson and co-workers got about 38×10^{-20} and our value is 28×10^{-20}.

Several plates were made for the determination of the absorption spectrum of hydrogen peroxide *solutions*. These were carefully compared (in a qualitative manner only) with the plates for equivalent values of concentration times path length for the vapor, and there is apparently no marked difference in the nature of the absorption in the two cases. The absorption increases steadily toward shorter wave-lengths, with no "sharp cut" at 2055A.

The determination of the exact value for the absorption coefficient at 2537A was carried out for both the aqueous solution and the vapor, for reasons previously cited. The average value of the absorption coefficient for *aqueous solutions* was found to be 7.6×10^{-20}, with a r.m.s. deviation of 0.3×10^{-20} between values from separate determinations. The value compares quite satis-

[9] L. A. DuBridge and H. Brown, Rev. Sci. Inst. **37**, 392 (1934).

factorily with the average of 7.9×10^{-20} obtained by several investigators mentioned previously.[10] Since the photoelectric technique employed is a better method of measuring relative intensities than the photographic method used by the earlier investigators, our value may be better than the average of the previous determinations, although we hesitate to say that it certainly is in view of the spread of values between individual determinations.

The figure reported is corrected for absorption by liquid water. This correction, although quite small, is necessary in order to obtain agreement between values of the absorption coefficient of hydrogen peroxide for solutions of various concentrations. The previous investigators mentioned did not indicate whether they made this correction or not; it may have been that they all worked with solutions concentrated enough to make it negligible anyway. If their concentrations were such that a correction should have been made and it was not made, this would help to explain the fact that we obtained a somewhat lower average value than that given in the literature. Obviously, such a correction need not be applied to the experiments on the vapor, since the concentration of water molecules is comparatively very much less.

The average value of 7.4×10^{-20} was obtained for *hydrogen peroxide vapor*. This is to be compared with a value of about 11×10^{-20} found by Furgusson and co-workers.[3] We believe that our value is to be preferred because of the refinements in technique employed. At any rate, the values obtained show quite clearly that there is no appreciable difference between the absorption coefficient for the aqueous solution and for the vapor at this wave-length. The value 9.0×10^{-20} obtained by Urey and co-workers[2] is also higher than our value for the vapor.

IV. DISCUSSION OF RESULTS

A. Measurements at 2537A

The fact that the absorption coefficients of the solution and the vapor at 2537A are the same is not unexpected. Furgusson and co-workers,[3] who observed a difference, very probably did so because of the very great difficulty of obtaining correct values for the concentration of the vapor by chemical analysis because of fog formation. This difficulty has been noted by others working with hydrogen peroxide vapor,[8] and resulted in the design of the special form of trap mentioned above. We found that special precautions had to be taken to avoid this trouble. At any rate, as Furgusson and co-workers point out, the usual explanations (*e.g.*, chemical reaction with the solvent to form a new compound in solution as in the case of aqueous chlorine solutions) would not be expected to apply to the case of hydrogen peroxide, so no difference is to be expected.

B. 1850 to 2200A Measurements

A formulation similar to that used by Urey and co-workers[2] in the discussion of their experimental observations seems to be the best available method for the interpretation of our results in this region. Hydrogen peroxide may be considered to be a pseudo-halogen, formed of two OH radicals in a way similar to the formation of halogen molecules from the individual atoms, even though the chemical and physical properties show little similarity to those of the halogens. This type of model is in accord with the structure proposed by Penney and Sutherland,[11] which is a non-planar structure, with the angle between OH groups as seen projected on a plane normal to the O—O bond of about 100°. This structure, incidentally, allows satisfactory explanation of the rather observed dipole moment of hydrogen peroxide. This large dipole moment has been taken by Sharma[4] as support for a different structure which he proposed on the basis of a "sharp cut" in the absorption spectrum at 2055A. The results of our measurements show that there is now no basis for Sharma's views. The infra-red absorption spectrum of hydrogen peroxide may also be interpreted as supporting the structure proposed by Penney and Sutherland.[12] Furthermore, the absence of such a "sharp cut" obviates the necessity of placing a limit on the energy of

[10] See Landolt-Bornstein, *Physikalisch-Chemische Tabellen* (Julius Springer, Verlag, Berlin, 1936), fifth edition, Eg. (IIIb), p. 1335.

[11] W. G. Penney and G. B. B. M. Sutherland, J. Chem. Phys. **2**, 492 (1934).

[12] L. N. Zumwalt and P. A. Giguere, J. Chem. Phys. **2**, 458 (1941).

dissociation of water vapor, which has been done by means of a rather involved indirect argument by Damköhler and Edse.[5]

The energy change for dissociation into two OH groups cannot be exactly calculated, but it can be approximated from the following thermochemical equations. All values are taken from the previously mentioned paper by Urey and coworkers, except that for the second equation, which is based on later measurements.[13] This

$HOOH=HOH+\frac{1}{2}O_2$	−25.2 cal.
$2HOH=2H+2OH$	236.4 cal.
$2H=H_2$	−102.5 cal.
$H_2+\frac{1}{2}O_2=HOH$	−57.8 cal.
$HOOH=2OH$	50.9 cal.

value (50.9 cal.) corresponds to a wave-length of 5620A, so the energy available over the range in which absorption is known to take place is certainly sufficient to dissociate the molecule in this way. The molecule might be expected, in analogy to the halogens, to dissociate into one normal and one excited OH, which would require more energy than that calculated above, but since the first excited level for OH is only 140 wave numbers (of the order of the rotational energy of the molecule), this factor does not modify our calculations appreciably. The main intensity of the absorption occurs far to the violet side of the long wave-length limit calculated here.

[13] R. J. Dwyer and O. Oldenberg, J. Chem. Phys. **12**, 351 (1944).

The continuous absorption spectra of the halogens each show a maximum in the range in which measurements have been made. This maximum is to be expected on the basis of a theoretical treatment which has been applied to the case of chlorine[14] with considerable success, even to a quantitative prediction of the temperature dependence of the absorption. If hydrogen peroxide has such a maximum (and it presumably does), it is farther in the ultraviolet than our measurements extended.

No such quantitative theoretical treatment for hydrogen peroxide as is possible in the case of the halogens seems possible. In the first place, the potential curves for the molecule are not known. The fact that this molecule consists of four atoms rather than two, as in the case of the halogens, introduces many new degrees of freedom. Our naive comparison of the process of dissociation by light to the similar process for the halogens is at best very approximate.

R. B. Holt and C. K. McLane wish to express appreciation for National Research Council Predoctoral Fellowships which made this investigation possible. The authors are grateful for financial support by the Rumford Fund of the American Academy of Arts and Sciences. The Buffalo Electrochemical Company kindly supplied the hydrogen peroxide used and furnished valuable advice on several points.

[14] G. E. Gibson, O. K. Rice, and N. S. Bayliss, Phys. Rev. **44**, 193 (1933); G. E. Gibson and N. S. Bayliss, Phys. Rev. **44**, 188 (1933).

The Effect of Variations in Surface on the Photolysis of Acetone*

E. W. R. STEACIE AND B. DEB. DARWENT
National Research Council, Ottawa, Canada

(Received December 5, 1947)

An investigation of the acetone photolysis in the "continuum" and in the "banded" region has been made in clean quartz vessels and in vessels coated with potassium chloride and with lead. No appreciable change in the C_2H_6/CO ratio occurs in the coated vessels. This is surprising since biacetyl formation is apparently at least partly heterogeneous, and the ratio would be expected to be sensitive to the condition of the surface.

A few experiments were also made on the mercury photosensitized decomposition of acetone. Very high C_2H_6/CO ratios were found. It is concluded that this is due merely to higher absorbed intensities for a given incident intensity.

INTRODUCTION

A GREAT many papers have been published on the photolysis of acetone. The products of the reaction are chiefly C_2H_6, CO, and biacetyl, and the reaction is frequently followed by the measurement of the ratio C_2H_6/CO. This ratio would be unity if no biacetyl formation occurred, and infinite if all acetyl radicals combined to form biacetyl. There is some uncertainty as to the extent by which the reactions

$$CH_3CO \rightarrow CH_3 + CO \qquad (1)$$

and

$$2CH_3CO \rightarrow (CH_3CO)_2 \qquad (2)$$

may occur heterogeneously. The evidence suggests that (2) is predominantly heterogeneous at lower pressures.[1] It follows therefore that an increase in the extent or effectiveness of the surface should increase the formation of biacetyl, and hence, increase the ratio C_2H_6/CO, while a decrease should decrease the ratio. The reaction would thus be expected to be sensitive to the condition of the surface.

An investigation has therefore been made of the C_2H_6/CO ratio in the products of the acetone photolysis in clean quartz vessels and in vessels coated with potassium chloride and with lead. Potassium chloride was used because it has been shown to make a pronounced change in the character of the surface as far as H-atom reactions[2] or oxidation processes are concerned,[3] and because it is transparent to the effective radiation and thus permits the coating of the entire cell including the incident face. Lead was used since a metal surface might have different properties, and because of some recent free radical work in which lead mirrors were present.[4]

EXPERIMENTAL

The usual type of vacuum system, etc. was employed. The reaction vessel was a cylindrical quartz cell, 5 cm diameter, 10 cm long, with plane polished ends. The light source was a Hanovia Type S lamp in a water-cooled reflector. For the "continuum" a chlorine filter, 10 cm long, 1 atmosphere pressure was used. This gave radiation mainly in the neighborhood of λ2537 (λ2537 itself was completely reversed). For the "banded" region the same lamp was used with a 6-mm Pyrex filter.

The potassium chloride coating was put on the cell by cleaning with fuming nitric acid, washing thoroughly, and rinsing out the cell with a saturated solution of KCl and drying. The lead coating was distilled on from a side tube in a high vacuum. The incident face of the cell was then cleared of lead by flaming.

Since the object of the work was merely to compare clean and coated cells, no attempt was made to determine quantum yields or to make a detailed investigation of pressure, intensity, etc. The amount of gas produced per second was used

* Contribution No. 1627 from the National Research Council, Ottawa, Canada.

[1] For a review see W. Davis, Jr., Chem. Rev. **40**, 201 (1947).

[2] K. H. Geib and E. W. R. Steacie, Zeits. f. physik. Chemie **B29**, 215 (1935).

[3] R. N. Pease and P. R. Cheesebro, Proc. Nat. Acad. Sci. (Washington) **14**, 472 (1928).

[4] M. H. Feldman, M. Burton, J. E. Ricci, and T. W. Davis, J. Chem. Phys. **13**, 440 (1945).

as a measure of $I_{abs.}$ as in the work of Spence and Wild.

Gas analyses were done by a condensation method. Gas from the reaction system was pumped by a mercury vapor pump into a cold trap. The non-condensable gas was pumped from the trap into a calibrated system by means of a Toepler pump. CO and CH_4 were pumped off at liquid nitrogen temperature, and C_2H_6 at -150°C. Trial runs with synthetic mixtures gave completely satisfactory separations. Agreement within the experimental error was also obtained in analyses by the Ward fractionation method.

In a large number of experiments the $CO-CH_4$ fraction was analyzed by combustion. The methane production was always small (6 to 8 percent) and was quite reproducible, and in the remaining experiments a correction to the "non-condensable" fraction was made for methane.

Acetone was Mallinckrodt's Analytical Reagent grade. It was distilled before used and stored over magnesium perchlorate.

RESULTS

A series of runs were first made at 150 mm pressure and approximately constant intensity. The results are given in Table I. In a second series of runs the pressure was varied. Since the variation in pressure produced a large change in $I_{abs.}$ pairs of runs were done under comparable conditions with a clean bulb and a KCl coated bulb. The results are given in Table II. The intensities were considerably lower in this series.

While no attempt has been made to do a complete investigation over a range of absorbed intensity and pressure, the results in Table II are in general agreement with previous work. Thus Herr and Noyes[5] found that at 3130A° a decrease in pressure raised the C_2H_6/CO ratio, while a decrease in $I_{abs.}$ lowered it. The pressure effect is somewhat larger than the intensity effect, and hence at constant incident intensity and decreasing pressure the ratio C_2H_6/CO should increase as found here. At λ2537 the effects are smaller, and the change is in the opposite direction.

DISCUSSION

From Tables I and II it is apparent that within the experimental error, the treatment of the surface with KCl has no effect on the C_2H_6/CO ratio. The results with lead are less reliable, but at least it may be said that with λ2537 a lead surface has no appreciable effect.

[5] D. S. Herr and W. A. Noyes, Jr., J. Am. Chem. Soc. 62, 2052 (1940).

TABLE I.*

Wavelength, A	P, mm	Gas produced cc per sec. ×10⁵	$\frac{C_2H_6}{CO}$	Remarks
2537	151	31.6	1.91	Clean cell
2537	150	41.8	2.30	
2537	150	43.1	2.40	
2537	151	37.3	2.46	Mean
2537	147	35.0	2.36	$\frac{C_2H_6}{CO}=2.26$
2537	152	37.5	2.11	
2537	150	41.9	2.20	KCl coated cell
2537	150	41.4	2.22	Mean
2537	157	37.7	2.26	$\frac{C_2H_6}{CO}=2.23$
2537	149	33.0	2.15	Lead coated cell
2537	150	31.8	2.23	Mean
2537	150	32.1	2.10	$\frac{C_2H_6}{CO}=2.16$
3000+	150	1.5	1.37	Clean cell
3000+	149	3.4	1.33	Mean
3000+	150	2.9	1.37	$\frac{C_2H_6}{CO}=1.36$
3000+	150	2.5	1.31	KCl coated cell
3000+	150	2.3	1.38	Mean
				$\frac{C_2H_6}{CO}=1.34$
3000+	151	0.7	1.11	Lead coated cell
				Mean
				$\frac{C_2H_6}{CO}=1.11$

* Temperature = 25°C.

TABLE II.*

Wavelength, A	P, mm	Gas produced, cc per sec. ×10⁵	$\frac{C_2H_6}{CO}$	Remarks
2537	151	5.3	1.72	Clean bulb
2537	150	5.3	1.75	KCl
2537	50	3.3	1.67	Clean
2537	50	3.4	1.60	KCl
2537	10.0	0.99	1.58	Clean
2537	11.0	0.99	1.55	KCl
3000+	153	0.42	0.92	Clean
3000+	150	0.46	1.01	KCl
3000+	50	0.066	1.21	Clean
3000+	50	0.12	1.20	KCl
3000+	18.5	0.055	1.48	Clean
3000+	18.5	0.025	1.58	KCl

* Temperature = 25°C.

TABLE III. Mercury photosensitized decomposition of acetone.*

Gas produced, cc per sec. $\times 10^5$	$\frac{C_2H_6}{CO}$
0.088	2.00
0.13	2.40
0.26	2.82
0.49	3.03
0.67	3.41
0.85	3.42
0.86	3.60
1.16	3.60**
1.23	3.94
3.3	4.50
19.9	4.76

* Pressure 50 mm; Temperature 25°C.
** KCl coated cell.

It is surprising that the ratio is not sensitive to the condition of the surface. While the present work cannot rule out the occurrence of surface reactions in the photolysis, it can at least be said that it offers no confirmation of the prominence of surface effects in the pressure range used.

MERCURY PHOTOSENSITIZED REACTION

In the course of a few preliminary experiments in which a resonance lamp was used as a source of λ2537, it was noticed that very high C_2H_6/CO ratios were obtained when mercury was present. From the absorption coefficient of acetone[6] and the "equivalent absorption coefficient"[7] of mercury vapor for λ2537 at 20°C it appears that about 98 percent of the radiation would be absorbed by mercury in a cell containing 50 mm of acetone saturated with mercury vapor. While this calculation ignores pressure broadening, etc., there seems to be no doubt that mercury will absorb most of the radiation. Also, by analogy with other substances the quenching cross section of acetone for excited mercury atoms would be expected to be very high. It therefore appears that the mercury photosensitized reaction can be investigated without much competition from the direct photolysis. The high C_2H_6/CO ratios were therefore presumably due to the photo-

[6] C. W. Porter and C. Iddings, J. Am. Chem. Soc. **48**, 40 (1926).
[7] A. C. G. Mitchell and M. Zemansky, *Resonance Radiation and Excited Atoms* (Cambridge University Press, Teddington, England, 1934) p. 203.

TABLE IV. Comparison of results (λ2537).†

Investigation	$I_{abs.}$ (relative)	Approximate $\frac{C_2H_6}{CO}$ ratio
Herr and Noyes*	1	1.7
This paper (Table I)	6	2.2
Spence and Wild**	12	2.4
Anderson and Rollefson***	250	3.6
Photosensitized reaction	2500	4.8

† Temperature 25°C; pressure 5 cm.
* See reference 6.
** R. Spence and W. Wild, J. Chem. Soc., 352 (1937).
*** H. W. Anderson and G. K. Rollefson, J. Am. Chem. Soc. **63**, 816 (1941).

sensitized reaction, and it seemed worth making a brief investigation of it.

The apparatus, etc. was identical with that described above. A few drops of mercury were placed in the reaction vessel. The light source was a low pressure, high voltage discharge with neon as a carrier. This gave most of its emission as λ2537 and light of longer wave-lengths was removed by a chlorine filter. Well over 90 percent of the total radiation absorbed by acetone was λ2537, and the direct photolysis was therefore almost negligible.

The results of a series of runs at 50 mm pressure and various intensities are given in Table III.

The products of the reaction were unaltered, and there seems to be no doubt that the basic mechanism was the same as that of the photolysis. At low enough intensities the ratio is approaching that of the photolysis, but at high intensities it is much higher.

The effect is satisfactorily explained as due merely to the much higher absorbed intensity near the face of the cell for a given incident intensity. The radiation will be largely absorbed in the first 3 or 4 mm when mercury is present in the cell. The effect will thus be to raise the absorbed intensity per cc. near the front of the cell by a factor of the order of 40. On this assumption the results then compare with those of previous workers roughly as shown in Table IV. The estimates of $I_{abs.}$, etc. in various investigations are very rough, but show the general trend clearly.

It thus appears that the C_2H_6/CO ratio in the photolysis continues increasing to very high values at very high absorbed intensities.

THE JOURNAL OF CHEMICAL PHYSICS VOLUME 16, NUMBER 3 MARCH, 1948

Simple Expressions for the Heat Capacities of Gases

BRYCE L. CRAWFORD, JR., AND ROBERT G. PARR
School of Chemistry, University of Minnesota, Minneapolis, Minnesota

(Received December 12, 1947)

A table of constants is given whereby one may at once write down, knowing the vibrational frequencies, the best approximation of the form $C_p^\circ = A_0 + A_1 T + A_2 T^2$ to the heat capacity of a gas with translational, rotational, and vibrational (harmonic) degrees of freedom.

THE heat capacities of gases (in the limit of zero pressure) are now quite frequently calculated from a knowledge of the vibrational frequencies, and estimates of any restricting potentials. This calculation is scarcely a difficult one if one wishes to find the heat capacity at a single temperature. However, in several common types of thermodynamic problem it is convenient to have a simple algebraic expression for the heat capacity as a function of temperature; even though the simple expression is only approximate, its convenience in use compensates for its inaccuracy. Such simple expressions are often fitted to values calculated for a few temperatures from the exact expressions.

Having observed that the necessary "fitting" could be done once for all, we proceeded to carry this out for the Einstein functions. Table I presents constants with whose aid one can at once write down, for any rigid molecule, the expression

$$C_p^\circ = A_0 + A_1 T + A_2 T^2 \qquad (1)$$

which will give the best possible (least-square) approximation in this form over the temperature range from 250° to 1500°K.

It is clear that similar tables could be calculated to give the "best" constants for other approximating forms, such as $B_0 + B_1 T + B_2 T^{-2}$; and, perhaps more valuable, similar tables for the contribution of hindered internal rotations.

USE OF THE TABLE

The table gives, for each frequency ω, the contributions a_0, $a_1 \times 10^{-3}$, $a_2 \times 10^{-6}$ to the constants A_0, A_1, A_2 in Eq. (1). One must add up the contributions of the several vibrational frequencies, giving double or triple weight to doubly or triply degenerate frequencies, and including a translational-rotational contribution $a_0 = 6.954$ for linear or $a_0 = 7.948$ for non-linear molecules. The constants used here give C_p° in cal./mole deg.; absolute temperatures (degrees Kelvin) should be used in (1).

In the first part of Table I ($150\ \text{cm}^{-1} \leq \omega \leq 600\ \text{cm}^{-1}$) and in the last ($\omega > 3000\ \text{cm}^{-1}$), the values given for the a_i are accurate to the last place; in the middle part, the values may be in error by one or two units in the last place. The two needed universal constants were taken to be $(hc/k) = 1.4385$ cm deg. and $R = 1.9869$ cal./mole deg. Since the significant parameter in the calculation is not ω but $\alpha = (hc/k)(\omega/1500)$, any change in the accepted values of (hc/k) can be compensated by the use of an adjusted value of ω in entering the table; thus if (hc/k) should increase by 5 percent, one would adjust all frequencies of the molecule of interest by 5 percent upward, and use Table I as given. A change in the accepted value of R will affect the value of C_p° from Eq. (1) directly; hence if R should increase 5 percent, one may compensate by increasing the final constants A_0, A_1, A_2 by 5 percent each.

It is unlikely that values of ω higher than those in Table I will be of interest. For ω less than 150 cm^{-1}, the a_i can be calculated from the series (20); a few terms will suffice.

EXAMPLES

Thus, the equation for the heat capacity of ethylene may be found from the vibrational frequencies[1] as follows, using linear interpolation in Table I:

[1] G. Herzberg, *Infra-Red and Raman Spectra of Polyatomic Molecules* (D. Van Nostrand Company, Inc., New York, 1945), p. 326.

ω (cm^{-1})	a_0	a_1	a_2
Trans.-rotn.	7.948	—	—
825	−.151	3.365	−1.391
943	−.402	3.620	−1.460
949.2	−.415	3.630	−1.462
995	−.492	3.690	−1.471
1050	−.579	3.741	−1.471
1342.4	−.816	3.573	−1.275
1443.5	−.834	3.400	−1.158
1623.3	−.815	3.009	−.922
2989.5	−.143	.181	.443
3019.3	−.132	.147	.454
3105.5	−.103	.057	.484
3272.3	−.05	−.10	.52

$$C_p^\circ = 3.016 + 28.313\times10^{-3}T - 8.709\times10^{-6}T^2$$

The accuracy of this approximation is shown in Table II.

The accuracy will of course depend on the distribution of frequencies for the molecule concerned; in general, we may expect the approximation to err by less than 2 percent. As a relatively unfavorable example, we consider carbon dioxide:[2]

ω (cm^{-1})	a_0	a_1	a_2
Trans.-rotn.	6.954	—	—
667.3 (twice)	.287	2.789	−1.182
1336.9	−.813	3.581	−1.280
2349.3	−.450	1.240	−0.004

$$C_p^\circ = 6.265 + 10.399\times10^{-3}T - 3.648\times10^{-6}T^2$$

The accuracy is again shown in Table II.

CALCULATION OF THE TABLE

The Normal Equations

The true heat capacity of a perfect gas is given by

$$C_p(T) = \sum_\omega c(\omega, T), \tag{2}$$

where the parameters ω may be regarded as generalized to include translation, rotation, etc., as well as the frequencies of vibration. We desired to approximate this in the range 250 deg. $\leq T \leq$ 1500 deg. by a function

$$\Gamma(T) = A_0 + A_1T + A_2T^2; \tag{3}$$

our criterion is that

$$I = \int_{250}^{1500} (C-\Gamma)^2 dT = \text{minimum}. \tag{4}$$

It seems worth while to give the fundamental theorem we use: that if we have a set of functions

$$\gamma(\omega, T) = a_0(\omega) + a_1(\omega)\times10^{-3}T + a_2(\omega)\times10^{-6}T^2 \tag{5}$$

each approximate to one of the set $c(\omega, T)$, so that for each ω

$$i(\omega) = \int_{250}^{1500} (c-\gamma)^2 dT = \text{minimum}, \tag{6}$$

then the function Γ satisfying (4) is

$$\Gamma(T) = \sum_\omega \gamma(\omega, T). \tag{7}$$

The proof is easily written out.

We have for the vibrational contributions to (2)

$$c(\omega, T) = c(x) = Rx^2e^x(e^x-1)^{-2}, \tag{8}$$

where R is the gas constant and

$$x = hc\omega/kT = 1.4385(\omega/T). \tag{9}$$

The requirement (6) on the approximate functions γ leads to the "normal equations" determining the a_k:

$$a_0(\omega)\Delta T^{(k+1)} + a_1(\omega)\Delta T^{(k+2)} + a_2(\omega)\Delta T^{(k+3)} = I_k(\omega); \quad k = 0, 1, 2. \tag{10}$$

Here

$$\Delta T^{(k)} = (10^{-3k}/k)(1500^k - 250^k) \tag{11}$$

and

$$I_k(\omega) = 10^{-3(k+1)} \int_{250}^{1500} c(\omega, T)T^k dT. \tag{12}$$

Equations (10) can be solved to give

$$\begin{aligned} a_0(\omega) &= 29.3184I_0(\omega) - 70.9632I_1(\omega) + 37.4784I_2(\omega), \\ a_1(\omega) &= -70.9632I_0(\omega) + 186.7776I_1(\omega) - 103.2192I_2(\omega), \\ a_2(\omega) &= 37.4784I_0(\omega) - 103.2192I_1(\omega) + 58.9824I_2(\omega), \end{aligned} \tag{13}$$

so that we need only evaluate the $I_k(\omega)$.

Calculation for $\omega \leq 600$ cm^{-1}

For small values of ω, it is convenient to calculate the $I_k(\omega)$ from their series expansions. Equations (8), (9), and (12) combine to give

$$I_k(\omega) = (1.5\alpha)^{k+1} \int_\alpha^{6\alpha} c(x)x^{-k-2}dx, \tag{14}$$

where

$$\alpha = 1.4385(\omega/1500) = 1.4385\mu. \tag{15}$$

Now expansion of (8) gives

$$c(x) = R\sum_{n=0}^{\infty} (1-n)(B_n/n!)x^n, \tag{16}$$

[2] Frequencies from reference 1, p. 274.

where the B_n are the Bernoulli numbers: $B_0=1$, $B_1=-\frac{1}{2}$, $B_2=\frac{1}{6}$, $B_3=0$, $B_4=-1/30$, $\cdots$. Substituting (16) in (14) and integrating term by term, one obtains

$$I_k(\omega)=R(1.5)^{k+1}\sum_{n=0}^{\infty}(1-n)(B_n/n!)C_{n-k-1}\alpha^n, \quad (17)$$

where

$$C_n=(1/n)(6^n-1). \quad (18)$$

Introduction of (15) and $R=1.9869$ cal./mole deg. into (17) yields

$$\begin{aligned}
I_0(\omega)&=2.483625-2.569660\mu^2\\
&\quad+3.81077\mu^4-6.78961\mu^6\\
&\quad+12.64625\mu^8-23.78977\mu^{10}\\
&\quad+44.8567\mu^{12}-84.6271\mu^{14}+\cdots,\\
I_1(\omega)&=2.173172-1.381264\mu^2\\
&\quad+1.39581\mu^4-2.12039\mu^6\\
&\quad+3.68842\mu^8-6.69087\mu^{10}\\
&\quad+12.3356\mu^{12}-22.9198\mu^{14}+\cdots, \quad (19)\\
I_2(\omega)&=2.224914-0.963623\mu^2\\
&\quad+0.59820\mu^4-0.70407\mu^6\\
&\quad+1.10641\mu^8-1.91167\mu^{10}\\
&\quad+3.42655\mu^{12}-6.25086\mu^{14}+\cdots.
\end{aligned}$$

Values of the $I_k(\omega)$ calculated from (19) for $0.10\leq\mu\leq0.40$ are given in Table I, along with the $a_k(\omega)$ found from them.

For values of $\mu=\omega/1500$ less than 0.10, the $a_k(\omega)$ may be calculated from the series

$$\begin{aligned}
a_0(\omega)&=1.9869-13.4345\mu^2\\
&\quad+35.0941\mu^4-74.9783\mu^6+\cdots,\\
a_1(\omega)&=23.8265\mu^2-71.4641\mu^4\\
&\quad+158.4446\mu^6-\cdots, \quad (20)\\
a_2(\omega)&=-10.5706\mu^2+34.0304\mu^4\\
&\quad-77.1265\mu^6+\cdots.
\end{aligned}$$

Calculation for $\omega>3000$ cm^{-1}

At the upper end, we may use

$$(1-e^{-x})^{-2}=\sum_{n=0}^{\infty}(n+1)e^{-nx} \quad (21)$$

to expand (8); then our integrals become, with a change of variable,

$$I_k(\omega)=R(1.5\alpha)^{k+1}\sum_{n=1}^{\infty}n^k\int_{n\alpha}^{6n\alpha}y^{-k}e^{-y}dy. \quad (22)$$

TABLE I.

μ	ω (cm^{-1})	I_0	I_1	I_2	a_0	a_1	a_2
0.00	0	2.48362	2.17317	2.22491	1.987	.000	.000
0.10	150	2.45830	2.15950	2.21534	1.856	.231	−.102
.11	165	2.45308	2.15666	2.21334	1.829	.278	−.123
.12	180	2.44739	2.15357	2.21116	1.801	.329	−.145
.13	195	2.44125	2.15022	2.20880	1.770	.383	−.169
.14	210	2.43467	2.14662	2.20625	1.737	.441	−.195
.15	225	2.42766	2.14278	2.20353	1.702	.502	−.221
.16	240	2.42023	2.13869	2.20063	1.665	.566	−.249
.17	255	2.41239	2.13437	2.19755	1.626	.633	−.279
.18	270	2.40415	2.12982	2.19430	1.586	.702	−.309
.19	285	2.39553	2.12503	2.19087	1.544	.774	−.341
.20	300	2.38653	2.12003	2.18728	1.501	.848	−.373
.21	315	2.37717	2.11480	2.18352	1.457	.924	−.406
.22	330	2.36747	2.10937	2.17960	1.411	1.002	−.440
.23	345	2.35744	2.10372	2.17552	1.364	1.082	−.474
.24	360	2.34708	2.09787	2.17127	1.317	1.163	−.509
.25	375	2.33642	2.09183	2.16687	1.268	1.244	−.544
.26	390	2.32547	2.08559	2.16231	1.218	1.327	−.580
.27	405	2.31423	2.07917	2.15760	1.169	1.411	−.616
.28	420	2.30273	2.07256	2.15724	1.118	1.495	−.652
.29	435	2.29098	2.06578	2.14773	1.067	1.579	−.687
.30	450	2.27898	2.05883	2.14258	1.016	1.663	−.723
.31	465	2.26676	2.05171	2.13729	.964	1.747	−.759
.32	480	2.25432	2.04443	2.13186	.912	1.831	−.794
.33	495	2.24169	2.03700	2.12169	.861	1.915	−.829
.34	510	2.22886	2.02942	2.12059	.809	1.997	−.863
.35	525	2.21585	2.02169	2.11476	.757	2.079	−.897
.36	540	2.20268	2.01383	2.10880	.706	2.160	−.931
.37	555	2.18935	2.00583	2.10271	.655	2.240	−.964
.38	570	2.17588	1.99770	2.09650	.604	2.319	−.996
.39	585	2.16228	1.98945	2.09018	.553	2.396	−1.027
.40	600	2.14857	1.98108	2.08373	.503	2.472	−1.058
.45	675	2.07852	1.93761	2.04980	.263	2.824	−1.196
.50	750	2.00687	1.89185	2.01336	+.044	3.124	−1.308
.55	825	1.93457	1.84432	1.97472	−.151	3.365	−1.391
.60	900	1.86236	1.79545	1.93417	−.320	3.547	−1.445
.65	975	1.79081	1.74561	1.89197	−.462	3.672	−1.471
.70	1050	1.72036	1.69513	1.84839	−.579	3.741	−1.471
.75	1125	1.65133	1.64428	1.80367	−.671	3.758	−1.448
.80	1200	1.58393	1.59331	1.75804	−.740	3.730	−1.404
.85	1275	1.51833	1.54241	1.71169	−.788	3.663	−1.342
.90	1350	1.45462	1.49176	1.66481	−.819	3.563	−1.267
.95	1425	1.39285	1.44152	1.61759	−.834	3.436	−1.181
1.00	1500	1.33307	1.39182	1.57019	−.836	3.288	−1.087
1.05	1575	1.27528	1.34276	1.52275	−.827	3.123	−.988
1.10	1650	1.21946	1.29444	1.47541	−.809	2.945	−.885
1.15	1725	1.16559	1.24694	1.42829	−.784	2.759	−.780
1.20	1800	1.11365	1.20034	1.38151	−.753	2.569	−.675
1.25	1875	1.06362	1.15470	1.33519	−.717	2.377	−.572
1.30	1950	1.01545	1.11007	1.28941	−.678	2.185	−.471
1.35	2025	.96910	1.06649	1.24424	−.637	1.996	−.374
1.40	2100	.92452	1.02398	1.19975	−.595	1.812	−.281
1.45	2175	.88168	.98257	1.15602	−.551	1.632	−.192
1.50	2250	.84052	.94229	1.11311	−.508	1.458	−.107
1.55	2325	.80101	.90315	1.07107	−.464	1.291	−.028
1.60	2400	.76310	.86517	1.02995	−.421	1.132	+.046
1.65	2475	.72674	.82835	.98977	−.380	.982	.114
1.70	2550	.69188	.79268	.95056	−.341	.840	.177
1.75	2625	.65848	.75816	.91236	−.302	.706	.235
1.80	2700	.62649	.72479	.87518	−.265	.581	.288
1.85	2775	.59586	.69256	.83904	−.231	.466	.335
1.90	2850	.56655	.66146	.80395	−.198	.359	.377
1.95	2925	.53853	.63147	.76991	−.167	.259	.415
2.00	3000	.51173	.60257	.73692	−.139	.168	.447
2.1	3150	.4617	.5480	.6741	−.09	.01	.50
2.2	3300	.4158	.4973	.6152	−.04	−.12	.53
2.3	3450	.3742	.4508	.5606	−.01	−.22	.56
2.4	3600	.3366	.4082	.5102	+.02	−.30	.57
2.5	3750	.3023	.3690	.4633	+.04	−.36	.57
2.6	3900	.2712	.3330	.4200	+.06	−.41	.57
2.8	4200	.2177	.2702	.3438	+.09	−.46	.54
3.0	4500	.1741	.2182	.2798	+.10	−.47	.50
3.5	5250	.0983	.1258	.1639	+.10	−.39	.36
4.0	6000	.0545	.0710	.0937	+.07	−.28	.24
5.0	7500	.0161	.0215	.0286	+.02	−.08	.07

These can be integrated by parts and in terms of the exponential integral

$$-E_i(-x)=\int_x^{\infty}e^{-x}x^{-1}dx \quad (23)$$

TABLE II. Accuracy of approximate formulas for ethylene and carbon dioxide.

	T(°K)	250	500	750	1000	1250	1500
Ethylene							
	$C_p°$ true[a]	9.346	15.165	19.471	22.501	24.691	26.276
	$C_p°$ calc.[b]	9.550	14.995	19.352	22.620	24.763	25.890
Carbon Dioxide							
	$C_p°$ true	8.325	10.664	12.063	12.938	13.493	13.854
	$C_p°$ calc.	8.637	10.553	12.012	13.016	13.564	13.656

[a] "True" values are calculated from Eq. (2).
[b] "Calc." values are computed from equations of the form (5).

to give

$$I_0(\omega)=R(1.5\alpha)[(e^{\alpha}-1)^{-1}-(e^{6\alpha}-1)^{-1}], \tag{24}$$

$$I_1(\omega)=R(1.5\alpha)^2\sum_{n=1}^{\infty} n[-E_i(-n\alpha)+E_i(-6n\alpha)], \tag{25}$$

$$I_2(\omega)=R(1.5\alpha)^3\{e^{-\alpha}\alpha^{-1}(1-e^{-\alpha})^{-2}-e^{-6\alpha}(6\alpha)^{-1}(1-e^{-6\alpha})^{-2}-\sum_{n=1}^{\infty} n^2[-E_i(-n\alpha)+E_i(-6n\alpha)]\}. \tag{26}$$

For $\omega>3000$ cm^{-1}, it is sufficient to take

$$I_0\cong R(1.5\alpha)(e^{\alpha}-1)^{-1}, \tag{27}$$

$$I_1\cong R(1.5\alpha)^2\sum_{n=1}^{5} n[-E_i(-n\alpha)], \tag{28}$$

$$I_2\cong 1.5R^{-1}e^{\alpha}(I_0)^2-R(1.5\alpha)^3\times\sum_{n=1}^{5} n^2[-E_i(-n\alpha)]. \tag{29}$$

These equations were used to calculate the I_k and a_k in the last part of Table I.

Calculation for Intermediate ω

As always, there is the intermediate range (600 cm^{-1} $<\omega\leq$3000 cm^{-1}) where neither series is convenient; we evaluated these $I_k(\omega)$ by numerical integration. It is convenient to calculate by Gregory's formula[3] a set of integrals

$$J_k(\omega_i,\omega_{i+1})=\int_{\alpha_i}^{\alpha_{i+1}} c(x)x^{-k-2}dx;\quad i=1,2,\cdots. \tag{30}$$

The α_i are an appropriate sequence of values of α. The $I_k(\omega)$ then follow from relations of the form

$$I_k(\omega)=(1.5\alpha)^{k+1}\sum_{\omega_i=\alpha}^{\omega_{i+1}=6\alpha} J_k(\omega_i,\omega_{i+1}). \tag{31}$$

Values of the $I_k(\omega)$ for $0.40<\mu\leq 2.00$ computed in this manner, using the table of Einstein functions given by Taylor and Glasstone,[4] are given in Table I, with the corresponding a_k.

Accuracy

The series expansions at either end were carried out far enough so that the last digit in the I_k should be off not more than 1; the a_k should be good to the last digit given. In the intermediate range the last digit given for the I_k is not significant, and the a_k may be off 1 or 2 in the last place.

The I_0 can of course be evaluated in closed form in terms of the heat-content function. We evaluated it by the same methods used for I_1 and I_2 chiefly to provide a check.

ACKNOWLEDGMENTS

Mr. T. Yamada helped with the calculations. We are also grateful to the Graduate School of the University of Minnesota for a grant in support of these calculations.

[3] Cf. for example, Margenau and Murphy, *The Mathematics of Physics and Chemistry* (D. Van Nostrand Company, Inc., New York, 1943), p. 459.
[4] Taylor and Glasstone, *Treatise on Physical Chemistry, Volume I* (D. Van Nostrand Company, Inc., New York, 1942), p. 655.

THE JOURNAL OF CHEMICAL PHYSICS VOLUME 16, NUMBER 3 MARCH, 1948

Poisoning of Platinum Catalysts at High Temperatures

ROBERT H. SAVAGE
Research Laboratory, General Electric Company, Schenectady, New York
(Received December 17, 1947)

Poisoning films of exceptional thermal stability are formed on a platinum catalyst when heated in a silicone vapor (hexamethyldisiloxane) at pressures of the order 10^{-3} mm. These films prevent the combination of hydrogen and oxygen at low pressures and are not removed until heated to about 1440 K in the presence of hydrogen (or to higher temperatures in oxygen). It is suggested that the film may consist of a silicon oxide oriented with the silicon atoms attached directly to the platinum and presenting an outer layer of oxygen atoms, effectively shielding the catalyst.

INTRODUCTION

THE poisoning of platinum catalysts by various gases at ordinary temperatures has been observed by chemists for over a century. The reaction between hydrogen and oxygen at low pressures provides a convenient means for studying this poisoning. At a known temperature the reaction velocity serves as a measure of extent of the active surface. Although large differences exist in the behavior of the known gases which cloak the platinum and which are responsible for the poisoning, it has been apparent that all of these gases are easily removed with restoration of the catalytic activity merely by heating the surface to incipient color. In this connection, Langmuir found[1] that the H_2+O_2 reaction is not sensitive to the previous treatment of the platinum when heated to the range 700 to 1900 K: the platinum in this temperature range showed no poisoning effect. This, in contrast to the known behavior of tungsten, certainly illustrates the ease with which adatoms on platinum are generally removed. Use of these characteristics is made, for example, in the microanalysis of gases,[2] where the usual procedure is simply to heat the platinum filament to a dull red to complete the combustion of oxygen and hydrogen (or of other mixtures).

In connection with a study of gas reactions occurring at low pressures in the region around the minute heated areas of carbon brush contacts, we found that a platinum filament used for the ignition of hydrogen and oxygen was mysteriously poisoned so that no combination of these gases would occur at the dull red heat. Upon raising the filament temperature, the inactivity was found to persist up to 1340K. Even at this temperature no reaction was detectable in the apparatus, which was sensitive to pressure changes of the order 0.1 micron. Finally the activity was restored by flashing at white heat; within 10 seconds, 50 percent of the gas mixture was cleaned up by condensation of the water in a cold trap. The unusual stability of the poison film, initially of unknown origin, led us to the following brief study of its nature and properties.

APPARATUS

The apparatus consisted of a Pyrex-Nonex vacuum system (10-mm average bore) containing McLeod and Pirani gauges, cold traps, mercury cut-offs, gas storage bulbs and, in a side arm, the tube containing the filament (a 10-mil diameter wire in the form of an inverted loop, spot-welded at the ends to the leads). This system had been used in other work and was not changed for the study of the poisoning (although other arrangements would clearly have been more convenient) because the source was indicated to lie in the system, and it was intended not to disturb this.

Gas or vapor pressures were read in terms of the unbalance current indicated by microammeters which were connected in a calibrated bridge containing the Pirani indicator and compensator. The filament brightness temperatures were measured with a disappearing-filament pyrometer and were corrected to absolute tem-

[1] I. Langmuir, Trans. Faraday Soc. **17**, 621 (1921).
[2] F. J. Norton and A. L. Marshall, Am. Inst. Mining Met. Eng. Tech. Pub. No. 1643 (1944).

peratures from data in the *International Critical Tables* (5, 245; 1929).

INITIAL EXPERIMENTS

Source of the Poison

At first, with this apparatus, many attempts were made to duplicate the original accidental poisoning by exposing the platinum at various temperatures to the gases which had been under study at the time. All of these failed. It was then recalled that the apparatus had been exposed to a silicone vapor (hexamethyldisiloxane*) a few days previously, and it was found that the glass walls were still evolving this vapor at a rate sufficient to build up a pressure of 1 to 2 microns when the pump had been closed off for an hour. The vapor was suspected as having contributed to the effect and, accordingly, a fresh quantity was admitted (25-micron pressure). Upon heating the platinum in this vapor for about 30 seconds, the poisoning occurred: mixtures of hydrogen and oxygen, tested subsequently, would not combine perceptibly although the platinum was held at the high temperature (1340 K) for several minutes, Fig. 1 (curve *A*). The test consisted in observing the gas pressure while the filament was heated and while one of the traps was chilled with liquid nitrogen to condense the reaction product.

Next it was found, consistent with the initial observations, that the film responsible for this poisoning was quickly destroyed and rapid clean up of the gases occurred immediately (Fig. 1, curve *B*) when the filament temperature was increased to 1440 K in the hydrogen-oxygen mixture.

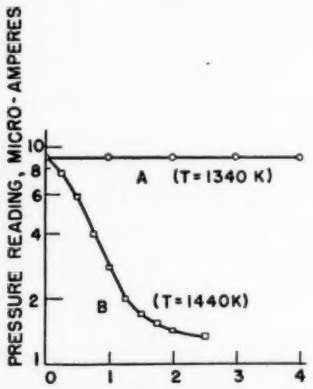

FIG. 1. Clean up of H_2+O_2 mixture by platinum at 1340 and at 1440 K after poisoning at 1340 K. For H_2, 1 microampere=1.8-micron Hg; O_2, 1 microampere=4.0 microns-Hg.

* $[(CH_3)_3Si]_2O$, vapor pressure 40 mm (mercury) at room temperature.

It was further found that the poisoning could be reproduced easily, a silicone pressure as low as 10^{-3} mm being adequate. The introduction of fresh silicone for each experiment was not necessary because the silicone continued to evolve slowly from the glass after a single exposure of the system to it, and this residual vapor was sufficient to provide an effective pressure for many trials although the apparatus was repeatedly evacuated below 0.01 micron. Thus when a low pressure of the silicone was required for an experiment, the system was exhausted and closed off from the pumps, and the trap chilled with liquid nitrogen; then after warming the trap to the range −110 to −80C, the residual silicone pressure would gradually build up to one or two microns, and these low pressures were used for poisoning.

METHOD OF TESTING

In order to estimate the relative extent of the poisoning resulting from the different experimental treatments which were tried, the filament was tested immediately after each treatment by heating to 1340 K in a mixture of hydrogen and oxygen** at a total pressure of 20 to 40 microns; then, from the observed clean-up rates, the half-time (τ) for hydrogen clean up was determined. This will be illustrated in the following paragraphs.

Effect of Temperature upon the Poisoning

The effect of the filament temperature (as maintained during exposure to the silicone) upon the poisoning subsequently evaluated is shown in Fig. 2. The slopes indicate the rates of gas clean up at the filament test temperature 1340 K, following exposure to the silicone at the different poisoning temperatures indicated for the pretreatments for each of the curves. Curve *A* gives the reference slope for the clean platinum.

From the known initial partial pressures of the component gases in these experiments, separate

** The concentration of oxygen was a few microns in excess of that necessary for complete combustion.

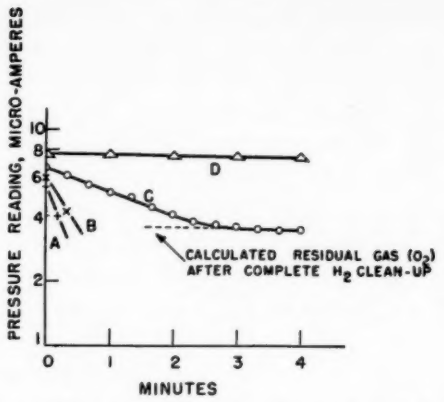

FIG. 2. Clean up of H_2+O_2 mixture by platinum at 1340 K. Pre-treatment: *A*—fire 1800 K, vacuum. *B*—heat 523 K, residual vapor. *C*—heat 723 K, residual vapor. *D*—fire 1340 K, residual vapor.

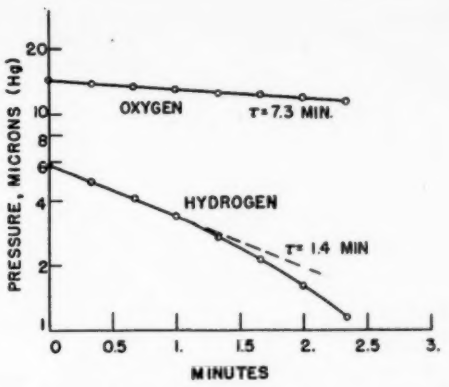

FIG. 3. Clean up of H_2 and O_2 by platinum at 1340 K after poisoning at 723 K (Fig. 2, C).

clean-up curves for each of the cases in Fig. 2 were plotted, as shown, for example, in Fig. 3. From the slopes of the hydrogen curves thus obtained, the half-times were determined. These are given in Table I. From these data it is seen that the poisoning effect begins at a platinum temperature between 523 and 723 K and is nearly complete at 1340 K ($\tau = 28$ minutes).

Stability of the Poison Film

It was mentioned earlier that the filament was cleaned by high firing to 1440 K or above in the gas mixture or in vacuum. Rapid clean up of the hydrogen-oxygen mixture followed reproducibly at the test temperature 1340 K. Further study showed that this reactivation process did not occur readily when the high firing was carried out in oxygen alone. For example, when the poisoned filament had been fired to 1610 K in oxygen and was tested subsequently in the gas mixture (test-temperature 1340), the half-time τ was found to be 50 minutes, indicating that only slight reactivation had occurred. In contrast, when the poisoned filament had been fired in the hydrogen-oxygen mixture, to the considerably lower temperature 1440, τ was found in the subsequent standard test to be 0.1 minute representing a clean filament. Thus the chemical stability of the poisoning film was much lower with hydrogen present than in oxygen.

This stability of the film was affected not only by the chemical environment when fired, after the poisoning, but also by the history of the platinum prior to the silicone exposure. For instance, the perceptible pressure fall noted on Fig. 2 after the 1340 treatment (curve *D*), for which $\tau = 28$ minutes in Table I, was inconsistent with earlier observations where the clean-up rate had been zero ($\tau = \infty$). It was finally shown that the film stability was lowered if the platinum had been exposed to a small amount of oxygen (about 0.5 micron) while being heated just before or during the exposure to the silicone. It was next found that the most stable film could be readily formed by cleaning the platinum in hydrogen and then poisoning it by exposure to a mixture of hydrogen and silicone vapor at 1340 K. This procedure effectively excluded oxygen. Thereafter the filament was completely inactive when tested in a hydrogen-oxygen mixture ($\tau = \infty$). In contrast, the effect of an oxygen pretreatment (before poisoning) was to lower the stability of the film subsequently formed so that when finally tested τ was found to be only a few minutes.

NATURE OF THE POISONING FILM

The composition of the film formed on the platinum by the silicone exposure is not known. The quantity of vapor required to form a monolayer on the filament in our apparatus (volume $= 530$ cm^3) would require a pressure difference of much less than 1 micron. As might be expected, no pressure changes have been observed during the film formation. The solid reaction products have not been isolated. The micromanipulation of gases in the system containing the silicone vapor has presented unexpected

TABLE I. Half-time for the hydrogen clean up in relation to platinum poisoning temperature.

Curve	Poisoning exposure minutes	Filament pre-treatment Atmosphere	Temperature °K	Filament test in H_2+O_2 mixture: half-time for H_2 τ (minutes)
A	0.	(Fired in vacuum) 15 seconds	1800	0.11
B	2.	Silicone vapor	523	0.10
C	2.	Silicone vapor	723	1.
D	0.5	Silicone vapor	1340	28.

complications, owing to preferential sorption effects between the silicone and water vapor, which compete for the glass surface. For example, following the condensation of the reaction product (water) in the cold trap during a clean up of the gas mixture, the condensate was sealed between the mercury cut-offs and the trap was warmed. Previously the silicone pressure had been low (1.3μ), and it was anticipated that the vapor from the trap would be mainly water. The total pressure of the evolved vapor (17.μ) was reasonably close to that of the water which was calculated as having condensed, but upon closer study this vapor was found to contain *only a small percentage water* (1.6μ) and was mainly silicone. This curious effect was noted repeatedly and was one of the factors which interfered with the analytical handling of the gas samples. It was proven to be the result of the competitive and preferential sorption already mentioned.

From the clean-up effects alone, however, some conclusions can be drawn regarding the nature of the films which poisoned the platinum. There are seemingly two types: (1) that which combined with the clean platinum and (2) that which combined with the oxygen-coated platinum.

It is suggested that the first of these, which is the more stable and which possesses the more reproducible characteristics, is an oxide of silicon, oriented so that the silicon atoms are attached directly to platinum atoms, the outer surface of the film being composed of oxygen atoms. (This is analogous to the carbon monoxide film which poisons platinum at low temperatures and which is known to be oriented with the carbon atoms attached directly to the platinum.)[1]

The observed properties of the film, as described, support this view in the essential details. A silicon monoxide film chemically bonded to the metal would show the low vapor pressure which is the outstanding characteristic of the present film and also would evaporate in some reproducible temperature range near white heat, as this film apparently does during the reactivation of the filament. Further, the evaporation would occur at a higher temperature in oxygen than in hydrogen-oxygen mixtures: with hydrogen present and at the lower temperature, the oxide would be reduced with the formation of a volatile product.

The formation of a silicon monoxide film would be expected to begin with the cleavage of the Si—O bond in the silicone molecule and adsorption of the organosilicon fragments on the clean platinum. The subsequent oxidation or loss of the methyl groups would then yield the stable silicon oxide on the metal and traces of CO_2 and water in the ambient. If this is correct, we should expect other alkyl silicones to produce similar poisoning.

A monolayer of silicon monoxide derived from the silicone vapor thus appears to account for the unusually stable poisoning film described. It is not known, however, whether the filming process would stop upon completion of the monolayer since at the rather high temperatures of these experiments, continued decomposition of the vapor may occur. Bearing upon this, it has been observed that the silicone vapor in the absence of oxygen is not cleaned up at a perceptible rate by the hot filament through the temperature range up to 1500 K; and this would indicate that the rate of film formation, after the initial monolayer, is, at most, relatively low. It is probable that the silicone molecule is much more stable toward the (suggested) monoxide surface than toward the clean platinum, in which case the rate may fall to zero upon completion of the initial layer.

In a later paper, it will be shown that carbon (or graphite) is coated similarly when heated in silicone vapor so that it also shows remarkable properties, among which is that of not combining with oxygen at temperatures up to at least 1200 K.

A New Method of Preparing Strongly Luminescent Thallium Activated Alkali Halides and Some Properties of These Phosphors

E. Hirshlaff Hutten* and Peter Pringsheim**
Department of Physics and Department of Chemistry, University of Chicago, Chicago, Illinois
(Received December 19, 1947)

Phosphors with a bright visible fluorescence and a long lasting afterglow can be prepared by grinding potassium chloride with small amounts of a thallous salt in a mortar. The character of the luminescence spectra and the phosphorescence decay depends on the thallium concentration. The behavior of other alkali halides under the same treatment and some conclusions concerning the probable carriers of the luminescence are discussed.

1. INTRODUCTION

IMPURITY activated alkali halide phosphors were prepared for the first time as single crystals by Pohl and his collaborators.[1] Most of their work, especially with respect to the emission process, was performed with thallium activated potassium chloride and bromide. Although the visible luminescence of such phosphors was mentioned on one occasion, the u-v emission was investigated almost exclusively.[2] Probably this was due to the fact that at the low thallium concentrations generally used in single-crystal phosphors the visible luminescence is relatively weak and does not extend far into the region of greater wave-lengths. Later it was shown that KCl(Tl) and KBr(Tl) phosphors of very high visible luminosity can be obtained by crystallization from a boiling aqueous solution saturated with potassium and thallous chlorides or bromides.[3]

2. PREPARATION OF THE NEW PHOSPHORS

It has now been found that phosphors with similar properties can be prepared by grinding potassium chloride together with a small quantity of a thallous salt in a mortar. The anion of the thallium salt is of no importance; identical results were obtained using TlCl, $TlNO_3$, and Tl_2SO_4. Exactly as in the single-crystal phosphors, only fluorescence is excited in the new phosphors when they are irradiated with light of wave-length 2537A, while phosphorescence is excited by light of wave-lengths below 2300A. In the following, the term luminescence is always applied in the sense of visible fluorescence under excitation with the Hg line 2537, if the contrary is not stated explicitly.

The source for 2537 line irradiation was a so-called "mineral light" lamp, a low pressure mercury arc with a filter transmitting the u-v down to 2400A. The quality of the finished phosphors was the same whether they were prepared in daylight, in the dark, or under "mineral light," but in the latter case, the formation of the phosphor can be demonstrated in a very striking manner. Under these conditions, bright spots appeared in the microcrystalline powder mixture practically at the instant when the pestle touched it, and after a minute of grinding the whole powder was converted into a uniformly luminescent material.

While this was the general behavior in all instances, the luminescence of the powder became much brighter and changed from a more bluish to a more yellowish white when the air was very humid or when the pestle was slightly moist. Although the quantity of water present under these conditions was so small that the finished phosphor powder seemed to be quite dry, this experience suggested that the introduction of thallous ions into the KCl lattice was due to the fact that the surfaces of the KCl crystals were first attacked by water. Therefore, all materials used (mortar, pestle, and the two salts) were baked in an oven for several hours at 150°C and put into a desiccator during the cooling period. The results obtained with these materials immediately after being taken from the desiccator did not differ from those obtained previously. It must be

* Now at the Department of Physics, University of London, England.
** Now at the Argonne National Laboratory, Chicago, Illinois.
[1] R. Pohl and E. Rupp, Ann. d. Physik **81**, 1161 (1926).
[2] W. Buenger, Zeits. f. Physik **66**, 311 (1930); W. Buenger and W. Flechsig, *ibid.* **69**, 637 (1931).
[3] Peter Pringsheim, Rev. Mod. Phys. **14**, 132 (1942).

TABLE I. Fluorescence bands of KCl(Tl) phosphors (wave-lengths in A).

Designation	*a*	*b*	*b'*	*c*
Band limits	2800–3300	3600–4050	4450–4700	5200–6300
Band peaks	3000	3850	4570	5400; 6100

admitted, however, that the grinding was performed in the presence of atmospheric air, so that some moisture was always present during the grinding, and it still seems probable that this is essential for the production of luminescence.

For the experiments described above, at first the crystalline powders of KCl and TlCl were heated in a common evaporating dish to 170°C, a small quantity of the thallium salt being placed on top of the potassium salt. After 12 hours of this treatment the whole surface of the KCl powder had become luminescent, with the strongest luminosity in the immediate neighborhood of the Tl powder, while the Tl powder itself remained completely dark. When the experiment was repeated at 135°C, the TlCl powder was surrounded by a narrow luminescent ring even after one hour, and after 12 hours the ring had extended into a halo about 1 mm wide. At 100°C and below similar effects could not be observed. In the final experiment the two salts (KCl and TlCl) were kept in separate dishes and mixed only after having cooled to room temperature.

In order to obtain some indications concerning the mechanism by which the activation takes place, a series of powders with varying thallium content were prepared. The starting mixture contained 1.5-g TlCl and 3-g KCl or 13.4 molar percent of TlCl. This was diluted successively with KCl, each time adding 3 g of KCl to 1 g of the preceding preparation, so that the second mixture contained one part (by weight) of TlCl in 12 parts of the total mixture, the following one part TlCl in 48 parts of mixture, and the seventh one part TlCl in 12288 parts of mass, corresponding to a change in molar percentage from 13.4 to 0.0025. Such a series was numbered C(10) to C(16), C(10) being the initial mixture. C(10) was relatively little luminescent after having been ground "dry," but became brilliantly luminescent with a yellowish-white color after grinding with a slightly moistened pestle. The luminescence of each following preparation was somewhat darker and more bluish than the preceding one, but even after prolonged grinding they never attained the luminescence intensity of C(10) and C(11) and all gained in luminosity by "moist grinding." The luminescence of the last samples, C(15) and C(16), was rather weak and more violet, but still very perceptible.

TABLE II. Relative intensities of the bands emitted by KCl(Tl) phosphors of different Tl concentrations.*

Phosphor	Tl%	*a*	*b*	*b'*	*c*
C(10)	13.4	none	*m*	*m*	*st*
C(11)	2.7	none	*m*	*m*	*st*
C(12)	0.66	*m*	*st*	*m*	*m*
C(13)	0.25	*m*	*st*	*m*	*w*
C(14)	0.05	*st*	*st*	*w*	none
C(15)	0.01	*st*	*st*	*v w*	none

st = strong; *m* = medium; *w* = weak; *v w* = very weak.

3. FLUORESCENCE SPECTRA

Fluorescence spectra of various samples were obtained by means of a Steinheil, one-prism glass spectrograph for the visible and with a Hilger, quartz G H spectrograph for the u-v. Eastman I F spectrographic plates were used for the long wave-length region; exposures with I N plates did not reveal the existence of any fluorescence bands with wave-lengths exceeding 6300A. The spectra were in good agreement with those described earlier. Altogether there were four bands or band groups which are listed in Table I, using the same nomenclature as in the earlier paper.[3]

It has been shown in this paper that the relative intensities of the various bands depend greatly on the wave-length of the exciting light, but it has already been mentioned there that the long wave-length band *c* had its greatest intensity at high Tl concentrations and was missing at the lowest Tl concentrations. This result was confirmed with the new phosphors and the color shift in the luminescence from whitish yellow to violet was found to be due to this change in the relative band intensities. The spectrograms made it clear that the apparent loss in luminosity with decreasing Tl concentration was not due exclusively to a corresponding loss of total fluorescence yield, but also to a transfer of energy to the u-v emission bands. Table II lists the relative intensities of the various bands emitted by phosphors of various Tl concentrations. Some of the spectra are reproduced in Figs. 1 and 2.

The relation between the excitation and emission spectra of these phosphors and the thallium concentration can be interpreted by the assump-

tion that the phosphors contain (at least) two types of centers. The first is characterized by a relatively narrow absorption band of great intensity and the luminescence bands of shorter wave-length; the absorption band of the second is much lower and more diffuse and overlaps the former on both sides, while the corresponding emission bands lie in the region of greater wave-lengths. Light of a wave-length which coincides with the peak of both absoption bands excites the centers of the first type strongly and those of the second type appreciably less. If the wave-length of the exciting light is shifted from the peak of the absorption bands to greater or smaller values, the excitation becomes more favorable for the centers of the second type. Finally, one must assume that higher thallium concentrations favor the formation of centers of the second type. It may be mentioned in this connection that the short wave-length absorption bands of KCl(Tl) phosphors become very broad and diffuse at high thallium concentrations.

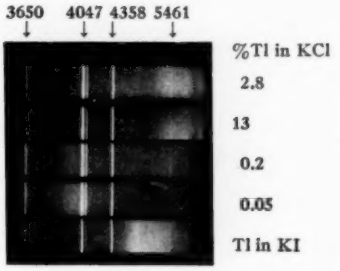

FIG. 1. Visible fluorescence spectra of KCl(Tl) phosphors of various Tl concentration and of a KI(Tl) phosphor.

4. PHOSPHORESCENCE

In all impurity activated alkali halide phosphors, *fluorescence* is excited only when the wave-length of the primary radiation coincides with the wave-length of the first absorption band of the phosphor (for KCl(Tl): $\lambda_1 = 2475$A), while *phosphorescence* in addition to fluorescence is excited by light of shorter wave-lengths covering the second absorption band of the phosphor (for KCl(Tl): $\lambda_2 = 1950$A). In this respect also the phosphors prepared by grinding behaved exactly like those prepared by crystallization and the original single-crystal phosphors.

The shape of the decay curve of these phosphors has been a matter of much controversy: strictly exponential or in other cases only slightly deviating from exponential according to Buenger and Flechsig[4] and Randall and Wilkins;[5] strictly hyperbolical and following the laws of a second-order reaction according to Antonov Romanowski[6] and Birus and Zierold[7] (all working with single-crystal phosphors and measuring the u-v afterglow); hyperbolic at first, later exponential, but not in agreement with the laws of a second-order reaction even during the hyperbolic phase according to one of the authors (P.P.).[3] In this last instance, the visible and the u-v phosphorescence of microcrystalline powder obtained by crystallization from aqueous solutions followed the same law of decay.

Decay curves of the visible afterglow were obtained with the new phosphors by means of a photo-multiplier tube hooked up to an Esterline Angus recorder which allowed the decay to be followed from 1 second after the end of the excitation for a period of 30 minutes through an intensity drop from 1 to $3 \cdot 10^{-4}$. This was attained by increasing the amplification of the photocurrent by a factor ten each time when the deflection of the galvanometer pen had decreased to one-tenth of its initial value. By connecting

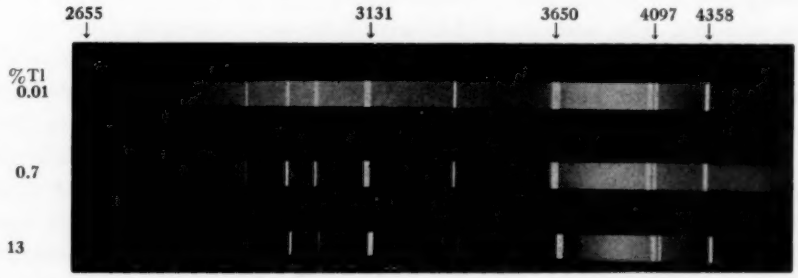

FIG. 2. Ultraviolet fluorescence spectra of KCl(Tl) phosphors of various Tl concentration.

[4] W. Buenger and W. Flechsig, Zeits. f. Physik **67**, 42 (1931).
[5] J. T. Randall and M. H. F. Wilkins, Proc. Roy. Soc. **184**, 366 (1945).
[6] W. W. Antonov Romanowski, Bull. Acad. Sci. U.S.S.R. **5**, 523 (1941); J. Phys. U.S.S.R. **7**, 153 (1943).
[7] K. Birus und H. Zierold, Naturwiss. **30**, 63 (1942).

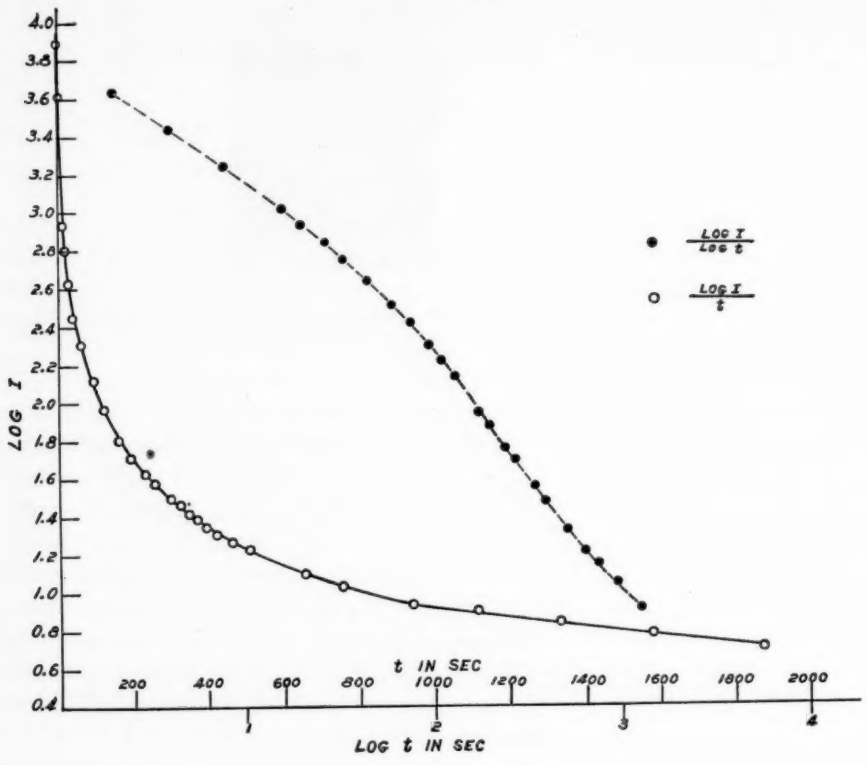

FIG. 3. Decay curve of a KCl(Tl) phosphor.

the multiplier tube directly to a sensitive galvanometer, the decay could be followed without difficulty for 24 hours. The phosphors were excited for 60 seconds with the radiation from a condensed spark between iron electrodes. The intensity of the irradiation could be altered in steps from 100 to 10 to 1 by varying the distance between the spark gap and the phosphor which was covered with a quartz plate.

The decay curves were similar, though not identical, for the various samples. Only samples of the type C(10), with the highest thallium concentration and the brightest yellowish white fluorescence exhibited a very weak afterglow of the same color which was perceptible only for a few minutes. The samples C(12) with 0.66 percent Tl and a bright white fluorescence and C(15) with 0.01 percent Tl and a relatively weak violet visible fluorescence showed equally strong and persistent phosphorescence. This is probably caused by the fact that the photo-cathode of the multiplier tube has its highest sensitivity in the violet.

The curve in Fig. 3 shows that the decay is certainly not exponential and is not represented by a straight line in a graph of log intensity *versus* time. It is better represented by a straight line in a graph of log intensity *versus* log time with a slope corresponding to the relation:

$$I = I_0 t^{-1.1}.$$

The following two experiments made it quite clear that the process follows neither a first-order nor a second-order law. In the first instance, the complete curves of the decay during the first 15 seconds were recorded after excitation with intensities 1:10:100. The absolute luminescence intensities differed greatly and were reduced in Fig. 4 by a factor such that they coincided at the end of 15 seconds. The initial slope of curve *a*, corresponding to the strongest excitation, is much steeper than that of *b* and *c*. For an exponential decay the three curves should coincide. However, the behavior shown in Fig. 4 is similar to that caused by a second-order reaction. In the second experiment, the sample was irradiated with light which in one case had an intensity ten times larger than in the other, but the high intensity curve was recorded only after it had dropped to the point from which the low intensity curve started. The two curves should coincide in a second-order reaction, but the curve in which the phosphor had already lost a great part of its

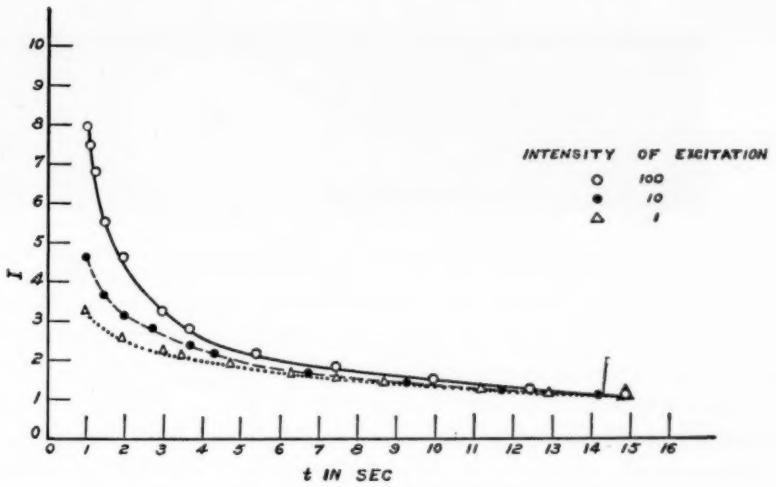

FIG. 4. Initial decay of a KCl(Tl) phosphor with three different excitation energies (phosphorescence intensities after 15 sec. reduced to same value).

initial intensity is appreciably less steep than the other (Fig. 5).

Such decay curves can, of course, be interpreted by assuming an adequate distribution of trap depths, but they might also be explained by second-order reactions which are strongly distorted by the microcrystalline and very inhomogeneous structure of the material.

5. OTHER ALKALI HALIDES

Mixtures of potassium bromide and thallous salts showed a behavior quite analogous to that of the chloride mixtures, and since this had also been observed with respect to the phosphors prepared by precipitation, no further investigation was deemed to be necessary. When potassium iodide was ground together with thallous chloride, it produced a phosphor with a very bright blue-green luminescence (spectrum in Fig. 1). While the non-luminescent pure powders of KI and TlCl or $TlNO_3$ were pure white, the color of the mixture turned into a light yellow the moment the grinding began.

Potassium fluoride did not become fluorescent when ground together with TlCl, but the powder mixture which had retained its white surface in daylight after having been ground, turned into a dark gray almost immediately after exposure to "mineral light." Instead of exciting photoluminescence, the light in this case produces a photo-chemical reaction of still unknown nature. The darkening was quite persistent, when the powder was kept in the dark for many days, nor did it change much when exposed to daylight. TlCl and KCl separately remain white after an indefinite time of exposure to mineral light. When the non-luminescent powder, even after being darkened, was reground together with some KCl, the new mixture became luminescent to about the same degree as corresponded to the quantity of thallium salt and potassium chloride in the mixture.

NaCl with an admixture of TlCl did not show the slightest trace of visible fluorescence after the same treatment which produced the highly fluorescent KCl(Tl) phosphors. It must be emphasized that, according to Hilsch and others, NaCl(Tl) phosphors prepared as single crystals from the melt have their first absorption and fluorescence excitation band at 2540A. No visible fluorescence could be obtained by prolonged grinding nor by grinding with a wet pestle. After excitation with the light from a spark between aluminum electrodes a very weak afterglow could

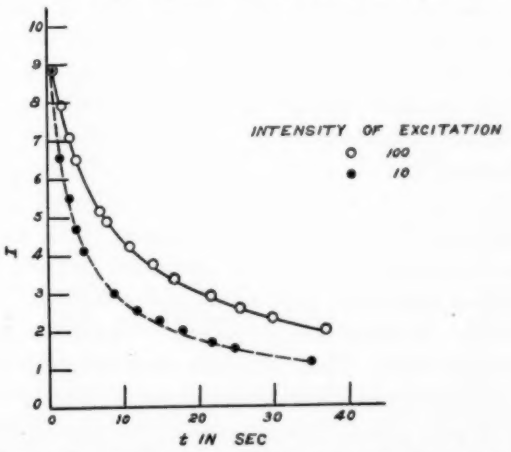

FIG. 5. Decay curve of a KCl(Tl) phosphor excited with different intensities and recorded at the same phosphorescence intensity range.

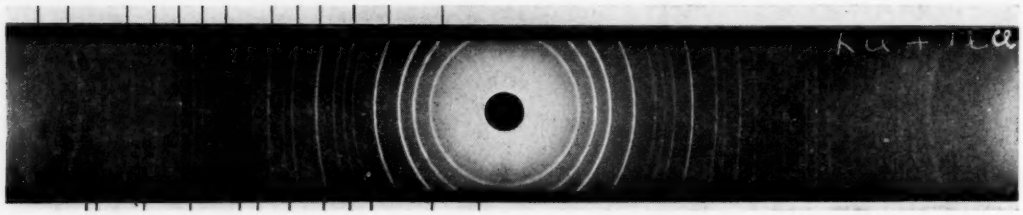

FIG. 6. X-ray pattern of a KCl(Tl) phosphor; lines marked above belong to KCl and those marked below to TlCl.

be perceived with dark-adapted eyes. When a small quantity of KCl was added to the powder and grinding restarted, luminescent spots began to appear immediately.

Grinding of cesium bromide together with a thallous salt produced a powder with visible luminescence; but its intensity was far weaker than that of potassium salts containing the same concentration of thallous ions and its color was more greenish. The facts enumerated in the last section seem to prove that potassium halides have a specific tendency to form luminescence centers with thallous ions. The only characteristic property which seems to favor potassium as compared with sodium is the smaller difference between the ionic radii of K^+ and Tl^+.

6. PROBABLE CARRIERS OF THE LUMINESCENCE

X-ray diffraction patterns of a strongly luminescent KCl(Tl) phosphor powder show the lines characteristic of KCl and TlCl exclusively. The KCl lines were not displaced by a measurable shift with respect to those characteristic of pure KCl; the lattice spacing was certainly not altered by more than 1:1000 (Fig. 6).*** Thus it seems certain that no large quantities of thallium ions had replaced potassium ions in the base lattice.

The crystal fragments forming the powder could be viewed under a microscope of low magnification (1:10) in transmitted light as well as in their own fluorescent light under mineral lamp excitation. It was quite obvious that those parts which looked bright and transparent in the first instance remained dark in the second, while the strongly luminescent parts were nearly opaque for white light. This indicates that the crystals, or perhaps only their surfaces, must have been more or less damaged in the parts which had been converted to the phosphorescent modification.

Since no complete incorporation of the thallium ions in the potassium chloride lattice seems to have occurred, one might assume that only a small fraction of the foreign activator does react with the base material. However, the very definite difference in the behavior of the various mixtures containing different concentrations of thallium is very striking. It is certain and has been verified repeatedly that the initial mixture containing 13.4 percent mole percent of thallium exhibits a much brighter and more yellowish fluorescence and a much weaker afterglow than the following phosphor containing only 2.7 percent Tl, which in turn differs very clearly from the phosphor with 0.66 percent Tl. Thus one is lead to assume that the amount of activator reacting with the base material is dependent on the quantity of Tl present in the mixture, although not all thallium present takes part in the formation of phosphorescent centers by prolonged grinding. The color change from white to yellow which is observed when KI is ground together with TlCl indicates that in this case the thallium salt is converted to TlI; the light yellow color which the mixture acquires matches very closely the color of TlI. Therefore, one is induced to suppose that also if other salts, such as Tl_2SO_4 and $TlNO_3$, are ground together with KCl or KBr, the thallium salts are converted to the corresponding thallium halides. If this hypothesis is correct, some alkali metal must be liberated in the reaction. This question will be cleared up when more x-ray diffraction pictures which are in preparation will be available. At any rate, the samples prepared with thallous nitrate and sulfate are indistinguishable with respect to their luminescence properties from those prepared with thallous chloride.

*** We are greatly indebted to Mr. R. W. Mattoon who not only took the x-ray picture, but also made a very careful analysis of the lines appearing on them.

Ultrasonic Velocity in a Series of 1-Olefins

R. T. LAGEMANN, D. R. MCMILLAN, JR., AND MARTHA WOOLSEY
Emory University, Emory University, Georgia

(Received December 18, 1947)

The ultrasonic velocity for the temperature range 10° to 30°C has been measured for seven members of a 1-olefin series. Densities and refractive indices were also measured. From the measurements, values of the molecular sound velocity, adiabatic compressibility, and molecular refractivity were computed. The ultrasonic velocity is found to vary linearly with temperature, while the molecular constant, $MV^{\frac{1}{7}}/d$, remains substantially constant. The constant is found to be strictly additive for the series members studied.

IT is becoming increasingly apparent that measurements of the velocity of ultrasonic waves in liquids can be of valuable aid in the study of molecular structure. In this regard, the velocity and, more especially, its derived molecular constant, will perhaps be found to compare favorably with the parachor and the molecular refractivity, for example. A major contribution in this direction was made by Rao[1] when he showed that there exists a molecular sound velocity characteristic of each substance, which is a function of the ultrasonic velocity, the density, and the molecular weight. Later Lagemann and Dunbar[2] pointed out the simple relationships existing between this new molecular constant and others longer established. The constant has been evaluated by Rao[1,3] for the members of a few series, for which fairly reliable data on velocity are available. These results indicated that the constant is additive, taking on additional increments of about 195 units[3] for the addition of each CH_2 group. The size of this increment varies more within a series and more from series to series than does, say, the parachor increment; whether this is real or due to poor measurement of velocity and density is not yet clear.

In view of the scanty data available on this new property, it seemed worth while to extend ultrasonic and density measurements to a series of olefins which was available. Particularly does this study appear appropriate when it is realized that much of the ultrasonic velocity data now available is not accompanied by accurate density measurements performed on the same sample. Often there is doubt as to the purity of the sample studied.

EXPERIMENTAL

The seven compounds studied are listed in Table I. They were obtained in very pure form through the kindness of Dr. C. T. Lester[4] who had prepared them for a study of the addition of 4-mercaptobiphenyl to a series of 1-olefins. Immediately before the ultrasonic measurements, the compounds were again distilled, all but one boiling within a one degree range.

TABLE I. Measured values of the ultrasonic velocity, density, and refractive index for a series of 1-olefins.

Compound	Ultrasonic velocity (M/sec.) 10°C	20°C	25°C	30°C	Density (g/cc) 10°C	20°C	30°C	Refractive index (D line) 10°C	20°C	30°C
1-Heptene	1189	1128		1082	0.7069	0.6995	0.6910	1.4060	1.4007	1.3953
1-Octene	1229	1184		1146	0.7238	0.7183	0.7100	1.4140	1.4091	1.4037
1-Nonene	1258	1218	1201	1179	0.7411	0.7330	0.7252	1.4209	1.4161	1.4111
1-Decene	1290	1250		1214	0.7510	0.7435	0.7359	1.4260	1.4218	1.4167
1-Undecene	1315	1275	1255	1235	0.7594	0.7523	0.7447	1.4301	1.4260	1.4212
1-Tridecene	1353	1313	1294	1276	0.7739	0.7670	0.7596	1.4373	1.4332	1.4290
1-Pentadecene	1390	1351		1313	0.7867	0.7800	0.7731	1.4436	1.4398	1.4352

[1] M. Rama Rao, Ind. J. Phys. **14**, 109 (1940).
[2] R. T. Lagemann and W. S. Dunbar, J. Phys. Chem. **49**, 428 (1945).
[3] M. Rama Rao, J. Chem. Phys. **9**, 682 (1941).
[4] C. T. Lester, G. F. Rodgers, and E. Emmet Reid, J. Am. Chem. Soc. **66**, 1674 (1944).

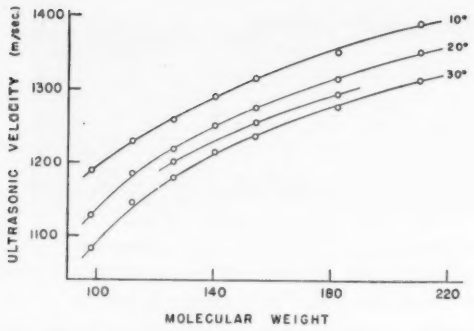

FIG. 1. Plot of the ultrasonic velocity *versus* molecular weight for a series of 1-olefins.

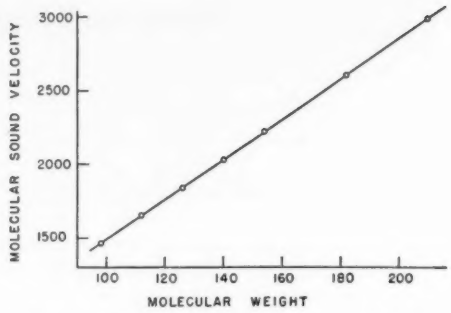

FIG. 3. Plot showing the additivity of the molecular sound velocity.

The ultrasonic velocity of each of the compounds was measured at 10°, 20°, 30°C, and in some cases at 25°C, using the ultrasonic interferometer described by McMillan and Lagemann.[5] The usual precautions to be taken with the interferometer were observed. The frequency used was 500,000±20 cycles per second. The temperature was maintained within ±0.03°C with Bureau of Standards calibrated thermometers. In most cases about 40 ml of each compound were available, giving sufficient nodal points in the interferometer to justify an estimate of 0.1 percent probable error in the measured velocities. In the case of 1-heptene and 1-octene, however, so small a volume was available that only two or three nodal positions could be measured, and for these compounds the error must be larger than that quoted above.

The velocities were measured with the liquids contained in a gold-plated brass cup. Despite the plating, some of the compounds turned lightly blue-green after 6 hours in the cup. Analysis showed the color to be due to copper. Drying with anhydrous sodium sulphate and redistillation yielded samples which remained uncolored on use in the apparatus. New velocity measurements were made, but these did not differ significantly from the earlier ones.

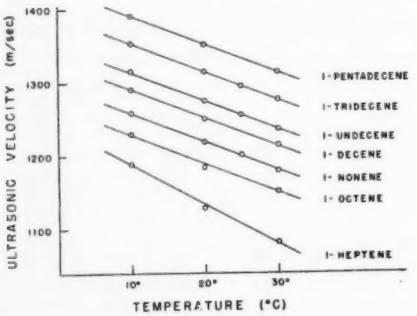

FIG. 2. Graph showing the variation of ultrasonic velocity with temperature for some 1-olefins.

The densities at 10°, 20°, and 30°C were measured using a 5-ml pycnometer such as that described by Lipkin, Davison, Harvey, and Kurtz.[6] Refractive indices were taken on a temperature regulated Abbe refractometer using a wavelength of 5893A.

RESULTS

Table I gives the measured values of the ultrasonic velocity, density, and refractive index. The plots of velocity *versus* molecular weight, shown in Fig. 1, are smooth curves. This is not generally the case within an homologous series.[2] It may be noted that the curve becomes more linear as one goes out the chain.

Figure 2 shows that the temperature coefficient, defined here as $\Delta V/\Delta t$, is constant for the temperature range studied and is the same for the five higher members. For 1-heptene and 1-octene the change of velocity with temperature does not appear linear, or, if assumed linear, the slope for 1-heptene, at least, differs from that of the others. It is unfortunate that larger quantities of these two were not available to check this point.

From the data in Table I it is possible to calculate the values of the molecular sound velocity, $MV^{\frac{1}{3}}/d$, given in Table II. The values for each compound remain substantially constant over the range 10° to 30°C, though there appears a

[5] D. R. McMillan, Jr. and R. T. Lagemann, J. Acous. Soc. Am. **19**, 956 (1947).

[6] M. R. Lipkin, J. A. Davison, W. T. Harvey, and S. S. Kurtz, Ind. Eng. Chem. (Anal. Ed.) **16**, 55 (1944).

TABLE II. Calculated values of the molecular sound velocity, adiabatic compressibility, and molecular refraction.

Compound	Molecular sound velocity			Molecular refraction (D line)			Adiabatic compressibility (Atm.$^{-1}\times10^6$)		
	10°C	20°C	30°C	10°C	20°C	30°C	10°C	20°C	20°C
1-Heptene	1471	1461	1459	34.13	34.09	34.09	101.4	113.8	125.3
1-Octene	1661	1653	1654	38.74	38.63	38.63	92.69	100.6	108.7
1-Nonene	1839	1839	1839	43.16	43.22	43.23	86.39	92.62	100.5
1-Decene	2033	2032	2033	47.85	47.89	47.90	81.08	87.23	93.43
1-Undecene	2226	2224	2223	52.50	52.55	52.56	77.17	82.86	89.21
1-Tridecene	2606	2603	2604	61.75	61.80	61.87	71.53	76.55	79.67
1-Pentadecene	2985	2982	2980	70.97	71.05	71.03	66.67	71.17	76.03

tendency for them to decrease with increase in temperature. Thus these olefins behave like other normal compounds in that there exists a molecular sound velocity which is constant for changes in temperature.

As CH_2 groups are added in successively building up the series, the constant increases and takes on nearly equal increments. Beginning with 1-heptene, the increase in the molecular velocity per CH_2 group is successively 193, 183, 194, 191, $2\times190/2$, and $2\times189/2$. The linearity between the molecular sound velocity and the molecular weight is well shown in Fig. 3. The average increment is 189 per CH_2 group, slightly less than the average of 195 for several series reported by Rao.[2] Assuming the experimental data used by Rao to be as accurate as the data given here, the change from 195 to 189 appears significant and indicates the constant is constitutive as well as additive.

Included in Table II are values of the adiabatic compressibility calculated by means of the relation

$$V=1/(\rho\beta_{ad})^{\frac{1}{2}},$$

where V is the ultrasonic velocity, ρ is the density, and β_{ad} is the adiabatic compressibility. Values of β_{ad} were converted from cm²/dyne to atmospheres^{-1} by use of the factor 1,013,000 ($13.590\times76\times980.66$), although g at the location of the experiment was 979.524 cm sec.$^{-2}$.

The CH_2 increments in the molecular refractivities listed in Table II vary more than those of the sound velocity. The average value of 4.620 is in good agreement, however, with the 4.618 proposed by Eisenlohr.[7]

ACKNOWLEDGMENTS

One of us (R.T.L.) wishes to acknowledge support of this work by the Georgia Academy of Science and the Research Corporation. It is also a pleasure to mention that William Woolf and John Evans assisted in the measurements.

[7] F. Eisenlohr, Zeits f. physik. Chemie **75**, 585 (1910).

THE JOURNAL OF CHEMICAL PHYSICS VOLUME 16, NUMBER 3 MARCH, 1948

An Asymptotic Expression for the Energy Levels of the Asymmetric Rotor. II. Centrifugal Distortion Correction*

S. GOLDEN**
Mallinckrodt Chemical Laboratory, Harvard University, Cambridge, Massachusetts

(Received December 19, 1947)

It has been found possible to develop perturbation operators for the centrifugal distortion terms that permit an approximate evaluation to be made of their contribution to the asymmetric rotor energy levels for large values of J. The procedure is based upon the asymptotic ($J\rightarrow\infty$) similarity between the matrices of the asymmetric rotor and that obtained from Mathieu's differential equation.

INTRODUCTION

THE general matrix formulation of the centrifugal distortion problem has been given by Howard and Wilson.[1] The explicit formulas applicable to symmetrical triatomic molecules, as well as the resulting secular equation, have been given by Wilson[2] and Shaffer and Nielsen.[3]

The secular equation given by these authors has been examined under conditions where J is increased indefinitely. It has been found possible to extend the asymptotic treatment described recently[4] to include the effect of the centrifugal distortion terms. Suitable perturbation operators are added to Mathieu's differential equation, permitting the asymmetric rotor problem to be reformulated with the result that the centrifugal distortion corrections, when small, require only an approximate knowledge of the effective moments of inertia. Their dependence upon the rotational state involves just the quantum numbers describing the state and the asymmetry of the rotor.

CENTRIFUGAL DISTORTION TERMS IN ENERGY OPERATOR

The centrifugal distortion contribution to the Hamiltonian has been given by Wilson[2] as

$$\mathbf{H}'=\tfrac{1}{4}\sum_{\alpha,\beta,\gamma,\delta}\tau_{\alpha,\beta,\gamma,\delta}\mathbf{P}_\alpha\mathbf{P}_\beta\mathbf{P}_\gamma\mathbf{P}_\delta, \qquad (1)$$

where

$\tau_{\alpha,\beta,\gamma,\delta}$ depends only upon the vibrational state;
α, β, γ, δ refer to the molecule fixed principal axes, x, y, or z;
$\mathbf{P}_\alpha$ refers to the component of angular momentum along the α-axis.

Formulas have been given by Wilson and by Shaffer and Nielsen that permit the τ's to be evaluated approximately.[5] The matrix elements of Eq. (1) evaluated in terms of a basis of symmetric rotor wave functions have also been given by the afore-mentioned authors. However, the choice of basis functions in both cases corresponds to the wave functions of the limiting oblate symmetric rotor. Since it is frequently desirable to expand in terms of the limiting prolate symmetric rotor functions, the effect of this change of basis will be examined.

The choice of a basis of symmetric rotor wave functions is determined by the manner in which the cartesian axes x, y, z are identified with the principal axes of the rotor a, b, c. Here a, b, c correspond to the axes of smallest, intermediate, and largest moment of inertia, respectively. In

* The support given by the Navy Department is gratefully acknowledged for some of the computational work herein reported. It was carried out under Task Order V of Contract N5ori-76 (Office of Naval Research) by Mrs. Grace C. Ek.

** National Research Council Predoctoral Fellow. Present address: Hydrocarbon Research, Inc., 115 Broadway, New York, New York.

[1] J. B. Howard and E. B. Wilson, Jr., J. Chem. Phys. **4**, 260 (1936).

[2] E. B. Wilson, Jr., J. Chem. Phys. **5**, 617 (1937); see also B. L. Crawford and P. C. Cross, J. Chem. Phys. **5**, 621 (1937).

[3] W. H. Shaffer and H. H. Nielsen, Phys. Rev. **56**, 188 (1939); see also H. H. Nielsen, Phys. Rev. **59**, 565 (1941).

[4] S. Golden, J. Chem. Phys. **16**, 78 (1948).

[5] B. T. Darling and D. M. Dennison, Phys. Rev. **57**, 128 (1940), give certain formulas that prove useful in this calculation.

an oblate representation z is identified with c, while in a prolate representation z is identified with a.[6] Although the extension of the present method to more general cases is clearly evident, only symmetrical triatomic molecules will be considered in any detail. The limiting prolate basis will be employed. This means that the matrices finally considered by Wilson are unaffected except that $(\mathbf{P}_x\mathbf{P}_y+\mathbf{P}_y\mathbf{P}_x)^2$ replaces his $(\mathbf{P}_x\mathbf{P}_y+\mathbf{P}_y\mathbf{P}_x)^2$.

The former matrix may be evaluated from the known values of $\mathbf{P}_z$ and $\mathbf{P}_y$.[7] Its non-vanishing elements are given below.

$$\begin{aligned}
&[(P_xP_y+P_yP_x)^2]_{J,K,M;\,J,K,M}\\
&\qquad=\frac{\hbar^4}{4}(2f+8fK^2-10K^2-8K^4);\\
&[(P_xP_y+P_yP_x)^2]_{J,K,M;\,J,K\pm2,M}\\
&=-\frac{\hbar^4}{4}(2K\pm1)(2K\pm3)\{[f-K(K\pm1)]\\
&\qquad\times[f-(K\pm1)(K\pm2)]\}^{\frac{1}{2}},
\end{aligned}\tag{2}$$

where $f=J(J+1)$.

ASYMPTOTIC FORM OF THE ENERGY MATRIX[8]

The results of Eq. (2) may be combined with those of reference 2 to obtain the energy matrix. When the procedure adopted in reference 4 is applied, the following non-vanishing elements are obtained for the reduced energy matrix when $K\ll J$. In arriving at these equations, the off-diagonal terms were expanded in powers of $(K+1)$ and powers greater than the second neglected. This conforms with the limiting situation for which the Mathieu equation method is applicable.

$$\begin{aligned}
&E'_{K;\,K}=\lambda A+(1+\lambda B)K^2+\lambda\theta_0''K^4,\\
&E'_{K;\,K\pm2}\simeq(\theta_0+\lambda\Delta\theta_0)-(\theta_0'+\lambda\Delta\theta_0')(K^2\pm2K),\\
&E'_{K;\,K\pm4}\simeq\lambda\theta_0'''-\lambda\theta_0^{\mathrm{IV}}(K^2\pm4K),
\end{aligned}\tag{3}$$

where

$$\lambda=\frac{2}{2a-b-c},$$

$a=\hbar^2/2I_a$, $b=\hbar^2/2I_b$, $c=\hbar^2/2I_c$,

$I_a\leq I_b\leq I_c$, the principal effective moments of inertia,

$$\begin{aligned}
A&=\frac{\hbar^4}{32}[(3f^2-2f)(\tau_{xxxx}+\tau_{yyyy})\\
&\qquad+(2f^2+4f)\tau_{xxyy}+4f\tau_{yzyz}],\\
B&=\frac{\hbar^4}{32}[(5-6f)(\tau_{xxxx}+\tau_{yyyy})-(4f+10)\tau_{xxyy}\\
&\qquad+8f(\tau_{xxxz}+\tau_{yyyz})+(16f-20)\tau_{yzyz}],\\
\theta_0&=\frac{1}{2}\left(\frac{b-c}{2a-b-c}\right)\left(f-1-\frac{1}{2f}\right);\\
-\Delta\theta_0&=\frac{\hbar^4}{32}\Big[\left(2f^2-6f+1+\frac{1}{f}\right)(\tau_{xxxx}-\tau_{yyyy})\\
&\qquad+\left(8f-4-\frac{2}{f}\right)(\tau_{xxxz}-\tau_{yyyz})\\
&\qquad-\left(6f+2+\frac{1}{f}\right)\tau_{yzyz}\Big],\\
\theta_0'&=\frac{1}{2}\left(\frac{b-c}{2a-b-c}\right)\left(1+\frac{1}{2f}\right),\\
-\Delta\theta_0'&=\frac{\hbar^4}{32}\Big[\left(4f-1-\frac{1}{f}\right)(\tau_{xxxx}-\tau_{yyyy})\\
&\qquad-\left(4f-4-\frac{2}{f}\right)(\tau_{xxxz}-\tau_{yyyz})\\
&\qquad+\left(8f+2+\frac{1}{f}\right)\tau_{yzyz}\Big],\\
\theta_0''&=\frac{\hbar^4}{32}[3(\tau_{xxxx}+\tau_{yyyy})+2\tau_{xxyy}\\
&\qquad-8(\tau_{xxxz}+\tau_{yyyz}+2\tau_{yzyz}-\tau_{zzzz})],\\
\theta_0'''&=\frac{\hbar^4}{32}\left[\left(\frac{f^2}{2}-5f-\frac{5}{2}\right)(\tau_{xxxx}+\tau_{yyyy}-2\tau_{xxyy})\right],\\
\theta_0^{\mathrm{IV}}&=\frac{\hbar^4}{32}\left[\left(\frac{f}{2}+\frac{1}{4}\right)(\tau_{xxxx}+\tau_{yyyy}-2\tau_{xxyy})\right].
\end{aligned}$$

The constant diagonal term, λA, may be removed immediately. It is convenient to divide the resulting equation by $(1+\lambda B)$, giving:

$$\begin{aligned}
&E''_{K;\,K}=K^2+\lambda\theta''K^4,\\
&E''_{K;\,K\pm2}\simeq(\theta+\lambda\Delta\theta)-(\theta'+\lambda\Delta\theta')(K^2\pm2K),\\
&E''_{K;\,K\pm4}\simeq\lambda\theta''',
\end{aligned}\tag{4}$$

where $\theta=\theta_0/(1+\lambda B)$, etc.

---

[6] G. W. King, R. M. Hainer, P. C. Cross, J. Chem. Phys. **11**, 27 (1943).

[7] See, for example, Eq. (5) of reference 6.

[8] The notation of reference 4 will be adopted here.

TABLE I. First-order corrections apart from factor θ_0''.

θ_0 \ Char. value	be_0	bo_1	be_1	bo_2	be_2	bo_3	be_3	bo_4	be_4	bo_5	be_5	bo_6
0	0.0000	1.0000	1.000	16.000	16.000	81.000	81.000	256.000	256.000	625.000	625.000	1296.00
1	1.5905	1.9726	2.580	17.650	16.107	82.154	81.549	256.951	256.904	625.957	625.956	1296.97
2	4.3043	4.0730	8.460	22.406	18.845	86.445	82.109	260.015	259.263	628.827	628.776	1299.87
3	6.9986	6.6056	18.863	29.771	26.417	94.553	82.679	265.727	262.104	633.652	633.271	1304.68
4	9.6479	9.2957	31.885	39.124	40.193	106.645	85.632	274.765	264.166	640.586	639.014	1311.38
5	12.3139	12.0438	45.628	49.879	61.071	122.584	93.653	287.756	264.698	649.923	645.294	1319.94
6	15.0106	14.8164	59.305	61.575	88.679	142.043	108.624	305.178	264.370	662.094	651.117	1330.45
7	17.7370	17.6010	72.791	73.886	121.223	164.581	131.960	327.316	265.452	677.632	655.331	1342.93
8	20.4884	20.3943	86.150	86.594	156.401	189.707	164.768	354.262	270.917	697.106	656.963	1357.66
9	23.2576	23.1950	99.456	99.564	192.426	216.937	207.559	385.955	283.433	721.059	655.682	1374.87
10	26.0473	26.0026	112.766	112.717	228.341	245.834	259.845	422.184	305.057	749.967	652.277	1394.95

The $(K^2 \pm 4K)$ terms have been neglected in $E''_{K;\,K\pm4}$, which is justifiable since θ^{IV}/θ''' varies as $1/f$, or $1/J^2$ when $J \to \infty$.

The reduced energy matrix is now given by

$$\mathbf{E}' = \lambda A \mathbf{I} + (1+\lambda B)\mathbf{E}''. \tag{5}$$

Apart from the diagonal K^4 terms and the $(K|K\pm4)$ terms, the $\mathbf{E}''$ matrix represents that of a modified asymmetric rotor. Suitable perturbation operators will now be given for the additional terms.

PERTURBATION OPERATORS

It is readily verified that the diagonal K^4 terms may be introduced by the perturbation operator[9]

$$\mathcal{P}_1(x) = -\lambda\theta'' \frac{d^4}{dx^4}. \tag{6}$$

The $(K|K\pm4)$ terms may be introduced by the operator

$$\mathcal{P}_2(x) = -\lambda\theta''' \cos 4x. \tag{7}$$

The modified Mathieu's equation becomes, to this approximation,

$$\left\{\frac{d^2y}{dx^2} + (\alpha - 2\theta\cos 2x)y\right\} + (\mathcal{P}+\mathcal{P}_1+\mathcal{P}_2)y = 0, \tag{8}$$

where $\mathcal{P}$ is defined by Eq. (24) of reference 4, with $(\theta'+\lambda\Delta\theta')$ replacing θ'.

APPROXIMATE SOLUTION

To find the characteristic values of Eq. (8), its matrix may be developed in terms of a basis of elliptic cylinder functions. The terms in braces then form a diagonal matrix. The off-diagonal terms (as well as some diagonal terms) arise from the evaluation of $(\mathcal{P}+\mathcal{P}_1+\mathcal{P}_2)$ in terms of this basis. The resulting matrix may now be approximately diagonalized to second order by the conventional perturbation theory. It may be pointed out that this procedure for diagonalization is equivalent to approximating the asymmetric rotor wave functions by their elliptic cylinder function equivalents, which assumes constant $(K|K\pm2)$ terms in Eq. (3), and then treating the variation of these terms with K together with the centrifugal distortion terms as a simultaneous perturbation on the asymptotic formulation of the asymmetric rotor problem.

The characteristic values, correct to second order, of the matrix obtainable from Eq. (8) may be formally written as

$$E''(\kappa) = \alpha(\theta+\lambda\Delta\theta) + (\theta'+\lambda\Delta\theta')\beta(\theta+\lambda\Delta\theta) + \lambda\theta''\gamma(\theta+\lambda\Delta\theta) + \lambda\theta'''\delta(\theta+\lambda\Delta\theta) + \epsilon(\theta+\lambda\Delta\theta,\ \theta'+\lambda\Delta\theta',\ \lambda\theta'',\ \lambda\theta'''), \tag{9}$$

where

- α is the appropriate characteristic value of Mathieu's equation;
- $(\theta'+\lambda\Delta\theta')\beta$ is the appropriate diagonal element of $\mathcal{P}$ evaluated in terms of elliptic cylinder functions;
- $\lambda\theta''\gamma$ is the appropriate diagonal element of $\mathcal{P}_1$ evaluated in terms of elliptic cylinder functions;
- $\lambda\theta'''\delta$ is the appropriate diagonal element of $\mathcal{P}_2$ evaluated in terms of elliptic cylinder functions;
- ϵ is the appropriate second-order perturbation correction.

[9] The basis functions used here are the normalized, imaginary exponentials, $y_0 = 1/(2\pi)^{\frac{1}{2}} e^{iKx}$. See Eqs. (11) and (12) of reference 4.

A characteristic value of the reduced energy matrix may now be written down.

$$\begin{aligned}E' &= \lambda A + (1+\lambda B)E'' \\ &= \lambda A + (1+\lambda B)\alpha(\theta+\lambda\Delta\theta) \\ &\quad + (\theta_0'+\lambda\Delta\theta_0')\beta(\theta+\lambda\Delta\theta) \\ &\quad + \lambda\theta_0''\gamma(\theta+\lambda\Delta\theta) + \lambda\theta_0'''\delta(\theta+\lambda\Delta\theta) \\ &\quad + (1+\lambda B)\epsilon(\theta+\lambda\Delta\theta,\ \theta'+\lambda\Delta\theta',\ \lambda\theta'',\ \lambda\theta''').\end{aligned} \tag{10}$$

Since the centrifugal distortion terms are generally small (i.e., $\lambda\Delta\theta/\theta \ll 1$) it is permissible to develop the quantities α, β, etc., in a Taylor series about the point θ_0 and retain only the zeroth- and first-order centrifugal distortion terms.

The factor $(1+\lambda B)$ represents a change in magnitude of the effective principal moments of inertia produced by the centrifugal distortion terms. The term $(\theta+\lambda\Delta\theta)$ involves what may be considered to be an effectively different asymmetry of the rotor produced by centrifugal distortion. The Taylor series expansion here involves the expansion of this term about the asymmetry of the rotor when centrifugal distortion is neglected.

Expanding,

$$\begin{aligned}E' &= \lambda A + (1+\lambda B)\left\{\alpha(\theta_0) + \frac{\partial\alpha}{\partial\theta_0}(\theta+\lambda\Delta\theta-\theta_0)\right\} \\ &\quad + (\theta_0'+\lambda\Delta\theta_0')\left\{\beta(\theta_0) + \frac{\partial\beta}{\partial\theta_0}(\theta+\lambda\Delta\theta-\theta_0)\right\} \\ &\quad + \lambda\theta_0''\gamma(\theta_0) + \lambda\theta_0'''\delta(\theta_0) \\ &\quad + \epsilon(\theta_0,\ \theta_0',\ 0,\ 0) + \lambda B\epsilon(\theta_0,\ \theta_0',\ 0,\ 0).\end{aligned}$$

Simplifying,

$$\begin{aligned}E' &= [\alpha(\theta_0) + \theta_0'\beta(\theta_0) + \epsilon(\theta_0,\ \theta_0',\ 0,\ 0)] \\ &\quad + \lambda A + \lambda B\{\alpha(\theta_0) + \epsilon(\theta_0,\ \theta_0',\ 0,\ 0)\} \\ &\quad + \lambda(\Delta\theta_0 - B\theta_0)\left\{\frac{\partial\alpha}{\partial\theta_0} + \theta_0'\frac{\partial\beta}{\partial\theta_0}\right\} \\ &\quad + \lambda\Delta\theta_0'\beta(\theta_0) + \lambda\theta_0''\gamma(\theta_0) + \lambda\theta_0'''\delta(\theta_0).\end{aligned} \tag{11}$$

Here it has been implicitly assumed that the off-diagonal terms from $\mathcal{P}_1$ and $\mathcal{P}_2$ are sufficiently small so that their effect upon ϵ may be safely neglected.

The bracketed term in Eq. (12) corresponds to the reduced energy of the asymmetric rotor when the centrifugal distortion terms are neglected. To find the change produced in the energy level of the rotor by centrifugal distortion, recall that the reduced energies must be multiplied by $(1-(b+c)/2)$ or $1/\lambda$. Thus one obtains for the centrifugal contribution to the actual energy

$$\begin{aligned}\Delta E_\tau^J &= A + B(\alpha+\epsilon) + (\Delta\theta_0 - B\theta_0)\left\{\frac{\partial\alpha}{\partial\theta_0} + \theta_0'\frac{\partial\beta}{\partial\theta_0}\right\} \\ &\quad + \Delta\theta_0'\beta + \theta_0''\gamma + \theta_0'''\delta.\end{aligned} \tag{12}$$

Examination of Eq. (12) reveals that the centrifugal distortion contribution requires information concerning the configuration of the molecule only to evaluate the quantities A, B, $\Delta\theta_0$, etc. (i.e., the $\tau_{\alpha,\beta,\gamma,\delta}$ of Eq. (1)). Except for this, it depends only upon the quantum numbers of the state and the asymmetry of the molecule.

Since the contribution from the diagonal K^4 terms appears to be most important, the diagonal matrix elements of $\mathcal{P}_1$ (i.e., γ) have been evaluated and are given in Table I. Other elements of $\mathcal{P}_1$ and those of $\mathcal{P}_2$ are readily evaluated using the Fourier coefficients of the elliptic cylinder functions tabulated by Ince.[10] The quantities α and $\partial\alpha/\partial\theta$ may be determined from the *Tables of Characteristic Values of Mathieu's Differential Equation*.[11] The quantities β (i.e., diagonal elements of $\mathcal{P}$) and ϵ have been given in reference 4.

ACKNOWLEDGMENT

The present treatment was carried out at the suggestion of Professor E. Bright Wilson, Jr., whose interest and encouragement are gratefully acknowledged. The author wishes, also, to express his appreciation to Mr. Robert Karplus for reading the manuscript and making several helpful suggestions.

[10] E. L. Ince, Proc. Roy. Soc. Edin. **52**, 355 (1931–32).
[11] AMP Report 165.1*R*, National Bureau of Standards.

Letters to the Editor

THIS section will accept reports of new work, provided these are terse and contain few figures, and especially few halftone cuts. The Editorial Board will not hold itself responsible for opinions expressed by the correspondents. Contributions to this section should not exceed 600 words in length and must reach the office of the Managing Editor not later than the 15th of the month preceding that of the issue in which the letter is to appear. No proof will be sent to the authors. The usual publication charge ($4.00 per page) will not be made and no reprints will be furnished free.

The UCl_3 Type of Crystal Structure

W. H. ZACHARIASEN
Argonne National Laboratory and Department of Physics, University of Chicago, Chicago, Illinois
January 14, 1948

THE UCl_3 type of structure was observed in the course of war research within the Manhattan Project. The crystal structure of the prototypic compound UCl_3 was first described in reports issued within the Manhattan Project in January and March 1944. Since that time seventeen additional compounds have been found to crystallize with the UCl_3 type of structure.

UCl_3 is hexagonal with two molecules per unit cell. The lattice periods are:

$$a_1=7.428\pm0.003\text{A}, \quad a_3=4.312\pm0.003\text{A},$$

corresponding to a calculated density of $\rho=5.51$. The density $\rho=5.44$ is reported in the literature.

The space group is $C6_3/m(C_{6h}^2)$ and the atomic positions are:

$$2\text{ U in }\pm(\tfrac{1}{3},\tfrac{2}{3},\tfrac{1}{4}),$$
$$6\text{ Cl in }\pm(x,y,\tfrac{1}{4})(\bar{y},x-y,\tfrac{1}{4})(y-x,\bar{x},\tfrac{1}{4}).$$

The parameter values are found to be

$$x=0.375\pm0.014, \quad y=0.292\pm0.014.$$

Each uranium atom is bonded to nine chlorine atoms, three at a distance of U−Cl=2.95A and six at U−Cl =2.96A. The closest distance of approach of two chlorine atoms is Cl−Cl=3.45A.

TABLE I. Lattice dimensions of isomorphous compounds XY_3.

Compound	a_1	a_3
$AcCl_3$	7.62 ±0.02A	4.55 ±0.02A
UCl_3	7.428±0.003	4.312±0.003
$NpCl_3$	7.405±0.010	4.273±0.005
$PuCl_3$	7.380±0.001	4.238±0.001
$AmCl_3$	7.37 ±0.01	4.24 ±0.01
$LaCl_3$	7.468±0.003	4.366±0.003
$CeCl_3$	7.436±0.004	4.304±0.004
$PrCl_3$	7.41 ±0.01	4.25 ±0.01
$NdCl_3$	7.381±0.004	4.231±0.003
$AcBr_3$	8.06 ±0.04	4.68 ±0.02
UBr_3[1]	7.926±0.002	4.432±0.002
$NpBr_3$	7.917±0.005	4.382±0.005
$LaBr_3$	7.951±0.003	4.501±0.003
$CeBr_3$	7.936±0.003	4.435±0.003
$PrBr_3$	7.92 ±0.01	4.38 ±0.01
$La(OH)_3$	6.510±0.005	3.843±0.005
$Pr(OH)_3$	6.47 ±0.03	3.76 ±0.03
$Nd(OH)_3$	6.42 ±0.02	3.74 ±0.02

[1] The approximate lattice dimensions of UBr_3 were first obtained by N. Baenziger and R. Rundle and given in a Manhatten Project report in April, 1944.

The structure of UCl_3 is of coordination type and the U−Cl bonds appear to be of predominantly ionic character.

Table I gives the lattice dimensions for the various compounds which so far are known to be isomorphous with UCl_3.

The decrease in lattice dimensions from $LaCl_3$ to $NdCl_3$, from $LaBr_3$ to $PrBr_3$, and from $La(OH)_3$ to $Nd(OH)_3$ illustrates the "lanthanide contraction" caused by the addition of electrons to the 4*f* shell. It is seen that there is a corresponding contraction of the interatomic distances in the series $AcCl_3-AmCl_3$ and $AcBr_3-NpBr_3$. The results of Table I thus represent experimental proof that electrons enter the 5*f* shell in the heavy element series.

The new compounds listed in Table I were prepared by various investigators as follows:

Sherman Fried——$AmCl_3$, $NpBr_3$,
Sherman Fried and N. R. Davidson——$NpCl_3$,
F. Hagemann——$PuCl_3$,
Sherman Fried and F. Hagemann——$AcCl_3$, $AcBr_3$.

A detailed account of the investigations will be published later.

The Non-Exchange of Radioactive Cobalt between Hexammino Cobaltic and Cobaltous Chlorides

K. J. MCCALLUM AND S. A. HOSHOWSKY
Department of Chemistry, University of Saskatchewan, Saskatoon, Canada
January 8, 1948

IN 1941, Flagg[1] reported that there was no exchange between radioactive cobaltous ion and hexammino cobaltic ion in neutral solution. The dissociation of the hexammino cobaltic ion through the reaction[2]

$$Co(NH_3)_6^{3+}\rightleftarrows Co^{3+}+6NH_3 \qquad (1)$$

should result in the presence of a small concentration of cobaltic ion in equilibrium with the complex. Because of the presumed ease of exchange between uncomplexed cobaltous and cobaltic ions by an electron transfer process, Flagg pointed out that exchange between the cobaltous and hexammino cobaltic ion might be expected. To explain the failure of exchange to occur, he suggested that the rate of reduction of the cobaltic ion by water might be greater than the rate of the electron transfer process. However, the reduction of the cobaltic ion would result in the gradual decomposition of the hexammino cobaltic ion, and in view of the observed stability of this ion, its rate of dissociation must be small, if Flagg's suggestion is correct.

In the present work, the exchange between hexammino cobaltic and cobaltous ion has been studied in solutions ranging from one molal hydrochloric acid to ten molal ammonia. According to Lamb and Larson,[2] in concentrated ammonia solution cobaltous ion forms the hexammino cobaltous ion, $Co(NH_3)_6^{2+}$.

In these experiments, hexammino cobaltic ion containing radioactive Co^{60} was synthesized.[3] A weighed amount

TABLE I. Apparent percentage of exchange. Solutions 0.011 molar in cobaltic and cobaltous cobalt.

Solutions	Time in hours	Apparent percent exchange
1 *M* HCl	3.5	0.03±0.05
neutral	3.5	0.02±0.07
neutral	24	0.03±0.07
3.6 *M* NH_3	3.5	0.19±0.24
6.5 *M* NH_3	3.5	0.05±0.13
6.0 *M* NH_3	24	0.03±0.25
9.5 *M* NH_3	3.5	0.02±0.07

of the complex and an equimolar quantity of inactive cobaltous chloride was dissolved in water and hydrochloric acid or ammonia water added to give the desired solution. After standing in the dark for a known time at room temperature, the solution was neutralized, ammonium chloride and ammonium thiocyanate added and the complex cobaltous thiocyanate extracted with amyl alcohol-ether mixture. The cobalt was removed from the organic layer by shaking with a dilute ammonia solution and then precipitated by the addition of ammonium sulfide. The cobalt sulfide was dissolved in aqua regia and the resulting solution boiled with sulfuric acid. The cobalt was deposited electrolytically on weighed copper disks and the radioactivity determined. Radioactivity measurements were made with a mica window end-on type of counter with a scale of 64 circuit.

All experiments were done in duplicate. Corrections were made for background and for the incomplete recovery of the cobaltous cobalt. Blank experiments indicated that less than 0.1 percent of the hexammino cobaltic ion was extracted under the conditions of these experiments.

The results are given in Table I. The initial activity of the hexammino cobaltic ion taken for each of the different experiments varied between 2400 and 3000 counts a minute. The results are reported as the apparent percentage of the hexammino cobaltic chloride undergoing exchange with all of the divalent cobalt present. The uncertainties were calculated taking the statistical error in the determination of the background and cobalt activity as the square root of the number of counts observed.

In all cases the apparent percent exchange is zero within experimental error. The results in neutral solution confirm those of Flagg. However, his suggestion that the nonexchange is due to the rapid reduction of the cobaltic ion by water is not by itself sufficient to account for these results. In his experiments the activity was present in the cobaltous state while in those reported here the hexammino cobaltic ion contained the activity. Dissociation of the complex by reaction (1) and reduction of the cobaltic to cobaltous ion would result, in these experiments, in activity being detected when the cobaltous ion was separated. Ascribing the total activity in the cobaltous state to such decomposition (as well as the results of additional blank experiments) indicates that less than 0.1 percent of the complex was decomposed in solution in twenty-four hours. Thus, either the dissociation of the complex to form cobaltic ions, the reduction of cobaltic ion, or both, must be slow processes.

The lack of exchange in strongly ammoniacal solution indicates that if, as Lamb and Larson conclude,[2] divalent cobalt exists as the $Co(NH_3)_6^{2+}$ ion under these conditions, exchange between the latter and $Co(NH_3)_6^{3+}$ does not occur by an electron transfer between the complex ions under the conditions of these experiments. Further experiments on the exchange reactions of the cobaltammines are in progress and will be reported elsewhere.

We wish to acknowledge the generous financial assistance of the National Research Council of Canada.

[1] J. F. Flagg, J. Am. Chem. Soc. **63**, 557 (1941).
[2] A. B. Lamb and A. T. Larson, J. Am. Chem. Soc. **42**, 2024 (1920).
[3] Biltz, Hall, and Blanchard, *Laboratory Methods of Inorganic Chemistry* (John Wiley and Sons, Inc., New York, 1928).

The Isomerization of Propane with C^{13} in One End Position

O. BEECK, J. W. OTVOS, D. P. STEVENSON, AND C. D. WAGNER
Shell Development Company, Emeryville, California
January 13, 1948

THE catalytic isomerization of propane with C^{13} in one end position, for which the nomenclature propane-1-C^{13} has been suggested,[1] was investigated over aluminum bromide at room temperature. It was found that the rate of isomerization of propane-1-C^{13} to propane-2-C^{13} with C^{13} in the middle position is comparable to the rate of isomerization of normal butane to isobutane under similar conditions. Within the accuracy of the analytical method the equilibrium distribution of the propanes-1-C^{13} and -2-C^{13} was found to be the statistical one, that is propane-1-C^{13}/propane-2-C^{13}=2, as would be expected since the introduction of C^{13} into the propane molecule changes the partition functions only very slightly. The result that no molecules containing two C^{13} carbon atoms are formed, unambiguously establishes the purely intramolecular character of the isomerization reaction. Finally, it was found that the probability for dissociation by electron impact in the mass spectrometer of the carbon–carbon bonds was decreased by roughly 5 percent for the $C^{13}-C^{12}$ bond and increased by the same amount for the $C^{12}-C^{12}$ bond below and over those in ordinary propane.*

Propane-1-C^{13} prepared through the reaction sequence:

$$KC^{13}N\ (16.7\ \text{atom percent}\ C^{13}) \xrightarrow{EtBr} EtC^{13}N \xrightarrow[H_2O,\ HCl]{C_8H_{17}OH} EtC^{13}OOC_8H_{17},$$

$$\xrightarrow[\text{hydrolysis}]{LiAlH_4} EtC^{13}H_2OH \xrightarrow{HBr} EtC^{13}H_2Br \xrightarrow[H^+]{Mg} EtC^{13}H_3$$

(16.7 atom percent C^{13})

gives in 30 percent yield a propane with the calculated isotopic and isomeric distribution shown in column 2 of Table I. The mass spectrometric technique used combines into one operation the usual steps of chemical degradation followed by isotopic analysis.

The relative concentrations of the four isotopic propanes can be calculated by well-known methods from the relative intensities of the ions of $m/q=47^+$, 46^+, 45^+, and 44^+ in the mass spectrum of a sample, when the relative intensities

TABLE I. Calculated distribution of isotopic species of C^{13}(16.7 percent)-propane.

Species	Propane synthesized	After intramolecular equilibration	After intra- plus intermolecular equilibration
$C_3^{12}H_8$	0.8150	0.8150	0.8237
$C^{12}H_3-C^{12}H_2-C^{13}H_3$	0.1720	0.1204	0.1100
$C^{12}H_3-C^{13}H_2-C^{12}H_3$	0.00856	0.0602	0.0550
$C^{12}H_3-C^{13}H_2-C^{12}H_3$	0.00182	0.00236	0.00734
$C^{13}H_3-C^{12}H_2-C^{13}H_3$	0.00172	0.00118	0.00367
$C_3^{13}H_8$	0.00002	0.00002	0.00025
$(46^+)/(44^+)\pm0.0003$[a]	0.0037	0.0037	0.0118
$(30^+)/(29^+)\pm0.0010$[a]	0.1020[b]	0.1300[b]	0.1265[b]

[a] Accuracy of measurement of these quantities.
[b] Calculated assuming equal dissociation probability for $C^{12}-C^{12}$ and $C^{12}-C^{13}$ bonds.

TABLE II. Mass spectral relative intensities in C^{13}-propane during isomerization.

Time[a]	$(30^+)/(29^+)$	$(46^+)/(44^+)$
0[b]	0.106(3)	0.0038
65	0.119(4)	0.0034
186	0.126(5)	0.0034
261	0.128(3)	0.0036
405	0.130(1)	0.0039
594	0.129(5)	0.0036
1074	0.133(6)	0.0039

[a] Time in hours of contact between vapor at approximately 450-mm pressure with a catalyst prepared by the addition of 0.023-gram H_2O to anhydrous aluminum bromide (0.40 gram).
[b] The propane-1-C^{13} as synthesized. The intensities of all of the C_3 and C_2 ions and ionic fragments agreed with the calculated values to within the experimental uncertainty.

of the ions of $m/q=44^+$, 43^+, 42^+, and 41^+ in the mass spectrum of $C_3^{12}H_8$ are known. Furthermore, the relative concentrations of the isomeric propanes, -1-C^{13} and -2-C^{13}, can be determined from the relative intensities of the ions of $m/q=30^+$ and 29^+ since the former species can give rise to but half as many ions $C^{12}C^{13}H_3^+(m/q=30^+)$ as can the latter species. This determination of the isotopic isomer distribution presupposes the knowledge of the concentrations of $C_3^{12}H_8$, $C_2^{12}C^{13}H_8$, $C^{12}C_2^{13}H_8$, and $C_3^{13}H_8$. Intramolecular equilibration requires the species distribution (statistical) shown in column 3 of Table I, while complete inter and intramolecular equilibration (statistical) requires the distribution shown in column 4. The relative ion intensities $(46^+)/(44^+)$ and $(30^+)/(29^+)$, which are measures of the relative species concentrations $C^{12}C_2^{13}H_8/C_3^{12}H_8$ and $C^{12}H_3-C^{13}H_2-C^{12}H_3/C^{12}H_3-C^{12}H_2-C^{13}H_3$, respectively, calculated from the mass spectrum of ordinary propane for the three situations, are shown in the last two rows of Table I.

In Table II there are shown the measured values of the relative intensities $(46^+)/(44^+)$ and $(30^+)/(29^+)$ for the prepared propane-1-C^{13} and after 65, 186, 261, 405, 594, and 1074 hours in contact with almost anhydrous aluminum bromide at 25°C. At 65 hours the $(30^+)/(29^+)$ ratio had undergone about one-half its maximum change, while even at 1074 hours the $(46^+)/(44^+)$ ratio was still unchanged (within the experimental error). The disagreement between the initial and final values in Table II and those given in Table I are believed to be due to a small (~5 percent) difference in the dissociation probabilities of $C^{12}-C^{12}$ and $C^{12}-C^{13}$ bonds. Similar experiments with butane are now in progress.

[1] J. W. Otvos and C. D. Wagner, Science **106**, 409 (1947).
* Recent measurements with a sample containing 54 atom percent C^{13} allow a more exact evaluation of the changes in these dissociation probabilities, with the result that the dissociation probability of the $C^{13}-C^{12}$ bond is decreased by 12 percent ±1 percent and that of the $C^{12}-C^{12}$ bond increased by 7 percent ±0.2 percent.

A Criterion for Normal Liquids

ROBERT L. SCOTT
University of California, Berkeley, California
January 23, 1948

IN a recent communication Parashad[1] has proposed a formula to distinguish between normal liquids and associated liquids. For liquids which we may regard as normal, he finds

$$\Delta E^v\beta/V\alpha=T, \tag{1}$$

while for abnormal liquids, the left-hand member is greater than T

$$\Delta E^v\beta/V\alpha>T. \tag{2}$$

ΔE^v is the energy of vaporization, β is the isothermal compressibility, V is the molal volume, α is the coefficient of cubical expansion, and T is the absolute temperature.

In reality, the criterion which Parshad proposed is not novel. Pure thermodynamics yields what has been called the "thermodynamic equation of state"

$$(\partial E/\partial V)_T=T(\partial P/\partial T)_v-P. \tag{3}$$

Since for liquids under normal conditions, P is negligibly small compared with the other two terms, we may write

$$(\partial E/\partial V)_T=T(\partial P/\partial T)_v. \tag{4}$$

Since $(\partial P/\partial T)_v=\alpha/\beta$, we obtain

$$(\partial E/\partial V)_T=T\alpha/\beta.$$

It remains for us to relate $(\partial E/\partial V)_T$ and $\Delta E^v/V$. Over a small range of volumes, we may represent E and $(\partial E/\partial V)_T$ in the functional forms:

$$E=a/V^n, \tag{6}$$

$$\partial E/\partial V=-na/V^{n+1}=-nE/V. \tag{7}$$

For most practical purposes the cohesive energy per mole E may be replaced by $-\Delta E^v$, and Eq. 5 may be rewritten

$$T\alpha/\beta=n\Delta E^v/V. \tag{8}$$

For a van der Waals liquid n is unity, and this last Eq. 8 reduces to the first. Although the van der Waals equation is certainly a poor approximation for liquids, Hildebrand and co-workers have measured $(\partial P/\partial T)v$ directly for a number of normal liquids and on comparison with $\Delta E^v/V$, it was found that n is, in fact, not far from unity.[2] For methyl alcohol and mercury, although for different reasons, the calculated n falls far short of unity, in agreement with Eq. (2).

[1] R. Parshad, J. Chem. Phys. **15**, 761 (1947).
[2] J. H. Hildebrand, Phys. Rev. **34**, 984 (1929); see also J. H. Hildebrand, *Solubility of Non-Electrolytes* (Reinhold Publishing Corporation, New York, 1936), second edition, pp. 93–101, and J. Chem. Phys. **15**, 727 (1947), particularly Table VII.